ABSTRACT

Title of Thesis: USING MODIS SATELLITE IMAGES TO CONFIRM DISTRIBUTED SNOWMELT MODEL RESULTS IN A SMALL ARCTIC WATERSHED

David F. Choy, Master of Science, 2009

Directed By Dr. Kaye Brubaker
Water Resources Program
Department of Civil and Environmental Engineering

Environmental analysts face the problem of obtaining distributed measurements to evaluate increasingly small spatiotemporal model output. This thesis explores the use of remotely sensed snow covered area (SCA) maps to confirm a time series of model maps. The measurements come from National Aeronautics and Space Administration (NASA) Moderate Resolution Imaging Spectroradiometers (MODIS). The United States Agriculture Department provided the model: TOPMODEL-Based Land-Atmosphere Transfer Scheme (TOPLATS). The Upper Kuparuk River Watershed (UKRW) on the North Slope of Alaska acts as the case study location. To meet the map-comparison goal, the Kappa statistic and probability functions expressing measurement uncertainty evaluate the ability of MODIS measurements to confirm the accuracy of TOPLATS model maps. Results show that composite statistics, like the proportion of agreement between two maps, can obscure spatiotemporally distributed confirmation information. Also, MODIS can confirm snowmelt predictions across areas less than 150 km^2, however, clouds and malfunctioning sensors limit such use.

CONFIRMING DISTRIBUTED SNOW COVERED AREA MODEL RESULTS IN A SMALL ARCTIC WATERSHED WITH MODIS SATELLITE IMAGES

By

David F. Choy

Thesis submitted to the Faculty of the Graduate School of the
University of Maryland, College Park, in partial fulfillment
of the requirements for the degree of
Master of Science
2009

Advisory Committee:

Dr. Kaye Brubaker, Chair
Dr. Richard H. McCuen
Dr. Glenn E. Moglen

COPYRIGHT

DEDICATION

This paper is dedicated to my grandpa Seymour Harrison and the engineers in my family: Sarah Ahmed, Cory Choy, Steven Choy, Arthur Harrison, Jesse Kovach, Amber Lee, Dean Li, Megan Li, and Marc Litz. We have catch-up work to do under an administration that is beginning to fund science and our planet.

ACKNOWLEDGEMENTS

Thank you to the Agriculture Research Service (ARS) at the Hydrology and Remote Sensing Lab at the United States Department of Agriculture which provided funding for this research and part of my education. Thank you to Dr. Wade Crow who provided the technical support to get a key computational model working on computers it was not intended to run on.

Thank you to the Center for Excellence in Project Management (CEPM) at the University of Maryland for funding my continued education and opening up a world of opportunity. Thanks to Dr. Miroslaw Skibniewski for developing the Web-Based Project Management class with me, Dr. Gregory Baecher for building the Water Policy Collaborative website with me, and Professor John Cable and Dr. Jimmy West for developing the CEPM website with me. These projects have kept me in school.

Thank you to the Water Resources Department and the unofficial Hydrology Club at the University of Maryland. Thanks to my committee members Dr. McCuen and Dr. Moglen for teaching me statistical and GIS approaches to engineering problems. (I am currently employing the skills I learned in your classes while developing web-based mapping applications.)

Thank you to King Cow Interactive LLC coworkers and partners for starting the generator, checking my email, and managing my accounts while I've been in the library writing this paper. Special thanks to Jesse Kovach and his family, Theo Ephraim, Jascha Ephraim, Dori Shivers, and Elliott Krimchansky.

Thank you to my family: Stevie Lew, Vincent and Spice, Clementine, Mineola, Kumquat, Sweet Penelope, Arthur Durham Bun Bun, my wife Sarah Ahmed

and her family, uncle Frank and uncle Arthur, Noelle, Collin, Rachael, Cory, my parents, and my grandparents. Thank you for wiring, dry-walling, plumbing, ripping-up carpet, and moving broken appliances up and down stairs in our home while I've been sitting in front of a computer screen.

I would like to thank my advisor Dr. Kaye Brubaker, more than everyone else, for developing a life-satisfying graduate program. During my time at the University of Maryland, Dr. Brubaker and I have competed in two Solar Decathlons and Dr. Brubaker has steered Sarah to both water resources graduate school and a job at the Interstate Commission on the Potomac River Basin. Thank you to David and Simon. Thank you to Maxine for waiting those extra weekday hours for Dr. Brubaker to get out of the office for your evening walk.

TABLE OF CONTENTS

CHAPTER 1: Introduction 1

1.1 Overall Research Goals 1

1.2 Need & Problem 1

1.2.1 Map Comparison Needs 2

1.2.2 Data Management Needs 4

1.2.3 Summary of Needs 5

1.3 Objectives 6

1.3.1 Preliminary Objectives: Resource Selections 6

1.3.2 Map Comparison Objectives 7

1.3.3 Data Management Objectives 7

1.4 Potential Contributions and Implications 8

CHAPTER 2: Literature Review 9

2.1 Watershed Background 9

2.1.1 Location & Area 9

2.1.2 Snowmelt 14

2.1.3 Meteorological Measurements & Geology in the UKRW 16

2.2 Remotely Sensed Measurements 18

2.2.1 Satellite Measurements Overview 19

2.2.2 MODIS Snow Measurements 27

2.3 Distributed Models 36

2.3.1 TOPLATS 39

2.4 Map Comparison 41

2.4.1 Background 41
2.4.2 Spatial Comparison 44
2.4.3 Temporal Comparison 58
CHAPTER 3: Resources and Methods 63
3.1 Resource Selection 64
3.2 Map Comparison 65
3.2.1 Spatial Comparison with Kappa and Kappa Variants 68
3.2.2 Temporal Comparison 71
3.3 Data Management 72
3.3.1 Measured Data 72
3.3.2 Model Calibration 84
CHAPTER 4: Results and Discussion 85
4.1 Measurements 85
4.1.1 DAAC Query Results 86
4.1.2 Influence of Availability, Collection Time, and Quality Assurance Filters on Measurement Uncertainty 90
4.2 Model Snow Maps 116
4.2.1 Snow Water Equivalent 117
4.2.2 Comparison with MODIS Maps 126
4.2.3 Snow Covered Area Threshold 131
4.3 Model Confirmation 146
CHAPTER 5: Conclusions 161
5.1 Accomplishments 161

5.2 Findings and Implications 162
5.2.1 Usefulness of MODIS for Modeling The UKRW 162
5.2.2 Quantifying Uncertainty In Scenes Containing Unavailable Measurements 164
5.2.3 Applicability of Kappa Statistics 165
5.3 Critique and Future Work 168
5.3.1 Other Statistics 168
5.3.2 Variable Time-Rate Composite MODIS Data 171
5.3.3 Comparing Data in Swath Format 172
5.3.4 Revaluate HEG-TOOL 174
5.3.5 Select Only High Quality Scenes Within Sub Time Intervals 174
5.4 Research Summary 175

TABLE OF APPENDICES

Appendix A. United States Global Change Research Program Organizations 178
Appendix B. Projected MODIS Measurements 179
Appendix C. Software Requirements 180
Appendix D. Comparison Overview Dataflow 181
Appendix E. MODIS Swath Scene Objects 182
Appendix F. Global Change Online Resources 183
Appendix G. Swath to Kuparuk (S2K) Code 184
Appendix H. Comparing Model and Measurements 185

LIST OF FIGURES

Figure 2-1. Upper Kuparuk River Watershed. 11

Figure 2-2. Location of the Upper Kuparuk Watershed with respect to Alaska 11

Figure 2-3. Watershed Shape and Bounding Study Area 12

Figure 2-4. Kuparuk River Watershed 13

Figure 2-5 Winter-Spring Hydrographs 15

Figure 2-6. Swath 22

Figure 2-7. Moderate Resolution Imaging Spectroradiometer (MODIS) 23

Figure 2-8. Terra and Aqua Launch Photos 24

Figure 2-9. Generic Confusion Matrix 51

Figure 2-10. Two-Category Confusion Matrix. 51

Figure 2-11. Kno and Kappa comparison. (Kno = 0.7500) > (K = -0.8025) 55

Figure 2-12. Example Triangle Probability Density Functions 62

Figure 3-1. MODIS-TOPLATS Confusion Matrix. 69

Figure 3-2. Interactive Map Comparison 70

Figure 3-3 Effect of Satellite Angle on Sample Point Quantity 79

Figure 3-4 Python Script, “ascii2kuparuk” Processes 83

Figure 4-1 Hydrograph Relationship to %SCA for years 2000, 2001, 2002 87

Figure 4-2 Sum of Snow-Covered Pixels Across Unfiltered and Filtered Melt Series 91

Figure 4-3 UKRW Elevation Zones 92

Figure 4-4 2000 Select MODIS Scenes 94

Figure 4-5 2001 Select MODIS Scenes 95

Figure 4-6 2002 Select MODIS Scenes 96
Figure 4-7 Year 2000 Quality Assurance, Collection Time, and Proportion SCA... 103
Figure 4-8. Year 2001 Quality Assurance, Collection Time, and Proportion SCA.. 105
Figure 4-9. Year 2002 Quality Assurance, Collection Time, and Proportion SCA.. 107
Figure 4-10. 2000 Probability as a Measure of Uncertainty 111
Figure 4-11. 2002 Morning Scenes Across The UKRW and Four Elevation Zones 113
Figure 4-12. 2002 Morning Scenes with a Proportion of 0.50 or Greater Good Quality Swath Points Across The UKRW and Four Elevation Zones..... 115
Figure 4-13 Select TOPLATS SWE Scenes for Albedo Values 0.75, 0.80, and 0.85 118
Figure 4-14 TOPLATS Watershed SWE (8,557 pixels) 119
Figure 4-15 TOPLATS Zone One SWE (3,015 pixels)..... 120
Figure 4-16 TOPLATS Zone Two SWE (4,173 pixels) 121
Figure 4-17 TOPLATS Zone Three SWE (1,184 pixels) 122
Figure 4-18 TOPLATS Zone Four SWE (185 pixels)..... 123
Figure 4-19 2002 Effect of the Albedo Parameter on SWE Model Results 128
Figure 4-20 2002 Effect of the Albedo Parameter on SWE Model Results for Good Quality Morning Points..... 129
Figure 4-21 2002 Effect of the Albedo Parameter on SWE Model Results for Good Quality Morning Points Ending for All Scenes Measured Before The Apparent End of Melt on Day 146. 130
Figure 4-22 Year 2002 0.80 Albedo Map Comparison for the Entire Watershed (Zone 0) 138

Figure 4-23 Year 2002 0.85 Albedo Map Comparison for the Entire Watershed (Zone 0) 144

Figure 4-24 Year 2002 0.80 Albedo and 0.85 Albedo SCA Error 145

Figure 4-25 Year 2002 0.80 Albedo, 0.75 cm SWE Threshold for Four Elevation Zones..... 151

Figure 4-26 Year 2002 0.85 Albedo, 2.50 SWE Threshold for Four Elevation Zones 155

Figure 4-27 SCA Maps for Measured, and Two Sets of Model SCA Results..... 156

Figure 5-1 Patchy Snow in the Kuparuk River..... 167

LIST OF TABLES

Table 2-1. Watershed Characteristics 17

Table 2-2. Model Area Characteristics 17

Table 2-3. Satellite and Instrument Characteristics for Sensing Snow & Ice..... 20

Table 2-4. Relative Visible and Near-Infrared Reflectance of Clouds, Land, and Snow 28

Table 2-5. MODIS Bands Used to Detect the Presence of Snow 28

Table 2-6. MODIS Snow and Ice Level Two , Collection Four Product Characteristics 32

Table 3-1. Functional Decomposition of Objectives 63

Table 3-2. MODIS Measurement Groups..... 67

Table 3-3. Kappa and Kappa Variant Interpretation..... 70

Table 4-1. Scene Filters 89

CHAPTER 1: INTRODUCTION

1.1 OVERALL RESEARCH GOALS

This study sought to develop a method for confirming modeled snow maps with remotely-sensed measurements, which inspired a second goal: to increase the usability of the remotely-sensed data. The following sections place this work in the context of global change research needs (1.2 Need & Problem), define research objectives (1.3 Objectives), introduce the Upper Kuparuk River Watershed (UKRW), the case study area, introduce the Moderate Resolution Imaging Spectroradiometer (MODIS) — a satellite sensor, and introduce the TOPMODEL-Based Land-Atmosphere Transfer Scheme (TOPLATS) model.

1.2 NEED & PROBLEM

The Global Change Research Act of 1990 established the U.S. Global Change Research Program (USGCRP). The USGCRP aims to "understand" and "respond" to "global change, including the cumulative effects of human activities and natural processes on the environment. . . ." Thirteen federal organizations, tabulated in Appendix A, participate in the program. Each organization contributes to seven research areas: (1) atmospheric composition, (2) climate variability and change, (3) global carbon cycle, (4) global water cycle, (5) ecosystems, (6) land use / land cover change, and (7) human contributions and responses (US Global Change Research Program, 2007). The U.S. Office of Management and Budget (2007) reports that the

USGCRP spent $5.9 billion in FY 2006 and proposes $7.4 billion for FY 2008 to study global change.

1.2.1 Map Comparison Needs

Analysts in all seven of the USGCRP research areas are constructing models of the earth more frequently and with greater complexity than ever before. As desktop processing advancements and web-based communication tools drive this growth, analysts struggle to systematically compare and confirm model results with measured data. Pontius (2002) describes this problem as it applies to landscape modeling:

> *Modeling Landscape Dynamics is an indication of the tremendous growth in the general field of landscape modeling. Our field abounds with variations on Markov Chain models, Cellular Automata models, agent-based models, multi-nomial logistic regression models, etc. In fact, we are now producing models faster than we can validate them.*

The research described in this thesis responds to the charter from the USGCRP for better understanding of global changes by recommending mechanisms to confirm both spatially and temporally distributed model map results with remotely sensed measurement counterparts. It aims to answer water resources questions set forth by the USGCRP (2003) described in Chapter 5 of "Strategic Plan for the U.S. Climate Change Science Program: Water Cycle." In particular, this study addresses ways to "merge measurements from different satellite[s]." It address aspects of Question 5.3 from the Strategic Plan, which ask for the "key uncertainties in seasonal . . . predictions . . . and . . . improvements . . . in . . . regional models to reduce these

uncertainties," "better understanding and improved model representations of . . . seasonal . . . interactions of the atmosphere with vegetation, soils, oceans, and the cryosphere," and "the role of mountains in the annual water cycle." This study also aspires to address new questions dealing with "Integration of Water Cycle Observations, Research, and Modeling" (USGCRP 2007) set forth in the 2008 strategic plan: "FY 2008 activities will focus on . . . an observing system aimed at measuring key elements required to close the terrestrial water cycle budget on a regional scale such as a river basin or watershed."

To address the USGCRP needs, this study uses snowmelt in the Upper Kuparuk River Watershed – measured by MODIS and modeled by TOPLATS – as a case study. This interest area and this remotely sensed dataset are both (a) strategically aligned with USGCRP needs and (b) practical choices for research for the following reasons: The interest area lies in the cryosphere; the interest area demonstrates seasonal variability; the interest area has a history of meteorological, geological, and hydrological measurements; the interest area has digital elevation information easily accessible to this research; the interest area exhibits spatial heterogeneity of snow cover during the melt season; the remotely sensed dataset exhibits a fine enough temporal resolution to monitor a short snowmelt season; the remotely sensed dataset is accessible at a low level of processing; and the remotely sensed dataset has other datasets available in the same location to check the measurements. With an interest area and data set selected, this study sets a goal to define methods for testing model accuracy both spatially and temporally.

1.2.2 Data Management Needs

Simultaneous to the increasing need for map comparison, the USGCRP spurs a need for better management of remotely sensed data. Most notably, the USGCRP funds management of three remote sensing projects: The POES and GOES program primarily developed by NOAA and NASA; the LANDSAT program developed by NASA, USGS, and NOA; and the overarching Earth Observing System (EOS) program maintained by NASA at the Goddard Space Flight Center in Maryland.

These programs (detailed in Chapter Two) contract, launch, and maintain satellite missions equipped with multi-spectral sensors. In space, sensors capture and broadcast images of the earth. On the ground, analysts receive, process, and archive the images. Growth of archived data at multiple levels of processing has created a need to better disseminate information over the World Wide Web. USGCRP set decade-long goals to make data free, available, and accessible via web-based technologies and GIS systems. The program calls for a "transparent" distribution service that allows end-users to focus on data. While first generation information systems are now in place, emerging web-based service technology indicate that "building this framework must be an evolutionary process" that will need to be "regularly updated . . . to respond to user requirements" (USGCRP 2003). Such web-based technologies that could answer user requests for improved data management include the implementation of model view controller programming patterns through web-standard technologies and the developing semantic web standards. These technologies could answer requests for better conveyance of quality assurance datasets (MODIS conference 2006), data in user-specified geographic projections

(MODIS conference 2006), and on-demand data delivery (CUAHSI 2009). Complementing USGCRP goals to make remotely-sensed data manageable, this thesis aims to employ web technologies, when appropriate, during the process of (a) converting low-level (Level 2), remotely sensed (MODIS) data into a geographic information system (GIS) compatible format and (b) comparing observed and simulated results.

1.2.3 Summary of Needs

In summary, this study address two needs set forth by the USGCRP in the early 1990s which have been reevaluated and reinforced in 2008. First, this study aims to develop methods to access the accuracy and uncertainty of a time series of model maps in comparison to a time series of measured maps. These comparison-methods should provide an example for future researchers calibrating, validating, or evaluating the performance of a model predicting snow water equivalent or snow covered area in any small, mountainous watershed like the UKRW. Second this study should begin the development of a tool for making low-level (MODIS Level 2) measurements manageable. Developing a MODIS data-management tool should reveal the ability and practicality of comparing MODIS measurement of snow and ice to modeled snow cover.

While these research needs are specific to snow cover during a quick snowmelt event, the methods and results developed in this study should be practical to analysts comparing other types of MODIS land cover measurements to other types of simulated results during quickly-occurring events. For example, wildfire modelers

could use MODIS forest-cover measurements and fire-cover measurements to calibrate their simulations. Flood modelers could similarly use MODIS water-cover measurements.

1.3 OBJECTIVES

The objectives of this study were to:

1. Select resources
    a. Select an interest area
    b. Select a time period
    c. Select remotely sensed measurements
    d. Select a model
3. Compare measured and modeled maps
    a. Spatially
    b. Temporally
4. Make measured and model maps compatible (manage data)

These objectives are briefly discussed below.

1.3.1 Preliminary Objectives: Resource Selections

Section 1.2 defines the preliminary objectives to investigate whether the UKRW snowmelt, MODIS, and TOPLATS meet the requirements for an interest area, a time period, measurements, and a model that will both help understand global change according to the USGCRP and act as the case study for developing methods for spatiotemporal map comparison. Chapter Three describes the reasons why these resources meet the needs of the USGCRP.

1.3.2 Map Comparison Objectives

This thesis aims to compare modeled and measured maps spatially and temporally. The selection of TOPLATS as the model narrows the spatial map comparison objectives to the evaluation of a single, binary land category because TOPLATS only assigns snow (in the form of a snow water equivalent) and snow-free categories to designated regions. TOPLATS does not, for example, assign ice or water to any region. This decision to limit categories, and given the fact that the MODIS measurements include other categories like clouds and lake ice, creates the need for another objective to develop a way to reduce the number of categories in the measured data. Finally, a no-data category needs to be considered to account for potential problems from either the modeled or measured data.

In line with USGCRP goals to uncover small scale mechanisms described in the "Revised Research Plan for the U.S. Climate Change Science Program" (USGCRP 2008) and to exploit the high temporal resolution of the MODIS orbit, the overall temporal map comparison objective aims to recognize the independence of each measured scene. This objective includes analysis of different elevation zones as well as the entire watershed, addressing the impact of elevation on snowmelt (Déry et al. 2004).

1.3.3 Data Management Objectives

Data management objectives in this thesis aim to make MODIS measurements comparable to the model output as explained in Section 1.2.2. Specifically, the NSIDC distributes MODIS data that has been minimally processed in a swath data

format, explained further in Section 2.2 Remotely Sensed Measurements (Figure 2-6). For comparison of measured and model data, either measurements in the swath format need to be converted into model output format, or model output needs to be converted into the swath format. Data management objectives include evaluation of existing software tools for their ability to manage swath measurements. Section 2.2.2.4 reviews these tools and reports results from attempting to benchmark them with measured data.

1.4 POTENTIAL CONTRIBUTIONS AND IMPLICATIONS

Potential contributions of this study include the creation of a mechanism to compare measured and modeled maps, the creation of a list of best practices to manage publically swath data, and possibly the foundation for a web-based GIS application to manage swath data and similar HDF-EOS files. Other USGCRP projects will both potentially review and improve on the map comparison mechanism and develop new data management systems influenced by the findings in this study.

CHAPTER 2: LITERATURE REVIEW

Four topics contribute to the literature review:

2.1 Watershed Background

2.2 Remotely Sensed Measurements with a focus on MODIS snow cover

2.3. Distributed Models with a focus on TOPLATS

2.4 Map Comparison

2.1 WATERSHED BACKGROUND

2.1.1 Location & Area

The Upper Kuparuk River watershed (UKRW), shown in Figure 2-1 and Figure 2-2, spans 147.6 km^2 on the North Slope of Alaska in UTM Zone 6.[*] It is located at the foothills of the Brooks Mountain Range in the USGS Philip Smith Mountains quadrangle. The UKRW is flanked by Toolik Lake (east) and Imnavait Creek (west) tributaries. Figure 2-3 shows the UKRW shape projected in UTM Zone 6.

Water flows from the mountains, northward, into the main Kuparuk River (Figure 2-4). For comparison, the entire Kuparuk River watershed is almost 60 times as large as the UKRW. It covers 8,421 km^2 and flows through three physiographic

[*] McNamara et al. (1998) delineate a 142 km^2 watershed area for the Upper Kuparuk. This study uses the value 147.6 km^2, derived from a glacial geology map of the Toolik Lake and the UKRW created by Walker et al. in 2003. This number agrees with the product of the number of pixels (8557 pixels) and the pixel size (131.34 m by 131.34 m) used by S. Déry et al. (2004).

provinces: arctic mountain, foothills, and coastal plains. The Kuparuk River watershed pours into the Arctic Ocean at Prudhoe Bay.

The UKRW is accessible to researchers via the Dalton highway (Alaska 11), also known as “Haul Road” for its use during construction of the trans-Alaska oil pipeline in the 1970s. The road and pipeline run along the west boundary of the watershed (Figure 2-1). The road crosses the Upper Kuparuk River, forming the north boundary. The road makes the UKRW a prime place for hydrological and meteorological stations.

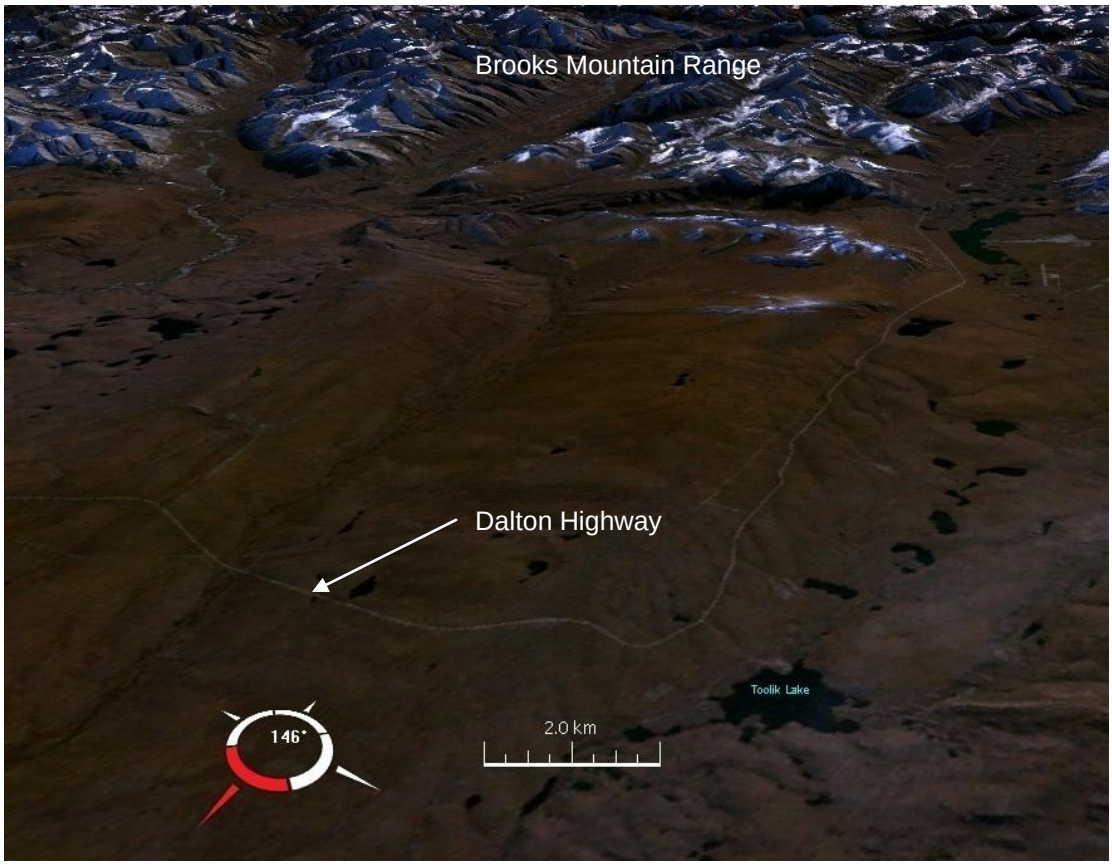

Figure 2-1. Upper Kuparuk River Watershed.
This is a World Wind 1.4 render of LANDSAT 7 false-color mapped onto USGS 30-meter DEM. The image is from the perspective of a person looking upstream, north of the watershed outlet. The thin gray line represents the Dalton Highway, which delineates the northern watershed boundary.

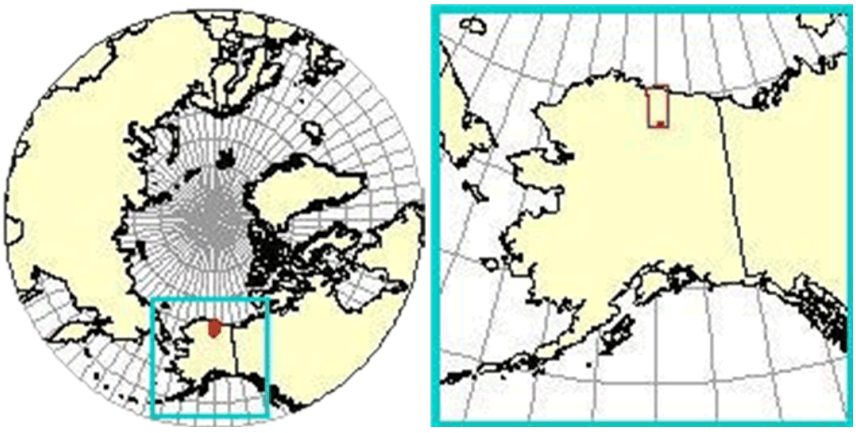

Figure 2-2. Location of the Upper Kuparuk Watershed with respect to Alaska
From NSIDC (http://nsidc.org/data/arcss017.html)

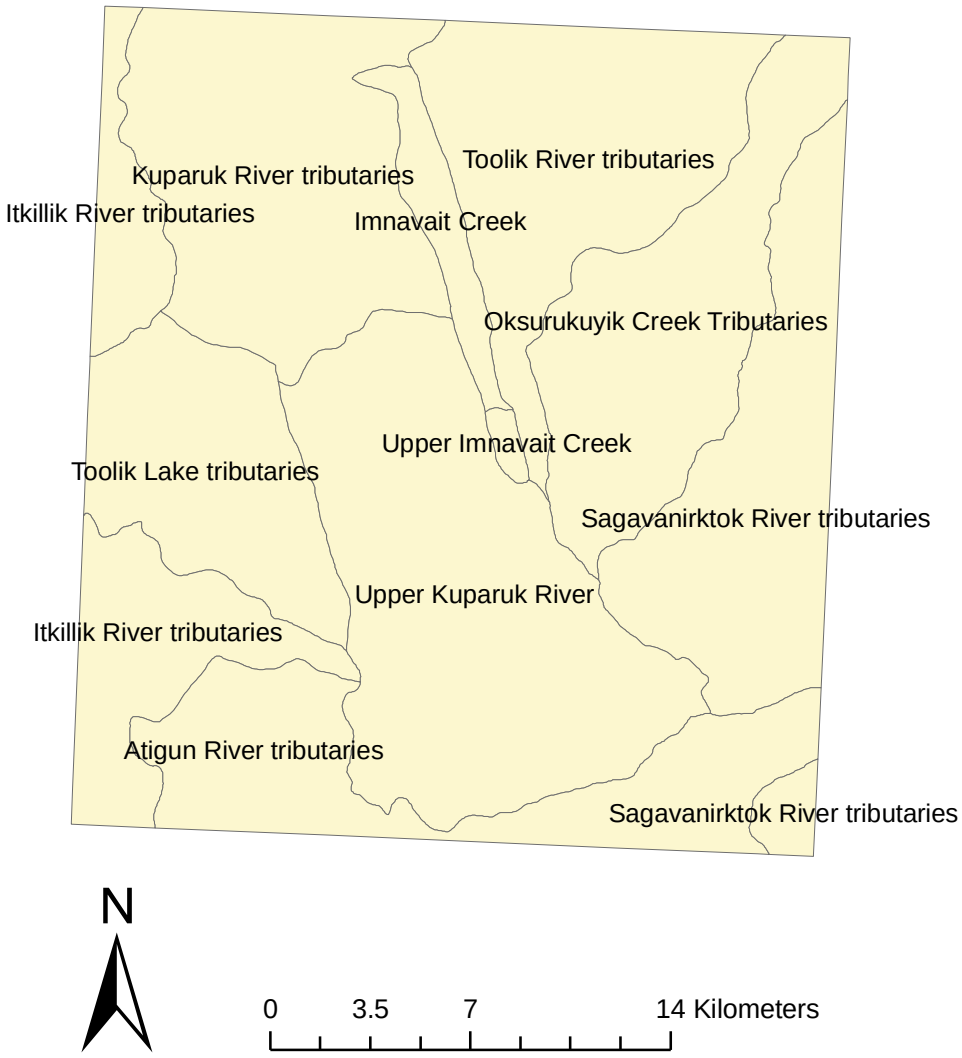

Figure 2-3. Watershed Shape and Bounding Study Area
This figure shows the UKRW in context with other tributaries in UTM Zone 6.

Figure 2-4. Kuparuk River Watershed
The entire Kuparuk River watershed is 8,421 km^2. Water flows from the Upper Kuparuk, through the Kuparuk River into the Arctic Ocean at Prudhoe Bay.

2.1.2 Snowmelt

Statisticians describe winter-spring snowmelt as a secular event, usually lasting less than three months, occurring annually. In mountainous arctic regions, the event usually starts with 100% snow-covered land and ends in none.[†] Plots of area-composite snow variables, like %SCA or mean SWE, against time show that hydrologists can describe snowmelt with a decreasing logistic function (biological death curve)

$$s(t) = \frac{1}{1 + e^{b(t-a)}}\ 100\% \qquad \textbf{2-1}$$

For proportion %SCA *s*, time *t*, and location parameter *a*, and scale parameter *b*, where both *a* and *b* are greater than zero. Statistical models forecast snow using both autocorrelation relationships detected within past snow measurements and indirect correlations involving temperature (McCuen 2003). The effect of ground elevation on snowmelt exemplifies an indirect effect involving temperature.

Snowmelt, in the UKRW specifically, usually accounts for a third of the annual runoff (Kane et al. 2000). This discharge from snow melt is due in part to both snow build up during the winter and thick permafrost limiting base flow in the arctic. The largest snowmelt event of the year in the UKRW usually begins in May (during bird migration season) and sometimes in June, when "hordes" of mosquitoes (Alaska

[†] This arctic example of snowmelt does not imply the definition of snowmelt excludes the general case of snowmelt in which interest areas are do not begin with 100% SCA. Land cover, land use, regional temperatures, wind, and other factors in various interest areas often prevent 100% SCA at the end of a given winter season. When snow melts in these situations, statisticians still call it snow melt..

Bureau of Land Management, 2006) make collecting measurements in the field particularly unattractive compared to gathering remotely-sensed data from an off-site location. This "winter-spring" (Liston, 1998) event usually causes the largest annual discharge shortly afterward. Figure 2-5 hydrographs shows these events for the years 2000, 2001, and 2002 in the UKRW. The peak discharge for each of these years rationally occurs at the time of the maximum rate of change in %SCA. This study uses this information to show that the UKRW snowmelt lasted six, ten, and seven days in years 2000, 2001, and 2002 in Chapter Four.

In addition to the importance of snowmelt on discharge, and in turn, traditional water resources and construction applications, Liston (1998) emphasizes the importance of snow cover on the balance of the earth's climate cycle. He attributes the effect of snowmelt on radiation due to the high reflectance and the low thermal conductivity of snow covered areas.

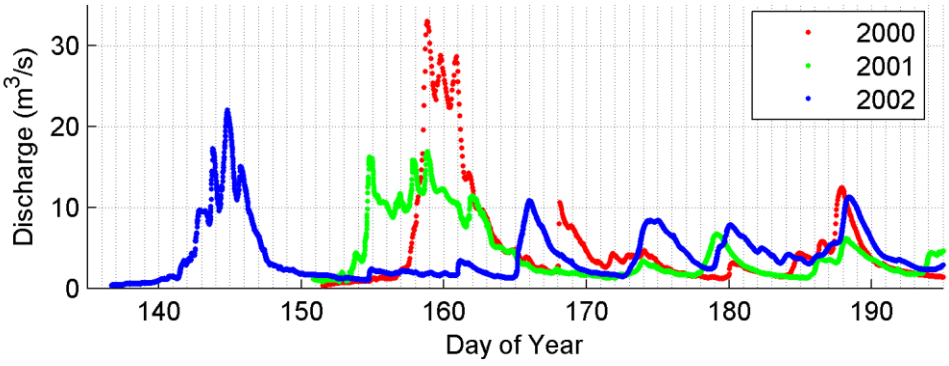

Figure 2-5 Winter-Spring Hydrographs
The peak discharge in the UKRW collected by Hinzman and Kane (2009) time during May and June, for each 2000, 2001, and 2002, guides the time period selection in each of this study's initial queries for snow cover. It also allows this study to cross reference MODIS Quality Assurance information for those times. Note that the day of year references UTC time, not UKRW local time which is nine hours ahead. May 1 occurs on day 135. (See http://modland.nascom.nasa.gov/QA_WWW/). See MATLAB® script "plot_hydrographs.m" to reproduce this figure.

2.1.3 Meteorological Measurements & Geology in the UKRW

Throughout the year, the U.S. National Weather Service (NWS) gauges the precipitation with a tipping bucket and Alter shields. During the snowmelt period, Kane, et al. (2003) make additional precipitation measurements. They measure precipitation twice daily. Wind contributes to the spatiotemporal variability of SCA along with accumulation and ablation (Zhang et al. 2000).

The Laurentide Ice Sheet shaped the foothills of the Brooks range (French 2007) during the Wisconsian Glaciation (Kaufman and Manely 2004) of the late Pleistocene epoch (Porter 1964, Hamilton 1986). Permafrost penetrates into the ground down to 600 meters in the Kuparuk River watershed near Prudhoe Bay (Osterkamp and Payne 1981), and down to 250 meters under the UKRW (Kane, et al. 2003).

Table 2-1. Watershed Characteristics

Characteristic		Measurement	Comments	
Area		147.6 km^2 (= 56.99 mi^2)	Small compared to the Kuparuk River watershed, which is 8,421 km^2. The watershed area is 18.12% of the model area.	
Perimeter		56.63 km	From vector area	
Number of Pixels		8,557	Includes only the Upper Kuparuk area shown in Figure 2-3	
Maximum Stream Length		22.24 km	(= 13.82 mi)	
Elevation	Min	736.4 m	The watershed starts in alpine foothills and drains into a relatively flat tundra.	
	Max	1,492 m		
	Range	755.8 m		
Centroid	X	404,610 m	Calculated with `.Centroid.X` and `.Centroid.Y` shape objects	
	Y	606,652 m		
Extent	*UTM Zone 6*		*Global Coordinate System*	
	Left	398,086 m	West	-149.508205°
	Right	413,190 m	East	-149.121345°
	Top	616,590 m	North	68.649343°
	Bottom	598,334 m	South	68.480656°

Table 2-2. Model Area Characteristics

Characteristic		Measurement	Comments	
Area		814.49 km^2 (= 314.47 mi^2)	Includes model area around the watershed shown in Figure 2-3	
Number of Pixels	Columns	208	$A = (131.34\ m)^2 \cdot 208 \cdot 227$	
	Rows	227	$= 814.5\ km^2$	
	Number	47,216	$= 314.5\ mi^2$	
Pixel Size	Width (x)	131.34 m	Same as cell size.	
	Height (y)	131.34 m	1 pixel = 17,250.20 m^2	
Projection		UTM Zone 6	Clarke 1866 Datum	
False Easting		500 km		
False Northing		-7,000 km		
Extent	*UTM Zone 6*		*Global Coordinate System*	
	Left	390,862 m	West	- 149.697228°
	Right	418,181 m	East	-148.998749°
	Top	627,228 m	North	68. 746202°
	Bottom	597,414 m	South	68. 469708°

2.2 REMOTELY SENSED MEASUREMENTS

Remote sensing of the Earth from satellites creates opportunity to analyze both the lay and utilization of the land. The process complements aerial remote sensing. In general, aerial sensors deliver higher resolution images than satellite sensors because of their proximity to the Earth; but aircraft paths are limited by flight zones, funding, and fuel constraints. At times, analysts using aerial images must composite output from different flights and different sensors to get a complete picture of an interest area. The National Operational Hydrologic Sensing Center (NOHRSC) at NOAA, for remote-sensing of snow, gathers, processes, analyzes, and distributes both satellite-sensed and aerially-sensed snow cover information from their website (NOHRSC 2009).

Builders and city planners can, in general, schedule single aerial flights for constructability analysis more easily than meteorologists, hydrologists, and other earth scientists can, in comparison, fund aircraft flights in order to monitor multi-day events and events that occur with little or no warning. These scientists, instead, predominantly use satellite imagery. Compared to sensors aboard aircraft, satellite sensors can potentially supply a persistent stream of images that blanket the earth. Satellites are expensive to build and maintain compared to aircrafts. When a problem occurs on a satellite, replacements parts (or a replacement satellite) cannot be as readily procured in comparison to a replacement part for an aircraft. Such problems, in conjunction with launches that are separated by years, lead to missing data.

2.2.1 Satellite Measurements Overview

As introduced in 1.2.2 Data Management Needs, the USGCRP funds and manages the POES and GOES programs primarily developed by NOAA and NASA, the LANDSAT program developed by NASA, USGS, and NOAA, and the MODIS (Moderate Resolution Imaging Spectroradiometer) satellite programs developed by NASA. The GOES, POES, LANDSAT, and MODIS missions compose part of NASA's Earth Observing System (EOS). For sensing snow and ice, NOAA uses the Interactive Multisensor Snow and Ice Mapping System (IMS) to process POES and GOES measurements. The resulting images are best suited for large-scale (four to 25 km cell size) meteorological forecasting in the northern hemisphere. LANDSAT missions deliver imagery with relatively high spatial resolution (15 m cell size) and relatively low temporal resolution (16 day earth coverage) while MODIS missions deliver imagery with relatively low spatial resolution (30 m to 500 m cell size) and relatively high temporal resolution (two-day earth coverage). Only MODIS measurements provide sufficient spatiotemporal resolution to monitor a seasonal land cover event like the snowmelt season in the UKRW. Table 2-3 summarizes the characteristics of the satellites and their instrument described in this section.

Table 2-3. Satellite and Instrument Characteristics for Sensing Snow & Ice

Satellite	**LANDSAT**	**AQUA & TERRA**	**POES**	**GOES**
Instrument	*ETM+*	*MODIS*	*AVHRR*	
Flight Pattern	near polar sun-synchronous			geostationary
Orbit Time	98.9 min		[98,102] min*	
Nominal Satellite Altitude	705 km		810 km & 850 km	36,000 km
Swath Width	185 m	2,330 km	up to 24,140 km**	not applicable****
Swath Scene Area***	3,145 m^2	3,154,820 km^2	nominally 1,000 km^2	
Scene Spatial Resolution (Cell Size)	15 m	500 m for snow and ice products	After processing through IMS: 25 km before 2004 4 km since 2004	
Time to sense every point on the earth.	16 days	2 days	1 day (14.1 polar orbits / day)	not applicable****

* Johnson 1996
** Swath widths vary between a "few" and 1,500 mi (NOAA 2006).
*** For comparison, the surface area of the earth spans 510,065,600 km2.
**** Geostationary satellites produce images centered around a single location on the earth.

2.2.1.1 LANDSAT

Scientists recognize the LANDSAT program as an old and comprehensive remote sensing project. Contractors are currently bidding on the development of the eighth LANDSAT satellite scheduled to replace the aging LANDSAT 5 (launched in 1984) and LANDSAT 7 (launched in 1999) satellites in 2011. Bergers (2006) estimates the value of the contract at $400 million. The LANDSAT 7 satellite orbits the earth once every 99 minutes in a near-polar, sun-synchronous pattern at an altitude of 705 km. While in orbit, the Enhanced Thematic Mapper Plus (ETM+) satellite sensor records a continuous strip of the Earth, called a swath, that is 185 km wide. The LANDSAT program divides swaths into segments, called scenes, that are 170 km long. The

LANDSAT 7 satellite takes 232 orbits or 16 days to record the entire earth (Williams 2007). Figure 2-6 evinces the components of a swath.

LANDSAT 7 produces digital images with pixels that have a cell size of 15m. This resolution makes LANDSAT 7 imagery especially useful in popular web-based mapping systems like Yahoo Maps and Google Maps. Additionally, desktop-based GIS like Google Earth and NASA World Wind uses false-color LANDSAT images in default views of Earth. While LANDSAT 7 provides enough resolution for many spatial applications, it does not provide enough temporal resolution for analysis of day-to-day events where significant change occurs in less time than the satellite takes to completely image the earth.

2.2.1.2 MODIS Satellites Aqua and Terra

In December 1999, NASA launched the first EOS mission by sending a Moderate Resolution Imaging Spectroradiometer (MODIS) sensor, among a total of 5 sensors, into orbit aboard the satellite called Terra. In 2002, NASA launched a sister satellite to Terra, called Aqua, with a second MODIS sensor. The satellites and their launches are pictured in Figure 2-7 and Figure 2-8. Like LANDSAT 7, both Aqua and Terra follow a near-polar, sun-synchronous orbit. Terra, also called EOS-AM, crosses the equator in the morning while Aqua, called EOS-PM, crosses the equator in the afternoon.

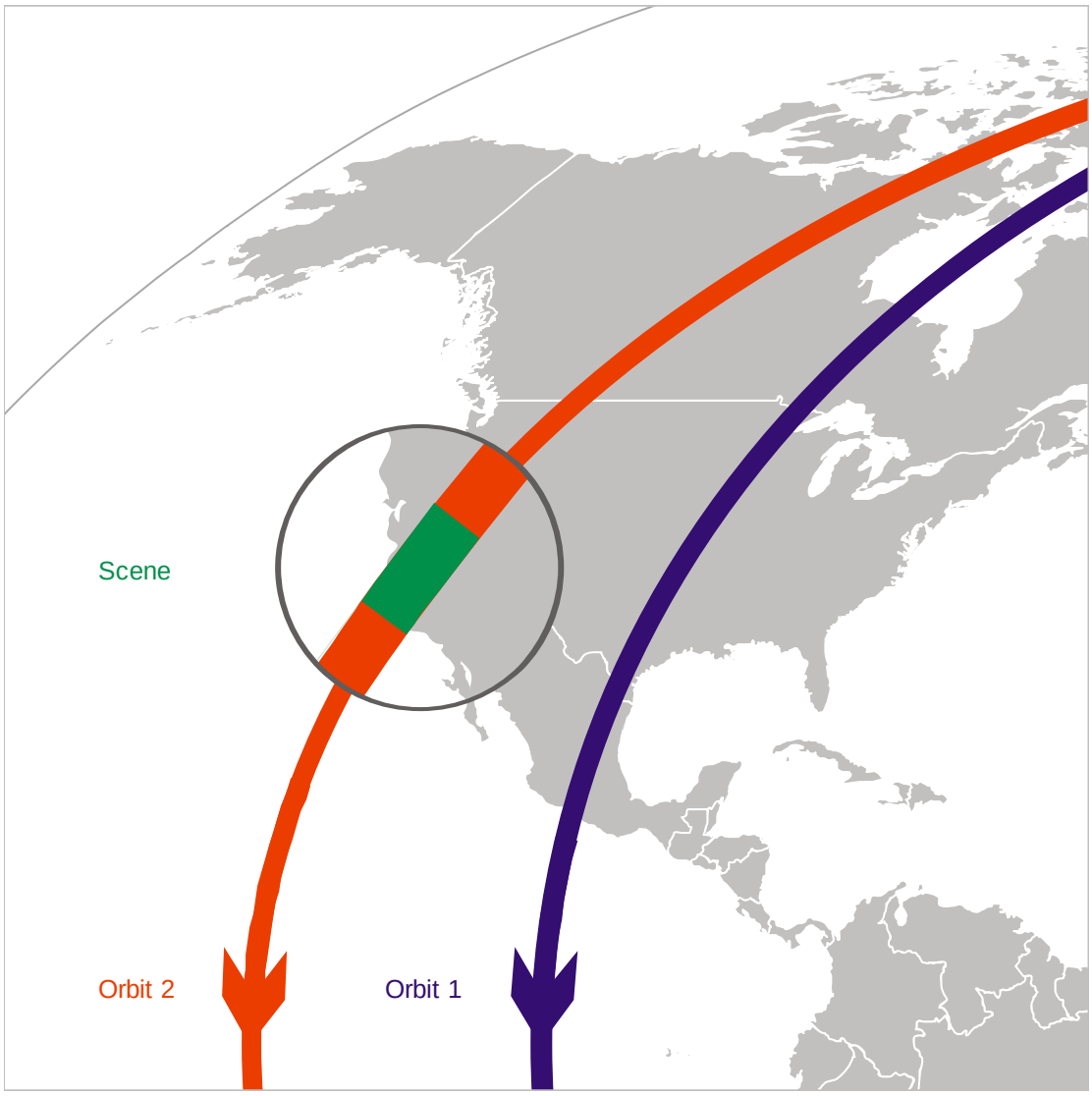

Figure 2-6. Swath
A swath is a continuous strip of land sensed from a satellite in orbit. A swath scene is a portion of a swath. This figure depicts the parts of a single swath taken from two consecutive orbits. It also highlights an individual swath scene. The swath shown is similar to the one produced by LANDSAT 7 in that the “swath orbits” converge near the poles. The swath is drawn on a pseudo-cylindrical Robinson projection.

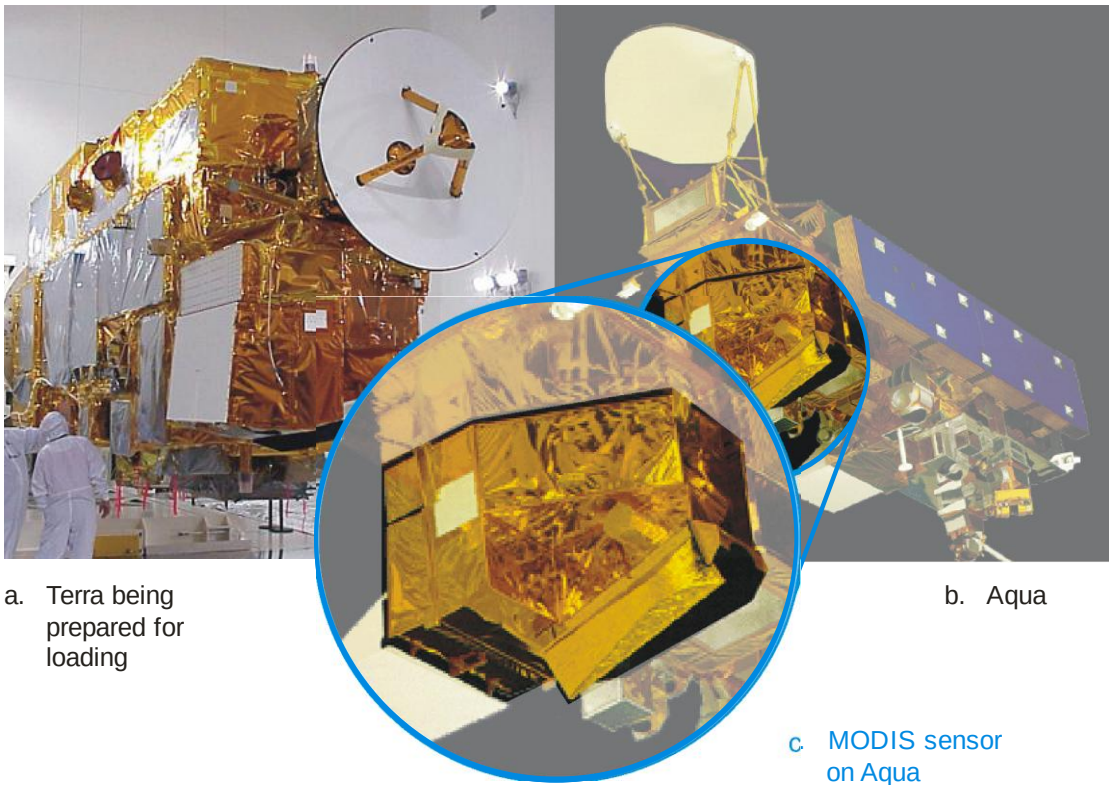

Figure 2-7. Moderate Resolution Imaging Spectroradiometer (MODIS)
MODIS is one of 5 instruments aboard Terra and one of 6 instruments aboard Aqua. (a) The relative size of Terra is shown as it is being prepared for loading into the C-5 aircraft. (b) Aqua is shown with (c) the MODIS sensor highlighted. (Photos from http://www.nasa.gov/.)

a. Terra Launch
December 18, 1999

b. Aqua Launch
May 4, 2002

Figure 2-8. Terra and Aqua Launch Photos
(a) C-5 aircraft lifting Terra on December 18, 1999 and (b) Delta II rocket lifting Aqua, at 2:55 a.m. PDT on May 4, 2002. Both satellites were launched from Vandenberg Air Force Base, CA. Photos from Wolfe (2002).

MODIS reports observations of clouds, fire, ice, land, ozone, snow, temperature, vapor, water, and more. It senses 36 different wavelengths ranging from below near infrared to mid-infrared (0.405 to 14.385 μm) at an average data rate of 6.1 megabits (about three-quarters of a megabyte) each second. MODIS records swath scenes that are 2,330 km wide — an order of magnitude larger than the LANDSAT 7 swath. The wide swath size, in comparison to LANDSAT, enables MODIS to see every point on the earth every two days, or less.

The USGCRP has defined seven research topics based on MODIS data since Terra was initially launched: atmospheric composition, climate variability and change, global carbon cycle, global water cycle, ecosystems, land use / land cover change, and human contributions and responses (US Global Change Research Program, 2007). Riggs et al. (2006) present both an overview of MODIS concepts and specific details pertaining to snow cover sensing. The overview favors Terra over Aqua because of the former satellite's ability to better detect snow in the mid-infrared waved lengths. Some detection bands on Aqua have failed. This study uses data collected by both Terra and Aqua.

2.2.1.3 GOES and POES Satellites

NASA, NOAA, the United Kingdom, and France developed the Geostationary Operational Environmental Satellite (GOES) project and Polar Operational Environmental Satellite (POES) project for weather forecasting among other environmental and social causes (GOES 2008 and POES 2008). While the POES satellite traces a sun-synchronous, thereby viewing different points of the earth at different times, the GOES satellite follows a geostationary orbits. This means that GOES remains above the same point on the earth at all times. Both projects currently launch several satellites each equipped with an Advanced Very High Resolution Radiometer (AVHRR) among other payloads. AVHRR includes a channel (3A) for sensing snow and ice at 1.58 μm to 1.64 μm wavelengths and channels (1, 3B, 4) for sensing cloud coverage among other channels (AVHRR 2008). While AVHRR can produce relatively high resolution images with a pixel size as small as 1.1 km (Robinson 2003), the final IMS product currently produces relatively lower resolution images with a larger pixel size of four kilometers. POES and GOES projects contribute to the oldest record of the northern hemisphere started by NOAA in 1966 when weekly products were created (Matson et al. 1986 and Robinson et al. 1993).

2.2.2 MODIS Snow Measurements

2.2.2.1 Sensing Snow

While clouds, snow, and water all highly reflect light in the visible spectrum, only clouds highly reflect light in the near infrared spectrum; snow and water absorb most near infrared light. Additionally, water reflects infrared light less than snow. The visible spectrum alone, therefore, cannot distinguish between snow, clouds, and water. The infrared spectrum, similarly, cannot solely distinguish between snow-covered areas and snow-free land. AVHRR, EDM+, and MODIS use both the visible spectrum (0.4–0.7 μm) and near infrared spectrum (0.75–5 μm) to discriminate between snow, clouds, and water (Table 2-4). These sensors can only report unknown snow coverage in areas where clouds block the earth. This leaves analysts the job of estimating the uncertainty of the existence of snow in these areas. (Section 2.4.3.1 further discusses missing data in partially-obscured scenes.) Hall et al. (2001) and Riggs et al. (2006) developed a snow mapping algorithm to test each point of the earth detected by MODIS for the presence of snow. The algorithm depends on the visible and near infrared bands of MODIS (Table 2-5) and consists of three Boolean requirements. Each point of the earth that MODIS detects must satisfy all three requirements in order for the algorithm to indicate the presence of snow at that point.

Table 2-4. Relative Visible and Near-Infrared Reflectance of Clouds, Land, and Snow

Coverage	*Relative Reflectance*	
	Visible	*Near Infrared*
Cloud	High	High
Snow	High	Low
Water	High	Very Low
Snow-Free Land	Low	Low

MODIS information from Riggs et al. (2006)

Table 2-5. MODIS Bands Used to Detect the Presence of Snow

Band	*Wavelength (μm)*	*Spectrum*
1	0.645	Visible
2	0.865	Near Infrared
4	0.555	Visible
6	1.640	Near Infrared

MODIS information from Riggs et al. (2006)

The first of the three requirements to detect snow is the calculation of the Normalized Difference Snow Index (NDSI) ratio

$$NDSI = \frac{band4 - band6}{band4 + band6} \geq 0.4\ \mu m \qquad \textbf{2-2}$$

which considers the difference between the visible reflectance on the 0.555 μm wavelength (band 4) less the near infrared reflectance on the 1.640 μm wavelength (band 6), all normalized over the sum of these two reflectance values (Hall et al. 2001 and Riggs et al. 2006). Normalizing the difference between visible and near infrared reflections helps determine the presence of snow in varying light conditions throughout the day.

The second requirement distinguishes water from snow. It checks the a near-infrared signal on the 0.865 wavelength (band 2). A reflectance greater than 0.11 indicates snow. Smaller values indicate water.

$$band2 > 0.11\ \mu m \qquad \textbf{2-3}$$

The third requirement checks that enough visible reflectance on the 0.555 μm wavelength is available to make a reading:

$$band4 > 0.10\ \mu m \qquad \textbf{2-4}$$

This last requirement, in other words, tests to make sure there is enough visible light to make a dependable reading of snow.

The conjunction of all three requirements (equations 2-2, 2-3, and 2-4) form the snow mapping of the MODIS snow and sea ice Algorithm Theoretical Basis Document (ATBD) in practice (Hall et al. 2001):

$$(NDSI \geq 0.4\ \mu m)\ \&\ (band2 > 0.11\ \mu m)\ \&\ (band4 > 0.10\ \mu m) \qquad \textbf{2-5}$$

Expanding 2-5 in terms of bands yields

$$\left(\frac{band4 - band6}{band4 + band6} \geq 0.4\ \mu m\right)\ \&\ (band2 > 0.11\ \mu m)\ \&\ (band4 > 0.10\ \mu m) \qquad \textbf{2-6}$$

The accuracy of the snow mapping algorithm varies with land cover, grain size, and pollution. Hall et al. (2001) explains that

> *. . . exclusive of clouds, the maximum, aggregated Northern Hemisphere snow-mapping error is expected to be about 7.5%. The error is expected to be highest (around 9-10%) when snow covers the boreal forest, roughly between November and April*

and that sensors detect snow best at solar noon. At this time, they are facing nadir — directly at the earth.

2.2.2.2 Snow Products

The Distributed Active Archive Center (DAAC) at the National Snow and Ice Data Center (NSIDC) provides a web-based service for researchers to order MODIS snow and ice data products (NSIDC 2008a). The NSIDC DAAC is one of a eight DAACs in the EOS Distribution System (EOSDIS) sponsored by NASA. NSIDC DAAC labels products according to sensor satellite (either Terra or Aqua) and processing information. The processing information of a product indicates the unit spatiotemporal size (i.q. the amount of compositing) and spatial-format for that product. The sensor abbreviations MOD and MYD represent, respectively, MODIS aboard Terra and MODIS aboard Aqua (NSIDC 2006). Six processing information abbreviations, 10_L2, 10A1, 10A2, 10C1, 10C2, and 10CM, indicate, respectively, 5-minute 500m swaths, 500m sinusoidal grids composited daily, 500m sinusoidal grids composited every eight days, 0.05 degree climate model grids (CMG) composited daily, 0.05 degree CMGs composited every eight days, and 0.05 degree CMGs composited monthly (NSIDC 2008a). Two satellites and six kinds of processing yield a total of 12 products. Of these 12 products, NSIDC refers to the two swath products (MOD10_L2 and MYD10_L2) as Level Two products. NSIDC builds Level Two products from fundamental MODIS reflectance data, MODIS geolocation data, and a cloud mask using the ATBD (Section 2.2.2.1). The remaining, gridded products comprise Level Three, which NSIDC builds from Level Two products.

All products are stored in the EOS-specified hierarchal data format (HDF) called HDF-EOS. This means, in application, that researchers download product files (also called product granules in this context) that have a ".HDF" file extension. The

National Center for Supercomputing Applications (NCSA) funded by the National Science Foundation (NSF) at the University of Illinois oversees continued development of the HDF file format. The HDF-EOS file format stores spatial information in three formats: swath, point, and grid. NSIDC distributes XML side-car files with each HDF-EOS granule that include metadata like database references, contributing products, time references, orbit number, the time the granule was last processed, and whether or not a granule is scheduled to be reprocessed.

NSIDC advances products by reprocessing them based on both current scientific research and NCSA updates to make HDF more manageable. NSIDC assigns a version number, synonymously called a collection number, to each reprocessing initiative. Version five, the current version in the completion stages of being processed, improves on version four by, for example, using a more conservative cloud mask, adding fractional snow information to the MOD10_L2 products and the MOD10A1 products, making products more manageable with new HDF compression techniques, and rendering preview images for each granule. Researchers have, in the past, found errors in data collections. NSIDC, when researchers correctly report processing errors, confirm the errors and temporarily remove access to error-effected data to patch it. NSIDC eventually deletes outdated collections. Table 2-6 lists the characteristics of the Level 2, Collection Four product.

Table 2-6. MODIS Snow and Ice Level Two , Collection Four Product Characteristics

Characteristic	Value
Spatiotemporal Properties	
Pixel Size	$(500\ m)^2$ or $0.25\ km^2$
Nominal Swath Coverage	2,000 km across track
	1,354 km along track
Scan Time	5-minute (1 Scene)
Contributing Products	
Cloud	MOD35_L2
Geolocation	MOD03
Radiance	MOD02HKM
	MOD021KM
Pixel Categories (Snow_Cover SDS)	
Missing Data	0
No Decision	1
Night	11
Snow-Free	25
Lake	37
Ocean	39
Cloud	50
Lake Ice	100
Snow	200
Detector Saturated	254
Fill	255

Data from Riggs et al. (2006), applicable to both MOD10_L2 (Terra) and MYL10_L2 (Aqua) products

Hall et al. (2001) describe the Level Three CMG products composited every eight days and recommends them for most model confirmation experiments (pers. com. 2006) because of their popularity, usability, and the accessibility of data tools built around them. Level Three products are easy to use with the NASA's HDF-EOS to GeoTIFF Conversion Tool (HEG-TOOL) developed by Raytheon Company, scripting libraries included with The MathWorks™ MATLAB® and ITT Visual Information Solutions™ Interactive Data Language® (IDL).

Hall acknowledges that the Level Three eight-day composite period is an arbitrary period in many applications (pers. com. 2006). The Level Three CMGs, also, "do not simulate the present Arctic climate very well" (Hall 2001 summarizing

Bromwich et al. 1994). The compositing process that NSIDC uses to create Level Three products, finally, marks pixels snow-covered if the snow mapping algorithm (Equation 2-6) is satisfied for at least one pixel among all location-coincident pixels in a composite period (Hall 2001). This means that the composite process maps a pixel as snow-covered even if only one location-coincident pixel within the composite period satisfies the snow requirements (Equation 2-6). Level Three temporal composites, therefore, are inadequate to confirm model results where model periods are close to or shorter than the eight-day measurement composite periods.

2.2.2.3 Quality Assurance

NSIDC (2006) explains that Collection Four, Level Two products include a layer called "Snow Cover PixelQA" that reports an eight-bit quality assurance report[‡] for each point recorded by the MODIS sensor in the swath. Bits zero and one represent the general quality of the product. The first two bits, bit zero and bit one read right to left, with values of [0,0] indicate nominal, usable quality. Values [0,1] (i.e. bit zero equals one and bit one equals zero) indicate abnormal quality. Values [1,0] indicate clouds, and values [1,1] indicate invalid data.

[‡] Various websites and literature use the word "quality assurance" and the word "quality assessment" interchangeably. This thesis uses the word "quality assurance." Further, a quality assurance report describes a mult-point layer of — or multi-pixel layer of — quality assurance eight-bit values in the context of swaths and grids, whereas a quality assurance value describes a single, eight-bit value in the context of a single coordinate or a single pixel.

Abnormal quality, cloudy, and invalid reports, indicate respective locations were sensed both out of an acceptable 150 degree to 210 degree range and with an observation coverage area limited to 20% of the potential coverage area (NSIDC 2006). The NSIDC does not further differentiate between these three quality assurance labels — abnormal quality, cloudy, and invalid — beyond the physical meaning inherent in the word "cloudy." (Data analyzed later in this thesis, however, infer that MODIS reports invalid locations throughout the day and night but reports abnormal locations predominantly during the daylight.)

Bits two through seven detail supporting quality information. Bit three flags measurements taken with broken ("dead") detector bands. Bit four flags measurements taken at sensor view angles greater than 45 degrees. Bit five flags measurements derived from "highly uncertain" band 6 radiance calculations. Bit six flags results given an undetermined cloud mask. Bit seven flags unusable sub-calculations. Bit eight is unused.

All other Collection Four (non Level Two) snow coverage products include a unique "Spatial QA" index, which is derived from the Level Two "Snow Cover PixelQA" and reported in four bits of eight bits. The first two bits report the same general quality information reported in the first two bits of the Level Two products. Bit three indicates a sensor azimuth angle between 150 degrees and 210 degrees. Bit four indicates an observation coverage of more than 20% of the are covered by the product. Bits five through eight are unused.

2.2.2.4 Swath To Grid Conversion Tools

Many software tools exist to interpret and project MODIS snow data for mapping and comparison purposes. Most of these tools, however, read grid data only. Few tools read and project data originally in the swath format, and of these tools, even fewer work with the MOD10_L2 product. This section extends the literature review to a software review of three swath to grid conversion tools:

1. MODIS Swath To Grid Toolbox (MS2GT)

   NSIDC distributes a combination of C programs, IDL scripts, and Perl scripts called in a package called MODIS Swath To Grid Toolbox (MS2GT). NSIDC make MS2GT specifically for converting swaths to grids (NSIDC 2003). MS2GT requirements, however, exceed the accessible resources of this research: comprehensive access to a UNIX platform with IDL and Level 1 MODIS data. NSIDC has only tested MS2GT on a SGI O2 workstation (NSIDC 2003).

2. HDF-EOS to GeoTIFF Conversion Tool (HEG-TOOL)

   HDF-EOS to GeoTIFF Conversion Tool (HEG-TOOL) converts most swath files into grids. HEG-TOOL converts and composites HDF-EOS products of all levels from all eight DAACs. The general tool works especially well compositing several Level Three granules (like MOD10C1) into a mosaic. The conversion tool, however, works only intermittently with the Level Two data. It seems to fail, although this study has not confirmed this, when converting swath granules with a large amount of no-data within bounds of an

interest area. In a batch conversion processes, implemented using HEG-TOOL's scripting interface, HEG-TOOL often halts mid-conversion.

3. MODIS Reprojection Tool for Swath Data (MRT Swath)

   The Land Process DAAC (LP DAAC) created the MODIS Reprojection Tool (MRT) for Swath Data (MRT Swath). The LP DAAC created the tool especially for LP data. MRT Swath incorporates Delaunay triangulation to map swath points to cells. MRT Swath, in an attempt to automate the conversion process of MOD_10L2 and MYD10L2 products with batch scripts, failed in situations similar to those that failed with HEG-TOOL. MRT Swath often halts mid-conversion. Neither HEG-TOOL or MRT Swath created files that were completely compatible with the projection descriptions used by ArcGIS Desktop.

2.3 DISTRIBUTED MODELS

> *"No real advance will be made if we continue to force lumped models based on empirical relationships to represent the complexity of distributed runoff."*
> *—Vieux (2004)*

Hydrologists have long relied on model concepts based on empirical observations, such as the unit hydrograph, and parameters that lump spatiotemporal-varying watershed characteristics into single values. The Natural Resources Conservation Service (NRCS) approach for estimating rainfall runoff and channel routing (Mokus 1972) exemplifies a lumped-parameter model. Soil group, impervious area, land cover, hydrologic condition, and land use are all lumped into the single NRCS curve

number. A watershed-averaged storage parameter is another example of a lumped parameter. Lumped conceptual models, in general, are called “grey-box” (Abbot et al. 1996) models because they are not based on purely black-box empirical relationships yet they do not fully account for sub-watershed processes in what Abbot et al. (1996) calls “white box” models.

Lumping concepts based on empirical observations of one type of watershed (e.g. a relatively large watershed) into a particular parameter can lead to problems if that parameter is used to predict runoff in a different type of watershed (e.g. a relatively small watershed). Further, a conceptual model or model parameter developed for one application could be used in another application for the wrong physical basis. As lumped-parameter models are scaled to meet the needs of different applications, the number of calibration parameters can grow and the inter-correlation between calibration parameters can increase. Modelers, to compensate for these problems, package application-specific calibration parameters alongside matching, application-specific run-time processes.

Remotely sensed measurements can uncover sub-watershed discrepancies between observations and lumped simulations. Such measurements drive the need to aggregate conceptual process models over smaller areas and smaller time intervals. Models that account for sub-watershed processes are called distributed models. The level to which a model is distributed is subjective and discussed further in relation to map comparison in Section 2.4.1. “The Saint Venant equations for overland and channel flow, Richards’ equations for unsaturated zone flow and Boussinesq’s

equation for groundwater flow" are examples of partial differential equations used in distributed modeling (Abbot et al. 1996).

The traditional comparison between empirical (black box), lumped-conceptual (grey box), and distributed physically-based (white box) models can be misleading. The common use of the words "physically-based" in combination with the word "distributed" supports the fact that distributed models enable the detailed simulation of physical processes and produce maps that are comparable to remotely-sensed measurements. The words "physically-based," however, are not exclusive of lumped conceptual models. Most models and model parameters have a physical basis, including lumped-parameters like the NRCS curve number. For the reason in these two points, the words "differential-equation-based" well-replace the words "physically-based" in the comparison of such white models with black, empirical ones.

The vintage of the programming techniques employed by a model does not determine if it is more lumped or more distributed. To efficiently create application-specific modules for time-tested lumped programs, programmers compartmentalize legacy procedural code into object-oriented classes. These classes can be used in combination with distributed process models when, for example, distributed calibration data is unavailable. Using a combination of lumped concepts and distributed concepts can, ideally, result in smaller errors of prediction with modest gains in model complexity. These models are called semi-distributed models. TOPMODEL, which stands for Topographic Model, exemplifies semi-distributed models (Vieux 2004 and Bevin 1998a). Hydrological Simulation Program--Fortran

(HSPF) is another model that incorporates "theory, laboratory experiments, and empirical relations from instrumented watersheds" (USGS 2008) with distributed modules. Critics of semi-distributed models like HSPF point out that there is a danger in significantly increasing model complexity to a point where there are minimal returns in increased model accuracy.

The process of creating distributed models has recently become more practical as a result of accessibility to geospatial products, desktop GIS, and cheap computer processing. Distributed models are now advancing the state of the art. Abbot et al. (1996) contend that models distributed in space and time "nearly always" limit uncertainty in comparison to lumped-parameter models. Abbot et al. (1996) cite this advantage of distributed models over lumped-parameter models in water resources applications for irrigation, erosion and land restoration, surface and ground water pollution remediation, flood and drought control, maintenance of aquatic ecosystems, and climate change assessment. "In mountainous terrain, topographically induced spatial variability makes distributed snowmelt models [especially] attractive" (Colee 2000).

2.3.1 TOPLATS

Snowmelt simulations analyzed in this study were produced by a model of the UKRW, built using TOPMODEL-Based Land-Atmosphere Transfer Scheme (TOPLATS). This study used TOPLATS because it was already implemented in the UKRW (Déry et al. 2004) and the input files were available from the USDA Agriculture Research Service (ARS) at the Hydrology and Remote Sensing Lab.

TOPLATS applies TOPMODEL surface water processes (Famiglietti and Wood 1994a,b) on a cell-by-cell basis. The model incorporates a soil–vegetation–atmosphere transfer (SVAT) scheme to simulate near-surface soil column energy balances (Peters-Lidard et al. 1997) and models physical representations of moss, snow, soil, and forest. The snow module divides snowpack into a thin surface layer and a thick subsurface layer. The surface snow layer interacts with the atmosphere and the subsurface snow layer exchanges heat with the soil. The forest module discriminates between an understory and an overstory.

Déry et al. (2004) add two "key topographic effects" to TOPLATS in order to "capture some of the small-scale physical processes" that effect snowmelt: the effect of elevation on air temperature and the effect of slope on radiation. They also review the effect of an adiabatic lapse rate on the ambient air temperature with elevation. For the effect of elevation on air temperature, they report that a difference of 5.58 °C persists between the highest point (1490 m above sea level) and lowest point (570 m above sea level) of the watershed throughout each model run. For the effect of slope on radiation, TOPLATS calculates the position of the sun using the method developed by Gates (1980) combined with DEM data.

TOPLATS prediction results consist of a time series of maps separated by regular time intervals. Déry et al. (2004) use a 10 minute time interval and maps projected in UTM Zone 6 grid with a 131.34 m cell size. Initial conditions include the beginning of season SWE (mm of water). Input variables include precipitation (mm), relative humidity (%), temperature (°C), incoming solar radiation (W/m^2), wind speed (m/s), air pressure (mbar). Model parameters include the UKRW DEM (m) and snow

albedo (a dimensionless ratio of reflected to incident solar radiation). Of all TOPLATS parameters, Déry et al. (2004) conclude that DEM and the adiabatic lapse rate of 6 °C / km^2 drive model results.

Déry et al. (2004) review the possibility of confirming model results in the UKRW with MODIS measurements. They conclude that although MODIS measurements could be reviewed, MODIS measurements "do not provide the location covered by snow within a single grid cell, nor the SWE contained in the snow cover" and "the persistence of low-level clouds in the Arctic during spring may also compromise its applicability." While the last two points — that MODIS does not measure SWE and that clouds can block the near infrared radiation that MODIS senses — are problems, the first point — that measurements are not provided in grid cells can be overcome by either interpolating swath measurements into grid values or interpolating model predictions into a sinusoidal projection. (In this thesis, the former is complete as described in Chapter Three.)

2.4 MAP COMPARISON

2.4.1 Background

Analysts evaluate the performance capabilities of spatiotemporal models by comparing model-created maps with measurements. Performance capabilities include simulation accuracy and predication capability. Maps consist of point, line, polygon, and pixel features, which delineate spaces into categories (e.g. snow, ice, snow-free) or continuous values (e.g. elevation) space. Maps with points (e.g. well locations) and maps with lines (e.g. topographic contours) that are relatively close together, and

maps with polygons (e.g. land use) and maps with pixels (e.g. snow cover) that are relatively small, best describe physical processes that span relatively small areas and take place in relatively small interest areas. Analysts call such maps with high spatial resolution "highly spatially distributed." Changes in features or states in these maps are illustrated by a series maps representing different times. The time difference between scenes indicates, likewise, the relative degree of temporal distribution in a map. For composite map scenes, each created from several sequential scenes in time, the time interval(s) encompassing the sequences define the relative degree of temporal resolution. The granularity[§] of measurements available in an interest area help modelers limit the physical processes that they choose to simulate when formulating a model. The increasing resolution of newer model results, in return, defines needs for developing sensors that capture images with higher resolutions for purposes of calibration and validation.

Error statistics indicate confidence in observed data. The most relevant error statistics for a data product are often distributed within that data product as complementary series of maps. The MODIS L2 Collection Five product, for example, includes quality assurance estimates for every coordinate measured in each swath scene. Sometimes analysts need to derive error information from data that is not necessarily included in a product. For example, supplementary meteorological

---

[§] Analysts often use the word granularity, which means increasing spatial resolution, in context with spatiotemporal data.

measurements, elevation measurements, and detection band information can be used to infer error in MODIS measurements. The error statistics derived from supplementary sources like these are not necessarily reported in the same measurement system or coordinate systems as the measurements themselves. For instance, if there is a high correlation between a land-use feature and errors, that pattern may be presented spatially as a polygon which masks many pixels. In this case, error is spatially-lumped. Error may be lumped temporally as well. The continuous volatility of the stock market, for example, may be lumped into individual variances that represent periods of time between abrupt events like interest rate cuts. An analogous example in hydrology is the lumping of error in a rainfall-runoff model into two periods, before channelization and after channelization.

The simplest process for comparing a modeled map with a measured map is to lay them side by side and visually assess similarities and differences. When a time series of maps need to be compared, the two series can be laid out side-by-side in chronological order. The comparison is easiest when the measured and modeled maps have a one-to-one relationship. Models, therefore, should ideally be set up to simulate conditions corresponding to the times the data in the measured maps were collected. Additionally, all maps should be presented in the same spatial resolution and coordinate system. Graphical software like GIS make this process of side-by-side comparison simple to execute. As the number of scenes increases, , however, visual comparison becomes increasingly onerous. The comparison problem provokes the need to find goodness-of-fit statistics that quantitatively capture the similarities or differences that visual inspection reveals. In addition, if map comparisons are to be

used for model evaluation or calibration, these statistics need to quantify the degree of agreement between modeled and observed maps.

2.4.2 Spatial Comparison

Analysts need objective measures of agreement if they want to use distributed, measured maps to evaluate the performance of distributed, modeled maps. They cannot rely on subjective visual comparisons between measurement images and model output. This section describes theoretical tools that have been developed for map spatial map comparison.

Calculating the change of a criterion that is spatially-lumped over an entire interest area accounts for the independence of each scene with respect to time, but ignores spatial processes within the interest area. For example, a comparison between the observed and modeled decline of snow covered area as a percentage of watershed area during a melt season could indicate a good agreement in the overall decline of snow. This comparison, however, does not confirm the correctness of — or reveal the absence of needed — sub-watershed processes in the model. (The effect of local elevation on the distribution of snow is an example of one of these sub-watershed processes.) Researchers using such a comparison exclusively could calibrate a model to correctly predict the change in a spatially-lumped coverage for the wrong physical reasons. Confirming model predictions of the decline of fuel in a wildfire is another example in which a agreement for a spatially-lumped statistic could lead to the oversight of small-scale, model failures.

2.4.2.1 Cohen's Kappa Statistic

Cohen's Kappa goodness-of-fit statistic, K (Cohen 1960 and, for a more abstract case, Fleiss 1971), provide insight into spatial agreement of feature-scale (e.g. pixel-scale or point-scale) physical processes without tediously comparing model maps and measured maps side by side. The statistic "gives a quick indication of the level of agreement between two maps." It is, more explicitly, "an indication of goodness-of-fit in comparison to a random situation" in which the pixels from each of the two maps being compared are relocated at random (Hagen 2002).

Cohen (1960) popularized the Kappa statistic to measure the agreement between two judges, categorizing single items in a series of trials. In this case, each judge must place each item in each respective trial into one and only one of several categories. Fleiss (1971) extended the comparison to include multiple judges. "Smeeton (1985) traces [Kappa's] history to Galton (1892)" (Pontius 2000). Two *maps* of a categorical variable in a spatial comparison are analogous to two *judges* considered by Cohen's Kappa. Location-coincident *pixels* in the two maps are analogous to individual *trials* being categorized by the two judges.

Kappa varies from negative infinity to one. Negative values of Kappa and Kappa equal to zero both indicate no agreement between two maps beyond what would be expected in the random relocation situation. Increasing, positive values of Kappa indicate increasing agreement between two maps. A positive value of Kappa close to zero indicates almost no agreement between two maps. A positive value of Kappa close to one indicates a strong agreement between two maps. Landis and Koch (1977) call negative values of Kappa "poor," and values from zero to one, in 0.2

intervals: “slight” (0 to 0.20), “fair” (0.21 to 0.40), “moderate” (0.41 to 0.60), “substantial” (0.61 to 0.80), and “almost perfect” (0.81 to 1). They call these labels “arbitrary” but “useful benchmarks.” Sim and Write (2005), in response to this scale, note that Kappa decreases with increasing categories because an increase in categories decreases the chance of agreement between two maps in the random relocation situation.

For the simple comparison of two raster maps I and II with pixels exclusively in any number of categories, Cohen’s Kappa statistic answers the following question: How well does the agreement between map I and map II compare to the agreement between theoretical maps, III and IV; where, the probability that location-coincident pixels in III and IV assume the same category equals the product of the following two fractions: (a) the fraction of that category in map I and (b) the fraction of that category in map II? The remainder of this section further details the calculation of Kappa and discusses complementary statistics Kno, Klocation, Kquantity all explained by Pontius (2000) and Khisto derived by Hagen (2002).

The first step in making a quantitative comparison between a model map and a measured map, which is also the first step in calculating Kappa, is to calculate the proportion of agreement, *PA*, between the two maps.

$$PA = \frac{area\ in\ agreement}{total\ area} = \frac{number\ of\ pixels\ in\ agreement}{total\ number\ of\ pixels} \qquad \textbf{2-7}$$

For example, two square maps, each with four-pixels and two-categories (snow or snow-free) that both have their two left-side pixels marked as snow and their two right-side pixels marked as snow-free have perfect agreement. In this example, there are no errors of commission (a false-positive detection of snow) and there are no

errors of omission (a false-negative missing detection of snow). In the case that the two left pixels of the measured map are observed to be snow-covered, and the model map shows the top two pixels as covered with snow, there is a 50% agreement: There is an error of commission in the upper right cell, there is an error of omission in the lower left cell, leaving two cells out of four (50% of the map) in agreement.

Calculating the proportion of agreement between two maps shows how well two maps agree on a pixel-by-pixel basis. Success, however, is measured with the assumption that there are the same number of pixels, *for* each category, between each of the two maps being compared. (This is not to say each category has the same number of pixels as every other category.) If there are an unequal number of pixels of a particular category between maps, there can never be 100% agreement. This study calls this issue the "unequal category count limitation" of the *PA* comparison.

The Kappa goodness of fit statistic addresses the "unequal category count limitation" of the simple *PA* calculation by comparing *PA,* for two given maps, with the proportion of expected agreement between those two maps when the cells in those two maps are rearranged.

$$K = \frac{PA - PE}{1 - PE} \qquad \textbf{2-8}$$

where, given two maps used to calculate *PA*, *PE* is the proportion of expected agreement between those two maps with a random rearrangement of cells.

The calculation of *PA* and *PE* with a confusion matrix, which tabulates the probabilities of the joint distribution of all combinations of discrete categories in the measured map and the modeled map, explains the two statistics further. The sum of all the proportions in the confusion matrix, because they are analogous to the

probabilities in a joint distribution, equal one. Figure 2-9 shows the confusion matrix (boxed) for the abstract case with n categories. The row header cells and the column header cells contain category labels C_1, C_2, …, C_n. The rows correspond to map one and the columns correspond to map two. The proportion of cells of C_i in map one with coincident cells of C_j in map two, p_{ij}, appear in the cell at row *i* and column *j*. For example, the proportion of category-three cells in map one with coincident category-four cells in map two would be expressed as p_{34} and appear in row three and column four of the confusion matrix. The matrix diagonal contains proportions of cells in which map categories agree. The matrix trace, therefore, equals the total proportion of agreement, *PA*, between the two maps:

$$PA = tr(confusion\ matrix) = \sum_{k=1}^{n} p_{kk} \qquad \textbf{2-9}$$

In the calculation of *PE*, the sum of proportions in each row *i* of the confusion matrix equals the proportion of category *i* cells in map one. These totals are expressed in an *n*-by-one column to the right of the confusion matrix.

$$\vec{\mathbf{p}}_{i*} = \begin{bmatrix} p_{1*} \\ p_{2*} \\ \vdots \\ p_{n*} \end{bmatrix} \qquad \textbf{2-10}$$

in which p_{i*}, for any category *i* where *i* = 1 . . . *n*, equals the proportion of cells containing category *i* in map one:

$$p_{i*} = \sum_{k=1}^{n} p_{ik} = sum([p_{i1} \quad p_{i2} \quad \cdots \quad p_{in}]) \qquad \textbf{2-11}$$

The proportion of category *j* cells in map two are similarly expressed in a one-by-*n* row below the confusion matrix. Map two proportion totals are expressed as

$$\vec{\mathbf{p}}_{*j} = [p_{*1} \quad p_{*2} \quad \cdots \quad p_{*n}] \tag{2-12}$$

in which p_{*j}, for any category j where $j = 1 \ldots n$, equals the proportion of cells containing category j in map two:

$$p_{*j} = \sum_{k=1}^{n} p_{kj} = sum\left(\begin{bmatrix} p_{1j} \\ p_{2j} \\ \vdots \\ p_{nj} \end{bmatrix}\right) \tag{2-13}$$

These total proportion vectors $\vec{\mathbf{p}}_{*j}$ and $\vec{\mathbf{p}}_{i*}$ (Equations 2-10 and 2-12) are the marginal probabilities of a joint distribution. The product of the total proportion vectors, $\vec{\mathbf{p}}_{*j}$ and $\vec{\mathbf{p}}_{i*}$, equal *PE*:

$$PE = \vec{\mathbf{p}}_{*j}\ \vec{\mathbf{p}}_{i*} = [p_{*1} \quad p_{*2} \quad \cdots \quad p_{*n}] \begin{bmatrix} p_{1*} \\ p_{2*} \\ \vdots \\ p_{n*} \end{bmatrix} \tag{2-14}$$

where, each independent k component product

$$p_{kj} \cdot p_{ik} \tag{2-15}$$

for $k = 1, 2, \ldots, n$, represents the probability of agreement for category k in every combination of cell pairs between — or, for random relocation of cells in — map one and map two. *PE*, thus, depends on the quantity of cells in each category in each map; *PE* does not depend on the location of cells within either map.

Comparing two four-pixel maps with two categories C_1 and C_2, for instance, if each map contains three C_1 pixels and one C_2 pixel, there are nine pairs of pixels in which both pixels are in category C_1 and there is one pair of pixels in which both pixels are in category C_2 out of sixteen possible pairs in a random situation. *PE* in this instance equals 9/16 (for C_1) + 1/16 (for C_2) = 10/16 = 0.625. Replacing a C_1 pixel

from map two with a C_2 pixel doubles the probability of C_2 pairs to 2/16 in the calculation of *PE*, but lowers the probability of C_1 pairs from 9/16 to 6/16 and lowers the overall *PE* to 2/16 (for C_2) + 6/16 (for C_1) = 8/16 = 0.5.

		Map Two Categories				
		C_1	C_2	...	C_n	Map One Totals, $\vec{\mathbf{p}}_{i*}$
Map One Categories	C_1	p_{11}	p_{12}	...	p_{1n}	p_{1*}
	C_2	p_{21}	p_{22}	...	p_{2n}	p_{2*}
	⋮	⋮	⋮	⋱	⋮	⋮
	C_n	p_{n1}	p_{n2}	...	p_{nn}	p_{n*}
Map Two Totals, $\vec{\mathbf{p}}_{*j}$		p_{*1}	p_{*2}	...	p_{*n}	1

Figure 2-9. Generic Confusion Matrix.
The generic confusion matrix (boxed) can be used to calculate *PA* and *PE* for the abstract case in which there are an unlimited number of categories in the maps being compared. PA equals the trace of the matrix. *PE* equals the product of the total vectors: $\boldsymbol{PE} = \vec{\mathbf{p}}_{*j}\,\vec{\mathbf{p}}_{i*}$.

		Measured Map Categories (true state)		
		Snow-Free	Snow	Modeled Map Totals, $\vec{\mathbf{p}}_{i*}$
Modeled Map Categories	H_0: Snow-Free	Agreement of Snow-Free Area	Type II Error of Omission (False Negative or Miss)	Proportion Snow-Free in Modeled Map
	H_A: Snow	Type I Error of Commission (False Positive)	Agreement of SCA (Hit)	Proportion Snow in Modeled Map
Measured Map Totals, $\vec{\mathbf{p}}_{*j}$		Proportion Snow-Free in Measured Map	Proportion Snow in Measured Map	1

Figure 2-10. Two-Category Confusion Matrix.
The two-category confusion matrix (boxed) shows four possible coincident-cell outcomes. In this example, H_0 equals the null hypothesis that indicates the model predicts that a cell is snow-free. H_A is the alternative hypothesis that indicates that the model predicts that a cell is snow covered.

2.4.2.2 Cohen's Kappa Statistic for Two Categories

Figure 2-10 simplifies the generic confusion matrix used in Cohen's calculation of Kappa for multiple categories (Figure 2-9) into a confusion matrix limited to two categories, snow-free and snow, used in this thesis. Figure 2-10 shows that the calculation of Kappa in this thesis can be thought of as *n* hypothesis tests, where *n* equals the number of cells in two maps being compared. This study calls each of these hypothesis tests a pixel test to distinguish them from the overall evaluation of agreement between two maps expressed by Kappa. In each pixel test, the null hypothesis indicates the absence of snow (snow-free) and the alternative hypothesis indicates the detection of snow:

$$H_0: \text{Snow Free} \quad \textbf{2-16}$$

$$H_A: \text{Snow} \quad \textbf{2-17}$$

This study calls the situation in which the model falsely indicates that snow is present in a pixel test a Type I error of commission. In other situations, Type I errors have been called α errors, false alarms, false positives, and producer's risk. This study calls the situation in which the model falsely indicates that snow is absent in a pixel test a Type II error of omission. Type II errors have been called β errors, non-detects or misses, false negatives, and consumer's risk.

The terms "producer risk" and "consumer risk," are only meaningful if the alternative hypothesis is undesirable (e.g. a polluted water sample or a defective product). A producer, in the case that an alternative hypothesis is undesirable, could incur unnecessary expenses (e.g. extraneously increase quality control in an acceptable system) due to a producer risk. A consumer, in the case that an alternative

hypothesis is undesirable, could suffer worse, unexpected ill-effects (e.g. sickness) due to a consumer risk. In this thesis both Type I and Type II errors are equally undesirable. False detection of snow is simply different, not worse, than a non detection of snow. This study, therefore, avoids the terms "producer risk" and "consumer risk." The calculation of Kappa, further, lumps both types of errors into *PE* (2-10, 2-12, and 2-14). Isolating Type I and Type II two errors could, however, reveal a systematic bias in the model.

2.4.2.3 Kappa Variants

This study cannot solely rely on Kappa to compare two maps. Cohen (1960) and Pontius (2000) warn that Kappa is best used only when the two judgments of a trail are independently made. Kappa, for example, appropriately explains a test of agreement between two biologists individually categorizing species of a random samples of nematodes, each isolated in separate Petri dishes. In this example, there is no known correlation between samples to the judges; judgments on a single sample are made separately from each other. In the general case of comparing model and measurement maps, in contrast, pixels are spatially correlated and therefore they are not independent. Pixels on a map, for example, are often dependent on spatial patterns like elevation. Researchers using Kappa to compare maps, therefore, should complement Kappa with additional information about model dependency, and model ability to predict, both the quantity of pixels in each category and the location of pixels.

Pontius (2000) generalizes Cohen's the calculation of Kappa (2-8) into,

$$K = \frac{PA - PE}{1 - PE} \xrightarrow{generalization} K = \frac{PA - PC}{PP - PC} \quad \textbf{2-18}$$

where *PC* (analogous to *PE* in Cohen's Kappa) equals the expected proportion of correctly categorized coincident cells made by a model, and *PP* (analogous to unity in Cohen's Kappa) equals the expected proportion of correctly categorized cells when the model is perfect. This generalization provides the foundation to develop Kappa variants that account for situations in which models choose categories based on

1. No
2. Medium
3. Perfect

ability to specify

1. The quantity or pixels in each category
2. The location of individual pixels

2.4.2.3.1 Kno

Models with "no ability" (Pontius 2000) to select either the quantity of pixels in each category or the location of individual pixels have a chance of 1/*n* to correctly predict a category at a specific pixel. Kappa for no ability, Kno (Pontius 2000) — also called κ_{nor} by Lantz & Nebenzahl in (1996), PABAK by Byrt et al. (1993), and random coefficient (RC) by Maxwell (1997) — exchanges *PC* in the generalized calculation of Kappa (2-18) with this chance that a model pixel could have the correct category at random, 1/*n*,

$$\text{Kno} = \frac{PA - \frac{1}{n}}{1 - \frac{1}{n}} \quad \textbf{2-19}$$

where, n is the number of categories. Hagen (2002) appropriately calls 1/*n* in this case the probability of agreement expected by the model due to the random selection of a category by the model, $P(E)_{RC}$.

Pontius (2000) contends that Kno improves Kappa because it considers the quantity of cells that could agree in a *completely* random situation. Figure 2-11 illustrates this point with a nine-pixel comparison in which snow rests in exactly one cell in each map. The strong agreement of snow-free pixels in this Figure 2-11 produces a relatively high *PE*=0.8025 (2-8), but yields a misleading negative Kappa of -0.1250. Kno, comparatively, only considers the number of categories, 1/*n* = 0.5000, yielding a rationally-positive Kno value of 0.7500.

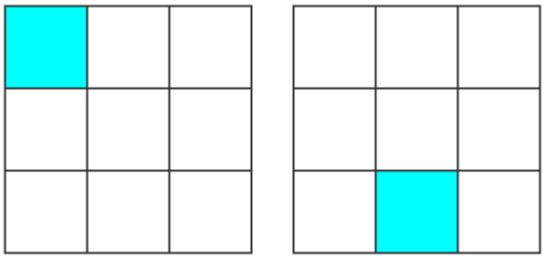

Figure 2-11. Kno and Kappa comparison. (Kno = 0.7500) > (K = -0.8025)

Kno could be useful in the case that one pair of maps in a series may have two categories and another pair of maps in the same series might have three. All maps reviewed by Hagen in 2002 and most maps in this study, however, do not have varying categories. The pertinence of Kno in these cases, therefore, diminishes to

$$\text{Kno} = \frac{n\,PA - 1}{n - 1} = \frac{n}{n - 1} PA - \frac{1}{n - 1} \quad \textbf{2-20}$$

which has a linear dependency on the probability of agreement, *PA*, despite the subjectively more-rational positive and negative values. This dependency diminishes the need to use Kno in an analysis where *PA* is already being used.

2.4.2.3.2 Klocation and Khisto

Both Kappa and Kno "fail to distinguish . . . between quantification error and location error" (Pontius 2000). Poor (low and negative) values of Kappa and Kno, in other words, do not explain whether a model has poorly predicted the quantity of pixels in each category or whether a model has placed the correct quantity of pixels in the wrong locations.

Klocation, introduced by Pontius (2000) attempts to correct Kappa and Kno by substituting *PP* in the generalized calculation of Kappa (Equation 2-18) with the maximum success rate of agreement that a model could achieve in the situation in which the number of pixels in each category predicted by that model does not change.

$$\text{Klocation} = \frac{PA - PE}{P_{max} - PE} \quad \textbf{2-21}$$

where

$$P_{max} = \sum_{k=1}^{n} \min(p_{k*}, p_{*k}) \quad \textbf{2-22}$$

Think of the calculation of P_{max} (2-22) in comparison to the calculation of *PE* (2-14). In the calculation of *PE*, the *product* the two map proportions for each category are summed. In the calculation of P_{max}, alternatively, the *minima* of the two proportions (one for each map) are summed. P_{max}, therefore is less than one except in

the perfect-quantity case in which the proportion of pixels in each category are equal between maps.

Klocation reports a lower agreement in comparison to the Kappa value when a cell of one category is displaced. Klocation, however, fails to consider the distance of a displaced cell. For example, in a mountain scene where it is known that snow is present on the mountain tops, but not in the valleys, a comparison between actual and simulated maps is made. In this example, Klocation will report identical values no matter if a pixel falsely reporting snow coverage is found either on a peak or in a valley. Despite this fallacy, Klocation is still valuable. It replaces the ideal 100% agreement used for *PP* (2-18) in standard Kappa calculation (2-8) with a realistic calculation for the maximum possible agreement, P_{max} .

Kquantity, also introduced by Pontius (2000) attempts to correct Kappa errors resulting from differences in the quantity of cells for each category between two different maps. It is "the success due to the simulation's ability to specify quantity divided by the maximum possible success due to a simulation's ability to specify quantity perfectly." Hagen (2002) renounces the statistic as "incomprehensible" and reports, with personal agreement from the Pontius, that the statistic is unstable. "Minor changes in the maps can lead to major change in the statistic" in cases where the denominator of the calculation is close to zero.

Hagen introduces an alternative to Kquantity, named Khisto, which is used in this study. It is called Khisto because it can be calculated from the histograms of two maps.

$$\text{Khisto} = \frac{P_{max} - PE}{1 - PE} \quad \textbf{2-23}$$

The product of Khisto and Klocation equals Kappa:

$$\text{Khisto} \cdot \text{Klocation} = \left(\frac{P_{max} - PE}{1 - PE}\right)\left(\frac{PA - PE}{P_{max} - PE}\right) = \frac{PA - PE}{1 - PE} = \text{K} \quad \textbf{2-24}$$

2.4.3 Temporal Comparison

2.4.3.1 Missing Data in Partially Obscured Scenes

Scalar statistics like %SCA or basin average SWE summarize spatially-distributed properties of a map scene for a point in time. Measuring model performance by comparing modeled and measured summary statistics over a period of time (e.g. comparing two SCA depletion curves) presents the problem of accounting for uncertainty in partially obscured measured scenes. While models predict complete results and complementary summary statistics, sensors yield incomplete measurements. Satellite orbit limitations (Table 2-3), for example, limit both the resolution and the frequency of scenes that a sensor can measure. Smoke that obscures the video camera mentioned in the previous wildfire example (described 2.4.2.1), or clouds that block a remote sensing instrument, as shown in this study, leave measured maps spatially incomplete. Smoke and clouds are only two possible physical causes of why a sensor could tag a spatial feature with a no-data label.

To compensate for missing data in measurement summary statistics, due to partially obscured scenes or other sensor problems, one could report a likely value based on either surrounding areas, surrounding scenes, or other spatiotemporal trends.

(The decrease of soil moisture over time in a watershed illustrates a spatiotemporal trend.) Making educated guesses like these, based on physical relationships and past observations, creates complete, usable products. Making these guesses in measurements, however, defeats the theoretical basis of comparing observed and modeled data; a "simulated measurement" is an oxymoron. Creating an artificial measurement, based on the same physical theories used in a model that the measurement is being compared to, can lead to artificially increased goodness-of-fit statistics. This problem reveals the need to calculate the uncertainty of a summary statistic for individual measured scenes, not based on external factors, but based on data from within the scene itself.

Many remotely sensed measurements, including many MODIS products (0), actually *are* composited over time to fill in the gaps of the missing data from clouds. NSIDC, for example, composites sea and snow ice data over time in the MODIS Level Three products (Section 2.2.2.2). NSIDC reports time intervals with Level Three composites — not only the mean points in time — so that analysts understand the implications of comparing model results to composite measurements. When composite time intervals are large compared to the time for physical processes to occur (like snow blown overnight by wind), those physical processes that occur out of sensing range (e.g. behind clouds), are missed. In the case of quick winter-spring snowmelt (0), which occurs in a matter of days in the Upper Kuparuk, Level Three MODIS data hides too much information from analysts to make reasonable judgments about physical processes in models.

2.4.3.2 Using Probability to Express Measurement Uncertainty

Brubaker et al. (2005) present a solution for comparing MODIS SCA measurements and IMS SCA estimates to surface station snow/snow-free reports across the continental United States while accounting for no-data fields. They develop a single triangle-shaped probability density function (PDF) of %SCA for each remotely-sensed map in a time series. Each PDF relies on the quantity of categorical data, including missing data, exclusively from within its respective scene. They plot the PDFs on a probability density (ordinate) versus %SCA (abscissa) axis.

Brubaker et al. (2005) use snow cover information in cloud-free areas of each scene to estimate a possible range of snow cover for the entire scene. They assume that the most likely value of %SCA in a scene is proportional to the fraction of the cloud-free part of the scene which is snow-covered.

$$\%\mathrm{SCA}_{likely} = \frac{\%\mathrm{SCA}_{cloud\ free}}{100\% - \%\mathrm{CCA}} \qquad \textbf{2-25}$$

In equation 2-25, all percentages are relative to the entire scene: $\%\mathrm{SCA}_{likely}$ is the likely estimate of %SCA relative to the entire scene, $\%\mathrm{SCA}_{cloud\text{-}free}$ is the cloud-free %SCA relative to the entire scene, %CCA is the percentage of cloud-covered area relative to the entire scene, and 100% – CCA% equals the percentage of cloud-free area relative to the entire scene.

The mathematically minimum possible %SCA equals $\%\mathrm{SCA}_{cloud\text{-}free}$. In this hypothetical case, snow-free land lies under the cloud-covered area. The mathematically maximum possible %SCA equals $\%\mathrm{SCA}_{cloud\text{-}free}$ plus %CCA. In this

opposite case, snow completely blankets the land under the cloud-covered area. These points define the triangular PDF because the area under any PDF equals unity,

$$1 = \frac{\overbrace{\left(\underbrace{\%\mathrm{SCA}_{cloud\ free}}_{\max\ \%\mathrm{SCA}} + \%\mathrm{CCA} - \underbrace{\%\mathrm{SCA}_{cloud\ free}}_{\min\ \%\mathrm{SCA}}\right)}^{\text{triangle base}} \overbrace{\mathrm{PD}(\%\mathrm{SCA}_{likely})}^{\text{triangle height}}}{2} \quad \textbf{2-26}$$

where $\mathrm{PD}(\%\mathrm{SCA}_{likely})$ equals the probability density of the most likely percentage of snow cover over the entire scene. Solving 2-26 for $\mathrm{PD}(\%\mathrm{SCA}_{likely})$ yields,

$$\mathrm{PD}(\%\mathrm{SCA}_{likely}) = \frac{2}{\%\mathrm{CCA}} \quad \textbf{2-27}$$

Take, for example, a PDF for an area measured with 30% snow, 30% snow-free, and 40% cloud-covered shown in Figure 2-12a. Solving equation 2-25 for the most likely percentage of snow cover in this example yields

$$\begin{aligned} \%\mathrm{SCA}_{likely} &= \frac{30\%}{100\% - 40\%} \\ &= 50\% \end{aligned} \quad \textbf{2-28}$$

Solving equation 2-26 for the probability density of most likely percentage of snow cover yields

$$\mathrm{PD}(\%\mathrm{SCA}_{likely}) = \frac{2}{40\%} = 0.05 \quad \textbf{2-29}$$

A congruent calculation for snow-free land yields a 0.05 probability density of likely snow-free area. A second example, plotted in Figure 2-12b, shows how the ratio of the same 30% SCA used in the first example to a reduced 20% snow-free area raises the overall likely %SCA. The apex %SCA in this case equals 60% (equation 2-27) and has a probability density of 0.04 (equation 2-29). In a final example, not shown, the probability density of the likely %SCA in a map with 100% coverage approaches infinity. In this case, the maximum and minimum %SCA equal the %SCA likely.

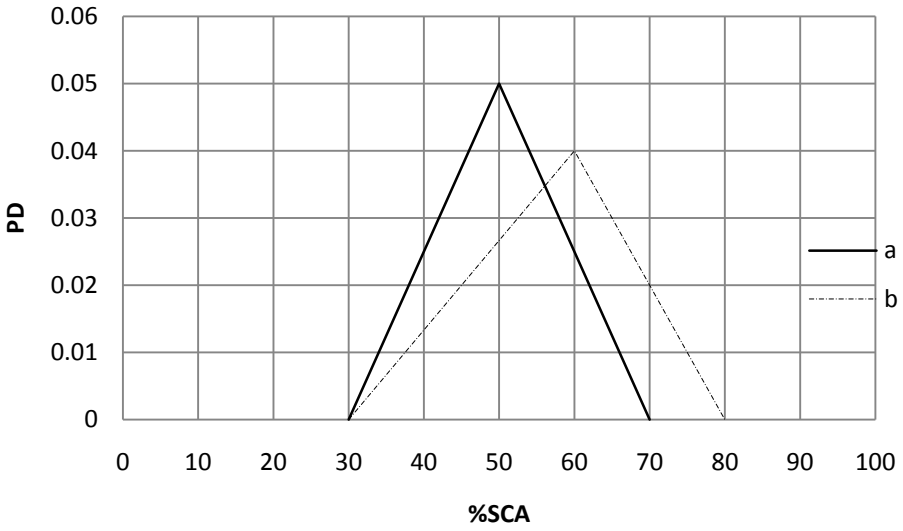

Figure 2-12. Example Triangle Probability Density Functions
Example PDFs for two cases where %SCA equals 30% and (a) %CCA = 40% (b) %CCA = 50%. The likely %SCA in the cloud-covered area depends directly on the proportion of snow-covered area in the cloud-free area. The likely %SCA in the cloud-covered area only depends on the quantity of cells in that scene; it does not depend on the location of known values in the scene or in scenes measured within a time period.

A generalized case of the triangle-PDF approach of estimating the most likely %SCA under a cloud-covered area can estimate the percentage of any category in an unknown area based on a known area. It is a quantity-only, scene-independent approach. The method, in other words, estimates uncertainty in obscured areas irrespective of the coverage in previous and subsequent scenes. Using this method in a comparison of modeled and measured maps, triangle PDFs of remotely sensed %SCA can be compared to model predictions of %SCA on a scene-by-scene basis.

CHAPTER 3: RESOURCES AND METHODS

This chapter explains the rationale for selecting resources (Section 3.1), describes the approach for comparing maps (Section 3.2), and lists procedures for managing measured and modeled data (Section 3.3). Table 3-1, a decomposition of objectives (Section 1.3.1 Preliminary Objectives: Resource Selections, 1.3.2 Map Comparison Objectives, and Section 1.3.3 Data Management Objectives), outlines the methods.

Table 3-1. Functional Decomposition of Objectives

1. Select resources
    a. Select an interest area
        i. In the cryosphere.
        ii. Is subject to past analysis, including
            1. Hydrologic study
            2. Meteorological study
            3. Other studies in the 7 USGCRP research areas listed in "Need & Problem"
        iii. Has measurements available
        iv. Has seasonal mechanisms
    b. Select a time period
        i. Over a seasonal event.
        ii. That includes an extreme event
        iii. That has obtainable measured and modeled data
    c. Select remotely sensed measurements
        i. With enough temporal resolution to monitor the seasonal event
        ii. With enough spatial granularity to see the impact of DEM
        iii. That reports snow and ice
    d. Select a model
        i. That has all the objective properties of the measurements listed above
        ii. That is ideally available to modify
        iii. That can be calibrated
        iv. That ideally has been validated in the past
2. Compare measured and modeled maps
    a. Spatially, by
        i. Statistical comparison, that accounts for
            1. Proportion agreement
            2. Location errors
            3. Category errors
        ii. Visual inspection
    b. Temporally, by statistical comparison of independent scenes, for the entire watershed and DEM zones
3. Manage data
   Make measured data and model output compatible, by either
    a. Converting measured data into the model format, or,
    b. Converting model output into measured the measured format

3.1 RESOURCE SELECTION

As introduced in 1.3.1 Preliminary Objectives: Resource Selections, this study selected the Upper Kuparuk River watershed (UKRW) for the interest area, an annual snowmelt season for the time period, MODIS data for the measurements, and TOPLATS to produce model results.

The interest area lies in the cryosphere, in a mountainous region. The entire Kuparuk area is well studied. "It has the longest history of research of any basin within Arctic Alaska, as both the Toolik Lake and Imnavait Creek watersheds are part of this system" (Nolan 2003). The area has glacial geology measurements (Walker et al. 2003), hydrological measurements (Kane and Hinzman 2009), and meteorological measurements (Kane and Hinzman 2009) all available online. Hinzman and Kane (2009) provide hydrological and meteorological measurements during snowmelt.

For remotely sensed measurements, this study selected MODIS Level Two products, LANDSAT, and high resolution DEM (Nolan 2003) measurements for their online availability and use in past research. Déry et al. (2005) have compared the MODIS measurements in this area to LANDSAT measurements in the area. MODIS Level Two products, although not as widely used or readily available to use in existing software packages, describe daily information compared to the eight day composites in Level Three products.

The model, TOPLATS, simulates spatial heterogeneity in the snow and considers interactions with environmental factors of interest to USGCRP, including vegetation and radiation from the sun. Déry et al. (2004) showed that TOPLATS can be used to model the UKRW with a time step as small as 10 minutes. The TOPLATS

model of the UKRW is set up to produce results in the same mask and the same coordinate system defined by Walter et al. (2003). Only the snow cover module of TOPLATS is investigated in this study. While TOPLATS was originally developed on a big-endian UNIX platform, updates to the model (Section 2.3.1) made by Déry et al. (2004) included modifying the code to enable it to run on a little-endian platform. This study modified the model again to enable it to run on the University of Maryland UNIX system. These updates included, mainly, updating file paths, updating the format of input files, and reverting byte-swapping subroutines that Déry et al. (2004) had last modified. In all updates, special characters and character encodings were considered.

3.2 MAP COMPARISON

This study uses two methods to compare model and measurement maps. In the first method, the proportion of agreement (PA), Cohen's Kappa goodness of statistic (Section 2.4.2.1) and Kappa variants (Section 2.4.2.3) show the agreement between maps accounting for the quantity and location of pixels categorized as either snow, snow-free, or not available. The second method compares model and measured %SCA depletion curves, where the quantity of categorized pixels in each independent scene are used to measure the uncertainty of MODIS %SCA. (as in Section 2.4.3.2).

For both methods, MODIS measurements and TOPLATS predictions need to be put into comparable formats. TOPLATS predicts SWE depths over grids of pixels in UTM Zone 6 while MODIS reports arrays of categories codes, each corresponding to a snow or sea ice feature, across point features in swath scenes. While this study

could have developed a procedure to convert TOPLATS grids to MODIS-comparable swaths, this study instead defined a way to convert MODIS swaths into a TOPLATS-comparable grid format. This study selected the latter procedure because (a) it is easier to visualize and analyze data in a grid format compared to a swath format and (b) it would be hard to assign MODIS categories like lake ice, night, and ocean to TOPLATS SWE values without updating the theoretical basis of the model and modifying the model code. The last part of this chapter lists the data management procedures used to make the model predictions and measurements comparable.

After completing the data management procedure, this study put MODIS measurement codes (Table 2-6) into groups (Table 3-2) where

- The "Available" group includes points that have been successfully identified by the sensor as either snow, lake, ocean, lake ice, or snow.
- The "Frozen" group includes points reported as either lake ice or snow; a subset of available measurements
- The "Snow" group is an exclusive subset of the frozen group
- The group labeled "Not Available" contains member points that MODIS has not decidedly identified or detected. This group also includes points reported by MODIS as "night" and points for a given granule which were outside the respective swath coverage

MODIS measurement groups are independent of quality assurance values and satellite detection angles. For purposes of evaluating a pixel as either snow-covered or snow-free in map comparison, this study generalizes the word "snow" to include "frozen" pixels including lake ice.

Table 3-2. MODIS Measurement Groups

Group	**Members**	
	Value	*Characteristic*
Available	25	Snow-Free
	37	Lake
	39	Ocean
	100	Lake Ice
	200	Snow
Frozen	100	Lake Ice
(called snow during map comparison)	200	Snow
Snow	200	Snow
Not Available	0	Missing Data
	1	No Decision
	11	Night
	254	Detector Saturate
	255	Fill

3.2.1 Spatial Comparison with Kappa and Kappa Variants

To compare MODIS and TOPLATS scenes, this study calculates PA, K, Kno, Klocation, and Khisto according to Figure 3-1 and evaluates the results according to Table 3-3. It also reports intermediate values P_{max} and PE. The criteria for interpreting the strength of agreement of the Kappa statistics in Table 3-3 reflects the number of categories being compared (two, snow and snow-free, rather than a multi-categorical test), the Kappa evaluation scale developed by Landis and Koch (1977), and visual comparison of maps. This scale should be revaluated by researchers that are seeking to reproduce these methods for a different location and/or for different categories.

This study plots these statistics using a set of MATLAB® comparison scripts (Appendix H) that filter model results and projected measurements with the following parameters: initial model albedo, SWE threshold, number of elevation zones, elevation zone, percent available threshold, and time of day. Model input files define the initial model albedo parameter. The SWE threshold parameter determines the minimum height of snow at a particular pixel simulated by the model that this study can consider to be snow-covered. This threshold enables this study to compare SWE predictions with SCA measurements. The number of elevation zones parameter determines the elevation boundaries between each elevation zone by dividing the difference of the maximum elevation and the minimum elevation into equal parts. The elevation zone parameter determines the elevation zone to report results for. The percent available threshold parameter determines the scenes to include in the comparison based on the percentage of cells available — where available means reporting either snow or snow-free, opposed to for example, cloud-covered or missing

— in the MODIS scenes. If the percent available threshold is set to 50%, for example, than the comparison script only evaluates scenes in which MODIS reports at least 50% of the pixels within the scenes as either snow or snow-free. Scenes that report more than 50% of cells as cloud or no-data, in this example, are excluded from the comparison. The time of day input parameter determines the scenes to include based on the time of day — morning or evening relative to solar noon. In each comparison this study shows the effect of changing each parameter.

This thesis provides an online tool to learn about the Kappa statistics for two categories. This learning tool shows the effect of varying grid size on Kappa and varying category assignments on Kappa (Figure 3-2).

		MODIS Map Categories (measurement)		
		Snow-Free	Snow	TOPLATS Map Totals, $\vec{\mathbf{p}}_{i*}$
TOPLATS Map Categories	H_0: Snow-Free	Agreement of Snow-Free Area	Type II Error of Omission (False Negative or Miss)	Proportion Snow-Free in TOPLATS Map
	H_A: Snow	Type I Error of Commission (False Positive)	Agreement of SCA (Hit)	Proportion Snow in TOPLATS Map
MODIS Map Totals, $\vec{\mathbf{p}}_{*j}$		Proportion Snow-Free in MODIS Map	Proportion Snow in MODIS Map	1

Figure 3-1. MODIS-TOPLATS Confusion Matrix.
The MODIS-TOPLATS confusion matrix (boxed) shows four possible coincident-cell outcomes: Agreement of snow-free area (upper-left box), agreement of snow covered area (lower-right box), error of commission where TOPLATS falsely predicts snow cover (upper-left box), and an error of omission where TOPLATS predicts a snow-free area in an area that MODIS reports to be snow covered (upper-right box).

Table 3-3. Kappa and Kappa Variant Interpretation

Statistic	Criteria	Agreement Strength*
PA	0.00	None
	0.01 – 0.40	Poor
	0.41 – 0.60	Low
	0.61 – 0.80	Moderate
	0.81 – 0.90	Substantial
	0.91 – 1.00	High
K, Klocation, Khisto	< 0.00	Poor
	0.01 – 0.10	Slight
	0.11 – 0.30	Low
	0.31 – 0.60	Moderate
	0.61 – 0.80	Substantial
	0.81 – 1.00	High

* Based on Landis and Koch (1977), adjusted for snow/snow-free categories and visual inspection of snow cover maps in this particular study location.

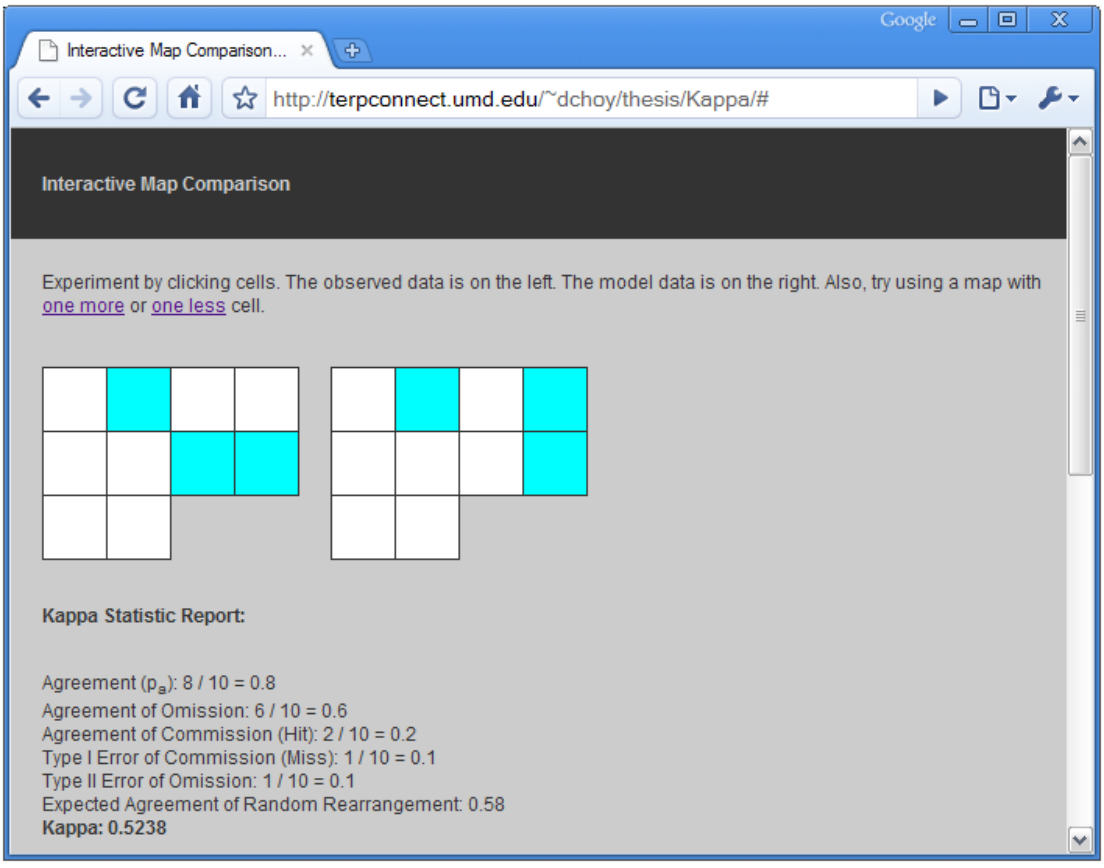

Figure 3-2. Interactive Map Comparison
Visit http://terpconnect.umd.edu/~dchoy/thesis/Kappa to interact with, and visually inspect, Kappa statistics for two categories. See the effect of varying grid size on Kappa and varying category assignments on Kappa.

3.2.2 Temporal Comparison

Varying the same parameters from the spatial comparison — initial model albedo, SWE threshold, number of elevation zones, elevation zone, percent available threshold, and time of day — this study compares MODIS and TOPLATS %SCA depletion curves and evaluates the sensitivity of changing the percent available threshold on the upper and lower limits of MODIS uncertainty. In this comparison, this study reports the most likely MODIS proportion of SCA, the minimum possible proportion of MODIS SCA, and the maximum possible proportion of MODIS SCA in probability distributions. Finally, this study visually compares TOPLATS performance to a logistic curve (death curve).

3.3 DATA MANAGEMENT

3.3.1 Measured Data

Each MOD10_L2 and MYD10_L2 swath needs to be converted into a projected grid in order to compare TOPLATS model results with MODIS measurements. After this study failed to batch-convert series of measurements using MS2GT, HEG-TOOL, and MRT Swath (reviewed in 2.2.2.4), and after exploring layers of swath information using NCSA's HDFView (version 2.3) application, MATLAB®, and IDL, this study created the methodology to convert swaths to grids. The conversion procedure builds on the theory and procedures documented by MS2GT, HEG-TOOL, and MRT Swath and produces grids comparable to TOPLATS output described in Table 2-2. This study names the procedure Level 2 Swath to TOPLATS Grid Tool for the Upper Kuparuk River Watershed and abbreviates it as Swath to Kuparuk (S2K). S2K creates grids with the same coordinate system (UTM Zone 6) used by Walker (2003) and the same cell size (131.34 m) used by Déry et al. (2004). S2K relies on MATLAB® to convert swath points to grid cells and ESRI ArcGIS to project, resample, and mask the grids that MATLAB® creates. (ESRI has yet to functionally realize hearsay plans for natively supporting HDF-EOS swaths in the ArcGIS application suite.) S2K can be modified to accommodate other watersheds by modifying interest area and projection variables, including a watershed polygon. S2K could, for example, capture measurements from nearby research areas like Toolik Lake with minimal modification.

To complete the S2K procedure the general data management procedure in this study adheres to the following general steps for MOD10_L2 and MYD10_L2 swath scenes overlapping the interest area: Download swaths, transform swath into grids, and make grids comparable to model results. The remainder of this section details this procedure.

3.3.1.1 Download Swaths

The process of downloading swaths begins with querying the NSIDC DAAC for MOD10_L2 and MYD10_L2 measurements via a web-based interface (NSIDC 2008c). This query includes a square bounding box in GCS coordinates (latitude and longitude) and time period. A query with coordinates bounding the watershed only, as expected, yields fewer granules than a query with coordinates bounding the entire model interest area. (Compare Table 2-1 and Table 2-2) The difference in the number of granules the DAAC returns, however, is not significant (e.g. <3% difference during the 2005 winter-spring snow melt). It is practical, therefore, to conservatively select the larger area to build a query.

The temporal correspondence between the winter-spring snowmelt and runoff shown in hydrographs (described in Section 2.1.2) guides the selection of the snowmelt time period in each query. For each year, this study initially selects a time period before the peak seasonal discharge. Plots of %SCA versus time reveal whether or not an initial time period inferred from hydrographs captures the melt period. In the case that a time period does not overlap with the melt period, this study modifies the query period in another trial. This trial and error process repeats until it identifies

a query that returns a time window in which the first several days of scenes show at least 99% snow- and ice-covered (frozen) area and the last couple days of scenes show at most 1% frozen area. In all queries, this study seeks to limit the number of granules returned to limit download time and S2K processing time. If download time and processing time could be executed one or two orders of magnitude faster (through, for example, a web-based controller of a server-side processing tool), the overall process of downloading swaths could practically mitigate the trial and error query process by initially selecting three months of data instead of a few weeks of data based on hydrograph plots. The NSIDC, in that vein, provides an option to skip night data in queries. This study always excludes night data from each query. The choice limits the number of scenes that cannot be well evaluated by the snow mapping algorithm (2-6) and halves processing time.

Most queries run shy of one hour and require a persistent connection to the internet to complete. After queries are complete, DAAC web users purchase granules (currently free) via a shopping cart interface. Next, NSIDC DAAC processes, compresses, and makes available the selected granules via an FTP connection. The time it takes NSIDC to process the granules and copy them to an FTP location is often shorter than a couple hours, but the process can take up to one day. This study always request NSIDC to compress all requested granules (using zip compression; HDF compression is currently unavailable) to limit the hard disk requirements for each year of data. Extracting 200 MB of compressed granule files yield about 5GB of uncompressed information. Users, therefore, need to check if there is enough available disk space at a their destination locations before uncompressing the HDF

files to them. At the end of each query execution, the DAAC provides a summary of search results. This summary, converted into a spreadsheet, keeps track of the scenes selected by a query. Search result summaries, additionally, ensure that the time periods encompassing results of each query trial overlap and therefore scenes are not overlooked.

3.3.1.2 Transform Swaths into Grids

3.3.1.2.1 Overview

The MATLAB® script "animate_series.m" (Appendix G) simultaneously animates a directory of HDF-EOS swaths in the GCS and creates a series of GCS ASCII files formatted for ArcGIS. The script depends on two subroutines, "expandgrid2.m" and "proccessDuplicates.m." Note that the script "animate_series.m" and its subroutines fully utilize a single processor and require at least 2GB of memory to interpolate up to 200 swaths in the UKRW. Without at least 2GB of memory, disk caching operations excessively increase the time to complete the interpolation of the swaths. If MATLAB® depletes all physical memory and starts paging information to the hard disk, break the script and run it again after moving the HDF files that have been already converted into a new folder. Be sure to delete, in this case, the last ASCII file the script created because that file is probably incomplete. The scripts instructs MATLAB®, for each file in a user-specified directory, to:

1. Read data: Use the inherent MATLAB® function, "hdfinfo," to read HDF granule data into a MATLAB® structure.

2. Extract three *grids of points* from the HDF MATLAB® structure into three matrices:
    a. Snow categories
    b. Latitudes
    c. Longitudes
3. Assign latitude and longitude coordinates to each snow category point by resampling latitude grids and longitude grids ten-fold. This means finding 100 intermediate points (ten by ten) for every set of four latitude values and four coincident longitude values forming four points.
4. Assign categories to duplicate coordinates using a modal decision (explained further in Section 3.3.1.2.3).
5. Fit an evenly spatially-spaced grid to the surface defined by the three duplicate-free snow category, latitude, and longitude grids using Delaunay triangulation built into the MATLAB® function "griddata."
6. Write fitted data to an ASCII file formatted for ArcGIS

After "processDuplicates.m" runs, "animate_series.m" could logically perform another modal decision to make measurement categories more comparable to TOPLATS categories by compositing all categories listed in Table 3-2 into two categories: snow and snow-free. The "animate_series.m" script, however, does not perform this secondary processing so that this study can evaluate MODIS measurement groups, later, during map comparison. By not consolidating all categories at this step, S2K could be readily modified to confirm results from

distributed snow-cover models that, unlike TOPLATS, account for categories like water and ice.

3.3.1.2.2 Extract and Resample Location Grids

The snow category matrix, the latitude matrix, and the longitude matrix, although presented in the HDF-EOS file as two dimensional grids and visualized by HDF View in a similar manner, are not regularly spaced in the GCS because the MODIS sensor, while in its sun-synchronous orbit, collects these grids in a 10-minute "long" flyby. If the points were regularly spaced, NSIDC could replace the latitude matrix and longitude matrix in the MODIS product with relatively simple metadata containing the position of a fixed point (e.g. the top left corner of a map) and a pair of values representing the x- and y-spacing between points.

The resolution of each snow category matrix, additionally, is ten times finer than both the latitude matrix and the longitude matrix. If, for example, a snow category matrix contained 20 rows and 20 columns, then both corresponding location matrices would contain two rows and two columns — a total of four cells in each location matrix. The first (upper left) cell in a snow category matrix maps to the first cell in both the latitude matrix and the longitude matrix. The tenth cell (ten cells below the first cell) in the snow matrix maps to the second cell (directly below the first cell) in the location matrices.

The "animate_series" script creates intermediate latitude values and intermediate longitude values spaced evenly between original location values to enable a one-to-one matching of snow category values with location values. To do

this, the script instructs MATLAB® to perform a bilinear interpolation on each location grid with the "interp2" function build into MATLAB®. MATLAB® executes this interpolation process in the "expand_grid.m" subroutine. (The subroutine does not increase the spatial extent of a grid.) The "expand_grid.m" subroutine, for example, expands a two cell by two cell square in an original matrix into a ten cell by ten cell square. Equation 3-1 demonstrates this example for a case in which the original cells are expanded by a factor of two rather than by a factor of ten.

$$\begin{bmatrix} 100 & 50 \\ 5 & 1 \end{bmatrix} \xrightarrow{expand\ \ grid\ \ 2X} \begin{bmatrix} 100 & \mathbf{75} & 50 \\ \mathbf{52} & \mathbf{39} & \mathbf{25} \\ 5 & \mathbf{3} & 1 \end{bmatrix} \qquad \textbf{3-1}$$

Equation 3-1 greatly exaggerates the actual expansion of GCS coordinates and shows interpolated values in bold. The values of neighboring cells in the latitude and longitude matrices vary only slightly, if at all, compared to the demonstration values shown in equation 3-1. The distance between originally spaced location points decreases between scenes as the MODIS sensor approaches nadir in relation to the UKRW as described in Figure 3-3.

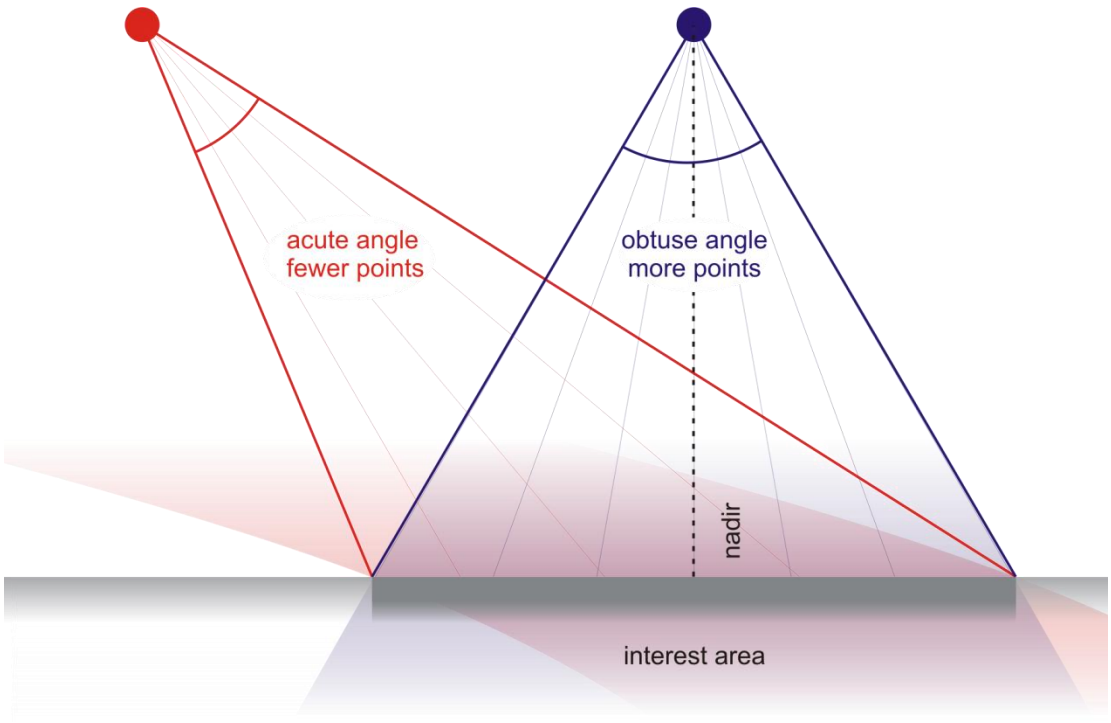

Figure 3-3 Effect of Satellite Angle on Sample Point Quantity
Assuming MODIS measures points at evenly spaced angles, the point density on the interest area is the greatest when MODIS is close to nadir. The sample point density under the acute angle (in red) is greatest on the left-hand side of the interest area and the smallest on the right-hand side of the interest area. The sample point density under the obtuse angle (in blue) is greatest at the center of the interest area and smallest at the edges of the interest area.

3.3.1.2.3 Assign Categories to Duplicate Coordinates

Given a limited floating point size for coordinate values, the "expand_grid.m" subroutine may produce duplicate coordinates while creating intermediate coordinates to match all snow category points in a granule. The "expand_grid.m" subroutine more likely produces duplicate coordinates from points that are sensed by MODIS close to nadir in comparison to coordinates that are relatively far apart on the earth. These duplicate coordinates, further, may have conflicting snow categories. When duplicate coordinate points all share the same snow category, "animate_series.m" removes all but one of the points from the surface. When duplicate coordinate points report conflicting snow categories, "processDuplicates.m" replaces these points with a

single point in the same location with a snow category derived by a modal decision algorithm. For an n-size sample of points with the same location:

1. Eliminate L1BMissingData points if there are points with other values
2. Eliminate DetectorSaturated points and NoDecision points if there are points with other values
3. Eliminate cloud-obscured points if there are points with other values
4. Eliminate night points if there are points with other values
5. Determine the frequency of categories reported by the remaining points.
6. If there is a maximum category frequency, replace all duplicate points with a single point marked with the maximum category frequency. If, otherwise, there is a "category-tie" among the remaining points, pick one of the tied categories at random

S2K alerts the MATLAB® command window in the case it finds duplicate coordinates. While running S2K, if many (e.g. 5%) duplicate coordinates are found, consider modifying the procedure by increasing the floating point size of coordinate variables. In this case, if the physical memory of a computer limits increasing the floating point size of coordinate variables, consider dividing the interest area up if the interest area is large, or ignoring snow-cover values at interpolated coordinates if the interest area is small.

3.3.1.2.4 Surface Fitting

After "processDuplicates.m" determines the snow category for points with duplicate coordinates in the swath surface, "animateSeries.m" creates an evenly spaced location

grid from the swath surface in the GCS. Input variables, that "animateSeries.m" reads at the beginning of the script, describe the evenly spaced surface

```
west = -149.53; %lons
east = -149.10;
north = 68.67; %lats
south = 68.47;
west_to_east_inc = .001;
south_to_north_inc = .001;
```

where the bounding variables (`west`, `east`, `north`, and `south`) describe the UKRW extent in the GCS and the increments (`west_to_east_inc` and `south_to_north_inc`) describe the spacing between each point in the evenly spaced grid. The MATLAB® function "griddata.m" performs Delaunay triangulation to populate the evenly spaced grid with categorical values from the swath surface. Categories are picked on a nearest neighbor basis. Note that `west_to_east_inc` and `south_to_north_inc` values smaller than 0.001 cause "griddata.m" to produce unexpected, irrational results in which categorical values are averaged rather than selected based on nearest neighbor sampling. Delaunay triangulation is used by other swath-to-grid conversion tools like the LP DAAC MRT Swath Tool (2). After "griddata.m" fits each swath surface into evenly spaced grids, "animate_series.m," in a final step, saves these grids as ArcGIS compatible ASCII files and animates the series on screen in the GCS.

3.3.1.3 Make Grids Comparable to Model Results

The third step in the S2K process begins with projecting GCS (WGS 1984) maps created by "animate_series.m" into the model projection system, Clarke 1966 UTM Zone 6. When an ArcMap user attempts to directly project an UKRW map from the

GCS into the model coordinate system and model extent, using for example an "ArcToolbox" wizard, ArcGIS unexpectedly shuts down. To compensate for this problem, the Python script "ascii2kuparuk.py" instructs the ArcGIS processor, called the "geoprocessor," to first project GCS maps into the Albers Equal Area Conic coordinate system, and then to secondly project the maps from the equal area coordinate system into the model coordinate system. (Note that ESRI makes the intermediate coordinate system, Albers Equal Area Conic, a standard that is easily available to ArcDesktop users. This coordinate system is available to users under the hierarchy of labels: Continental, North American, Alaskan. The Albers Equal Area Conic system could be useful in confirming model results spanning larger arctic areas like the entire Kuparuk River.)

In a final step, "ascii2kuparuk" masks the raster in the model coordinate system with a watershed raster defined by a cell size and extent comparable to TOPLATS output

```
gp.extent = "390862.8 597414.74 418181.52 627228.92"
gp.cellSize = "131.34"
```

where the values, in order, of "`gp.extent`" define minimum easting, minimum northing, maximum easting, and maximum northing values, all in meters. The parameter, "`gp.cellSize`," defines the cell size of the mask, 131.34 m, which equals the cell size output by TOPLATS. The mask is simply a rectangular grid in the model projection system defining the extent of the interest area. Watershed pixels in the mask report unity while all other pixels report zero (re-classed from null values). Once a granule is masked, "ascii2kuparuk" saves it in a floating point file for comparison to the model.

Figure 3-4 Python Script, "ascii2kuparuk" Processes
The python script, "ascii2kuparuk," instructs the geoprocessor to transforms GCS grids created by "animate_series.m" into raster images that are comparable with model output.

Figure 3-4 charts the process "ascii2kuparuk" performs on each GCS grid. In order to reproduce this procedure ArcMap users must set up their workspace; they must

1. Add the "ascii2kuparuk.py" script to their tool box or load it from an existing toolbox.
2. Obtain the Spatial Analyst extension and set the Spatial Analyst options to match the extent of the mask:
    a. top: 627228.92
    b. left: 390862.8
    c. right: 418181.52
    d. bottom: 597414.74
3. Set the cell size variables in the Spatial Analyst options (accessible in ArcMap via Spatial Analyst → Options > Cell Size Tab) and the environment settings (accessible via Tools menu → Options → Geoprocessing Tab → Environment Settings Button) to:
    a. Cell size: 131.34
    b. Number of rows: 227
    c. Number of columns: 208

Warning: Only raster multiplication will correctly mask the watershed for an individual granule. The “Extract by Mask” command, alternatively, consistently produces an offset error and, sometimes, produces maps with a number of cells incomparable with model output. This is why this process does not use the “Extract by Mask” command.

3.3.2 Model Calibration

The entire modeling process consists of model conceptualization, model formulation, preliminary application, model calibration, and model confirmation. This thesis focused on developing tools for the model calibration and confirmation steps. The conceptualization, formulation and preliminary application steps had already been accomplished by the USDA ARS at the Hydrology and Remote Sensing Lab (Déry et al. 2004). The calibration processes in this study sought to determine whether the map comparison methods would be sensitive to changes made in model parameters and therefore useful in setting the values of model parameters that cannot be directly measured. The process includes determining the winter-spring melt time period from MODIS measurements.

CHAPTER 4: RESULTS AND DISCUSSION

Chapter Four presents MODIS measurements independent of TOPLATS results (4.1), presents results from running TOPLATS with three different albedo values and varying the SWE threshold (4.2), and presents, finally, map comparison results to show how well MODIS confirms TOPLATS (4.3). Chapter Four limits its discussion of implications of each result to their effects on steps presented in Chapter Three, (including evaluation of statistics via Table 3-3), while Chapter Five summarizes all results, critiques the methods, and suggests future work. Note: Throughout Chapter Four and Chapter Five, unless lake ice is specifically mentioned, snow refers to both members of the MODIS measurement group "frozen" defined in Table 3-2 — lake ice and snow.

4.1 MEASUREMENTS

This study needs to download and review MODIS measurements before running TOPLATS because model input parameters depend on the winter-spring melt period revealed by MODIS. Additionally, the quality assurance of MODIS measurements determines the usability of individual scenes in model confirmation. This section shows measurement results from this review exclusive of model results. It shows swath plots and grid plots of MODIS snow cover, cloud cover, quality assurance, and other categorical data throughout the S2K procedure described in Section 3.3.1. It shows the effect of observation time during the day, the effect of cloud coverage, and the effect of elevation on snow cover measurements. The results in this section reveal ambiguities in MODIS measurements, and ultimately aid this study in selecting a set

of observations that this study believes are closest to "ground truth." This study uses these observations — the ones that this study has the most confidence in — for both selecting the times to get model results in Section 4.2 and confirming model results via map comparison in Section 4.3. Probability quantifies this study's uncertainty of measurements at each scene through the triangle-shaped probability density function described in Section 2.4.3.2. Plots of %SCA versus time of day and plots of %SCA versus day of the year, along with plots of supporting quality assurance information like cloud coverage and like overall quality, support qualitative explanations of this study's confidence in individual MODIS scenes to confirm model results.

4.1.1 DAAC Query Results

Given that the peak annual discharge of the UKRW usually occurs shortly after the winter-spring snow melt in the UKRW, as explained in Section 2.1.2, the peak winter-spring discharges shown in the UKRW hydrographs for years 2000, 2001, and 2002 (Figure 2-5) guided the time period for this study's initial queries to the NSIDC DAAC. Figure 4-1 shows final results of the trial and error process described in Section 3.3.1.1 of downloading granules and plotting %SCA versus day of the year in relationship to the these hydrographs. Notice that the %SCA data Figure 4-1 shows many, unrealistically rapid (within time intervals of less than one day) melt and accumulation periods during the course of an overall melt period confined by a smooth, logistic-shaped, upper envelope.

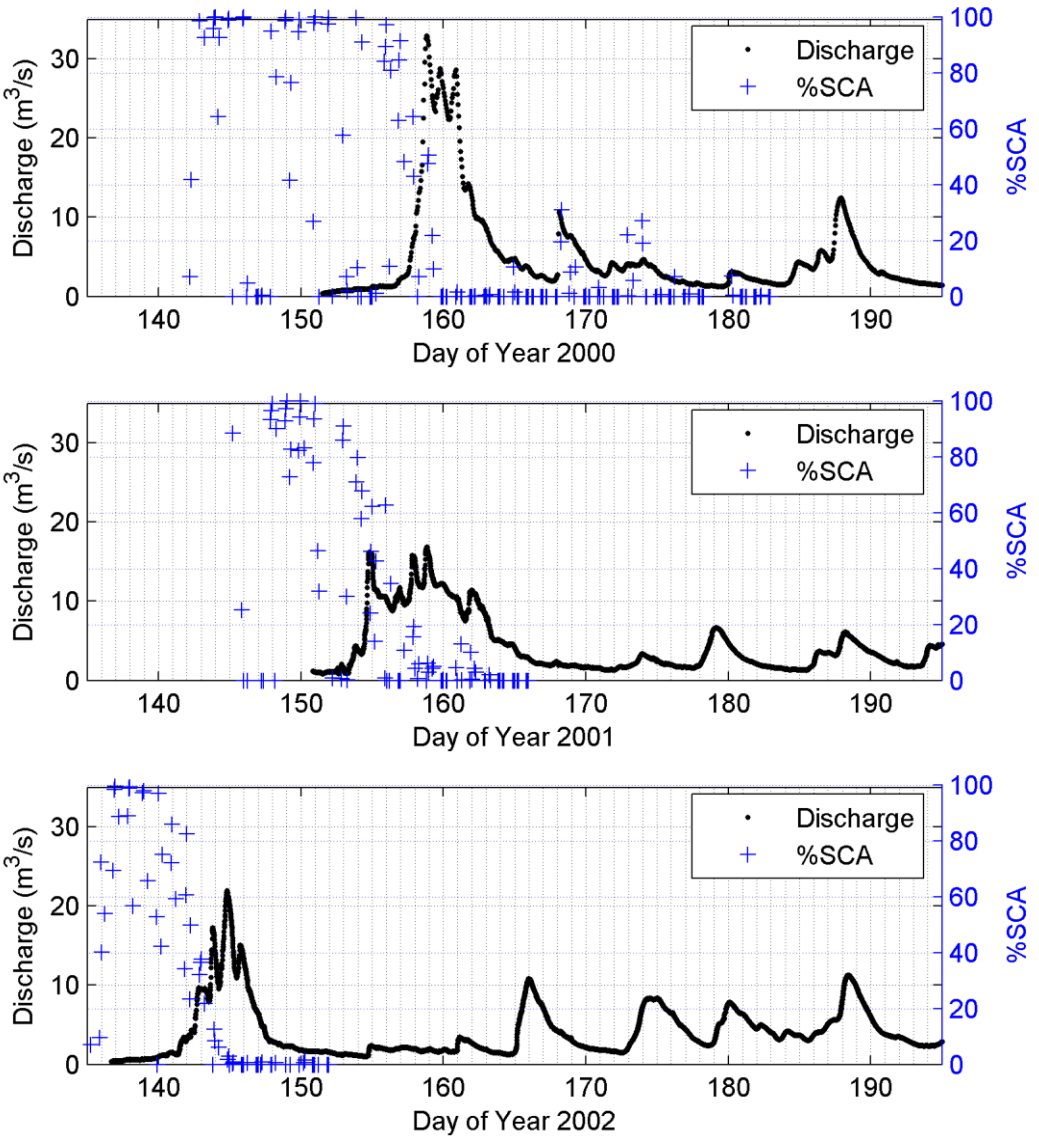

Figure 4-1 Hydrograph Relationship to %SCA for years 2000, 2001, 2002
The beginning of the winter-spring melt in the UKRW occurs within ten days prior to the peak winter-spring discharge in each of the years, 2000, 2002, and 2002, shown. The %SCA series shows results of each scene returned by the DAAC from the day-time query, irrespective of cloud coverage, day of year, measurement quality, or any other scene-excluding factor. %SCA in this plot is calculated over the watershed area, not the model bounding box. See MATLAB® scripts “compare_calculate_all.m” and “plot_hydrographs.m” to reproduce these figure.

The reason why Figure 4-1 reports an unrealistic result, is because the figure shows %SCA results irrespective of the following filters (a) supporting quality assurance information (Section 2.2.2.3), (b) collection time information (besides night time), (c) elevation information, and (d) satellite. This unfiltered[**] %SCA series only considers categories listed in Table 3-2 and the decision to request only daytime granules from the DAAC. Table 3-2 categories plus the daytime query flag, even though they yield the overall unrealistic %SCA series in Figure 4-1, do sufficiently indicate a rough (plus or minus a few days) time period to narrow collection of model input parameters and perform map comparison. Figure 4-1 indicates that model confirmation for the winter-spring snowmelt depends on model results between day 150 and day 165 in the year 2000, day 145 and day 165 in the year 2001, and day 135 and day 150 in the year 2002. Appendix G shows the MATLAB® script, "plot_hydrographs.m", which shifts the hydrograph data from Kane (2009) in Alaska local time into coordinated universal time (UTC) and plots results with MODIS snow cover.

All MODIS scenes can be viewed using the application at http://choy.me/david/research/thesis/filter.php, where MODIS maps can be sorted by the filters described in Table 4-1. The application colors unavailable pixels, including

[**] The word "unfiltered," when exclusively describing measurement maps in this study or comparison results in this study, refers to the scenes corresponding to the measurement times described in this passage. "Filtered" scenes, alternatively, refer to a subset of scenes defined by one or more variables Table 4-1 lists most of these filters.

cloud-covered pixels, grey; it colors snow blue; and it colors snow-free land brown. Complete sets of unfiltered MODIS snow cover maps support their unrealistic %SCA series counterparts from Figure 4-1. The unfiltered maps show patches of snow cover that appear and disappear from one scene to the next. The maps suggest that either physical factors like wind possibly moved snow across the watershed between measurement times, or that the snow cover observations do not fully consider the impact of supporting quality assurance information — such as a broken detector band, an obtuse sensing angle, an uncertain radiance calculation, or clouds (Section 2.2.2.3). Chapter Five suggests additional factors, not necessarily completely inherent to HDF-EOS quality assurance information, that could contribute to measurement error.

Table 4-1. Scene Filters
View http://choy.me/david/research/thesis/filter.php to apply these filters on MODIS data in the TOPLATS model system where each cell has a side length of 131.34 meters. Grey cells represent clouds, blue cells represent snow, and brown cells represent snow-free land.

Filter	Description / Values	
	Temporal	
Year	All	(2000, 2001, 2002)
	2000	
	2001	
	2002	
Day of Year Range	Time since the beginning of a year in decimal days	
Time of Day	All	(Morning and evening)
	Morning	(Near solar noon)
	Evening	(Near night)
Sequence Number	Rank of a map among all unfiltered maps for a year	
	Spatial	
Quality Rage	Proportion of good quality swath points in a GCS bounding box	
Proportion Available Range	Proportion of snow-covered or snow-free pixels	

4.1.2 Influence of Availability, Collection Time, and Quality Assurance Filters on Measurement Uncertainty

While the unfiltered maps seem to indicate patches of snow moving from one scene to the next in short time intervals (under one day), time-composite maps of counts of SCA pixels over the entire melt period of each year, shown in Figure 4-2, indicate that snow consistently persists the longest during the melt period at locations in the lower elevation zones (Figure 4-3) across all three years evaluated. The color of each pixel in this figure represents the number of scenes in a series that show that pixel covered with snow. Figure 4-2a does not provide clear results compared to Figure 4-2b because clouds and invalid data influence the plots shown in Figure 4-2a while Figure 4-2b considers three filters: 90% available coverage, 50% or greater quality of points, and the morning time period (close to solar noon) times.

Figure 4-4, Figure 4-5, and Figure 4-6 show sets of filtered scenes from respective years 2000, 2001, and 2002. Each set contains images that start with close to 100% likely SCA and end in none. The filter selections in each of these figures maximize the useful information for each year. In Figure 4-4, nine sequential morning scenes from year 2000 between noon (UTC) at day 151 and the end of day 154 reveal unavailable pixels, resulting from mainly clouds, obscure the melt window. Changing the morning filter to an evening filter in this figure reveals a series which include a similar amount of cloud coverage and likely, mis-detected points. These evening scenes can be viewed by adjusting Figure 4-4 at the website location specified in the caption of this figure.

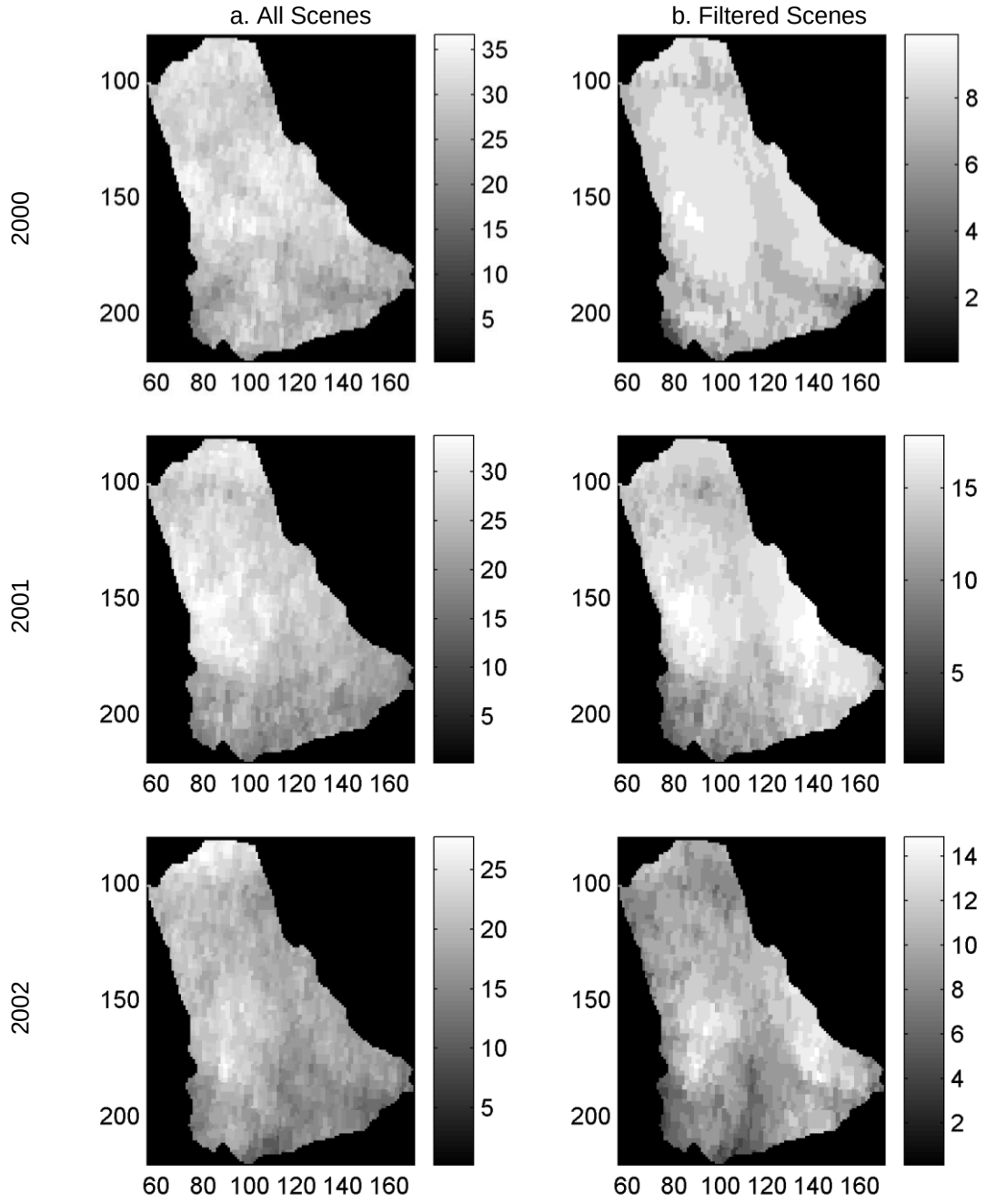

Figure 4-2 Sum of Snow-Covered Pixels Across Unfiltered and Filtered Melt Series
Brightness-normalized plots of the sum of the number of pixels where snow lasts during a melt series indicates either the location of possible physical features that should be considered by a model to limit snow melt, or the location of features that limit MODIS from correctly sensing snow. In the UKRW, clouds and poor quality measurements confuse the plots derived from the unfiltered scenes (a). The plots derived from the filtered scenes (b), however, clearly show two areas flanking the river path where snow lasts the longest. Maps are shown in the model coordinate system where southing and easting units are pixels widths of 131.34 m. See MATLAB® script “plot_cumulative_sca.m” to reproduce these figure.

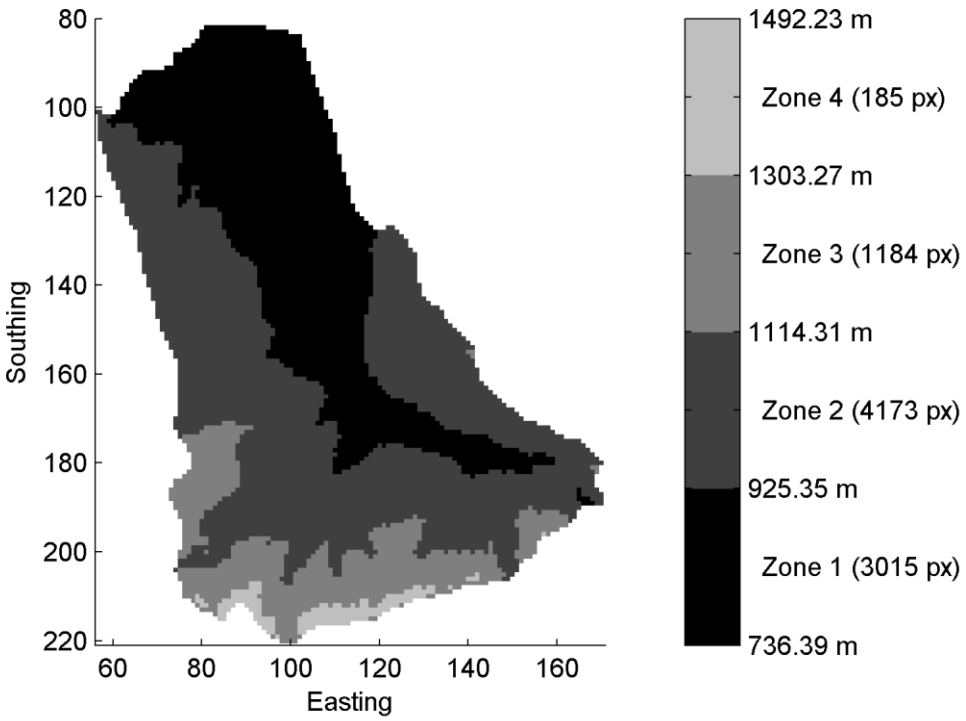

Figure 4-3 UKRW Elevation Zones
Elevations equally spaced at 736.4 m (minimum elevation), 925.4 m, 1,114.3 m, 1,303.3 m, and 1,492.2 m (maximum elevation) above sea level bound four 189.0 m elevation zones in the UKRW. In the 131.34 m model grid (Table 2-2), zone one covers 3,015 pixels (52.01 km^2), zone two covers 4,173 pixels (71.99 km^2), zone three covers 1,184 pixels (20.42 km^2), and zone four covers 185 pixels (3.191 km^2). Note that easting and southing units are pixel widths in the model grid. See MATLAB® script “elevationszones.m” to reproduce this figure and see a side views of the watershed elevation zones.

Figure 4-5 shows nine sequential morning scenes from year 2001 between day 151 and day 159 with 0.40 or greater proportion of good quality swath points. These scenes represent the beginning of the melt period inferred from Figure 4-1, which appears to last from day 150 to 160. The middle of the melt period, occurring between day 154 through day 157, is absent from these filtered results. During this time, in the middle of the melt period, the proportion of good quality swath points falls below 0.40. The figure reveals a strong correlation between the proportion of points available in the scene and the quality assurance information. Changing the time-of-day filter parameter to evening yields nine scenes with unavailable information, blanketing the series. Evening scenes may be viewed by adjusting Figure 4-5 at the website location specified in the caption of this figure.

Figure 4-6 shows fifteen sequential morning scenes with a proportion of quality swath points greater that 0.50 between day 138 and day 146 during the year 2002. The year 2002 contains more available coverage with higher quality measurements during the melt period than either the year 2000 or the year 2001. Unlike the series shown in Figure 4-4 for the year 2000, this figure shows no cloud coverage. Unlike the series shown in Figure 4-5 for the year 2001, this figure contains scenes that are more evenly sampled across time during the melt period. Notice that all of the scenes in this figure have 100% available coverage, which means the estimate of uncertainty in these measurements due to unavailable pixels is zero. Like Figure 4-4 and Figure 4-5, adjust Figure 4-6 at the website location specified in the caption of the figure.

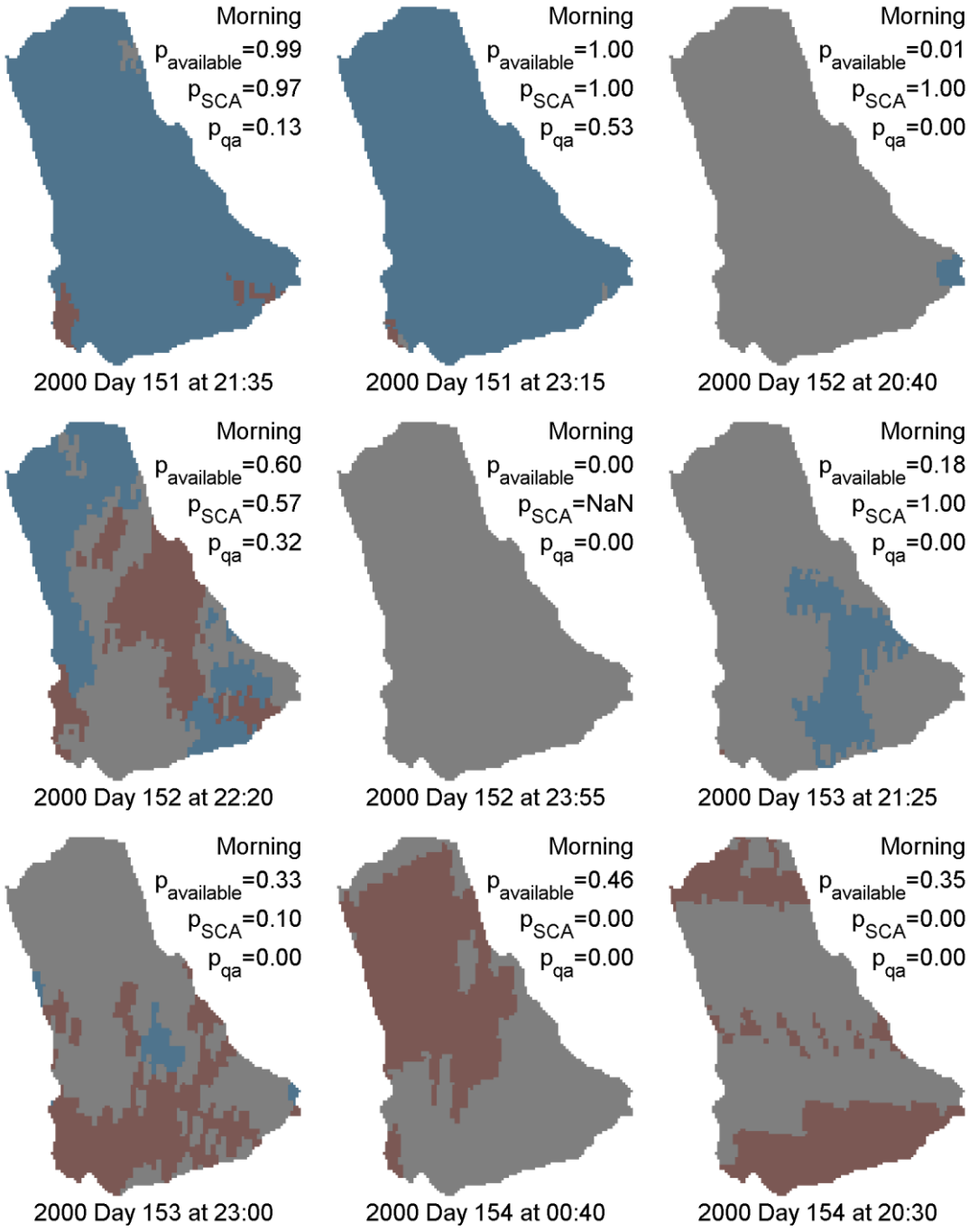

Figure 4-4 2000 Select MODIS Scenes
Blue = snow; brown = snow-free; grey = unavailable data, including cloud.
Unavailable data, caused predominantly by cloud coverage, obscures the most important scenes during the 2000 melt period. This figure shows morning scenes during the melt period. See evening scenes, which include a similar amount of cloud coverage and likely, mis-detected points by adjusting this figure at http://choy.me/david/research/thesis/filter.php?Y=2000&Tmin=151.5&Tmax=154.9&M=Morning&Qmin=0.00&Qmax=1.00&Amin=0.00&Amax=1&Nmin=1.00&Nmax=500&go=Submit.

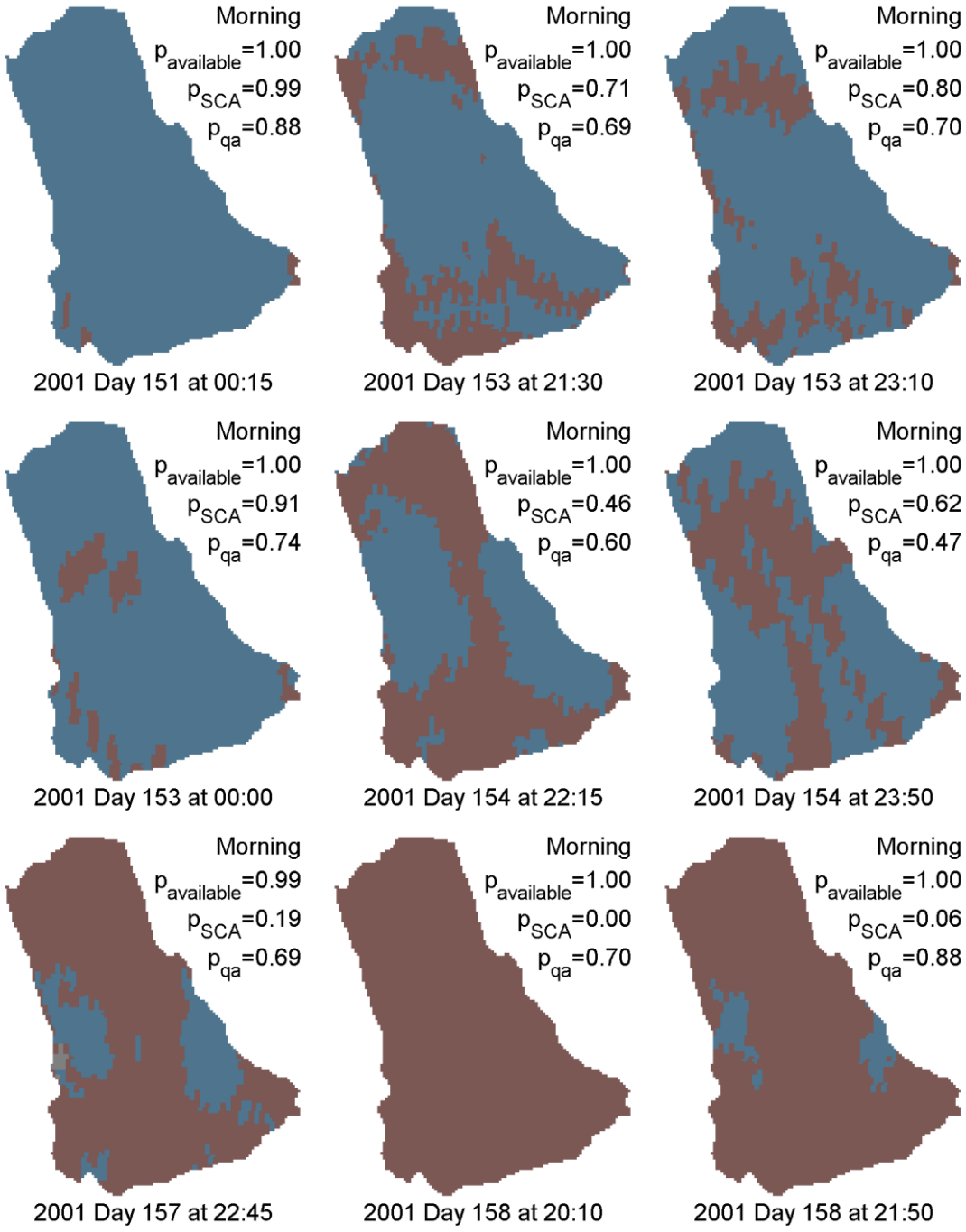

Figure 4-5 2001 Select MODIS Scenes
Blue = snow; brown = snow-free; grey = unavailable data, including cloud.
Morning scenes with 0.40 or greater proportion of good quality swath points show the beginning of the melt period inferred from Figure 4-1, which appears to last from day 150 to 160. The middle of the melt period, between day 154 through day 157, is absent from these filtered results. At these times the proportion of good quality swath points falls below 0.40.
Adjust this figure at
http://choy.me/david/research/thesis/filter.php?Y=2001&Tmin=151&Tmax=158.91&M=Morning&Qmin=0.4&Qmax=1.00&Amin=0.00&Amax=1&Nmin=1.00&Nmax=500&go=Submit.

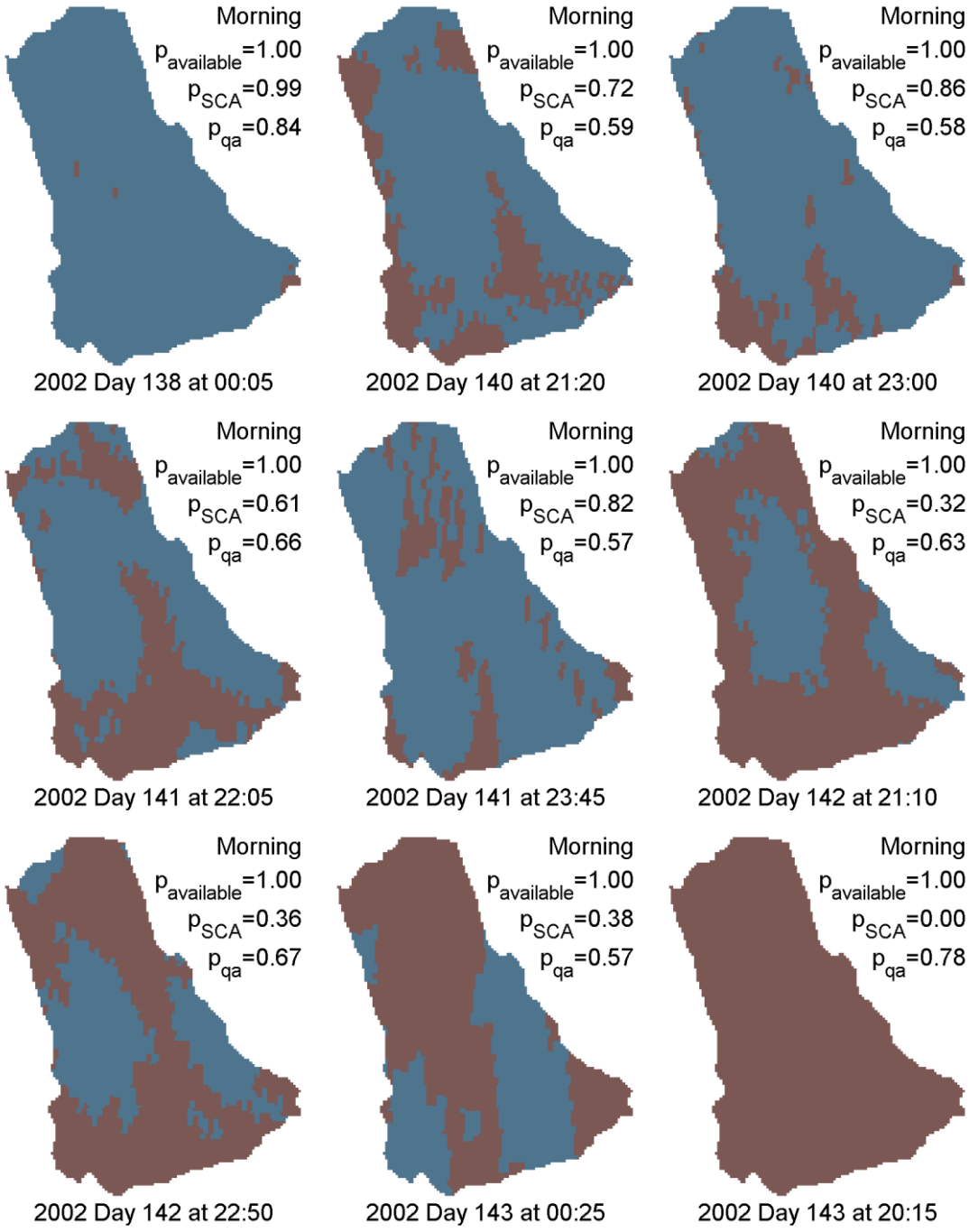

Figure 4-6 2002 Select MODIS Scenes
Blue = snow; brown = snow-free; grey = unavailable data, including cloud.
Continued on the next page, the fifteen 2002 morning images with a proportion of good quality swath points greater than 0.50 shows more clear information than the images from previous two years. Unlike year 2000, this figure shows no cloud coverage. Unlike year 2001, this figure contains scenes that are evenly sampled during the melt period. View more at http://choy.me/david/research/thesis/filter.php?Y=2002&Tmin=138&Tmax=145.85&M=Morning&Qmin=0.5&Qmax=1&Amin=0.00&Amax=1&Nmin=1.00&Nmax=500&go=Submit.

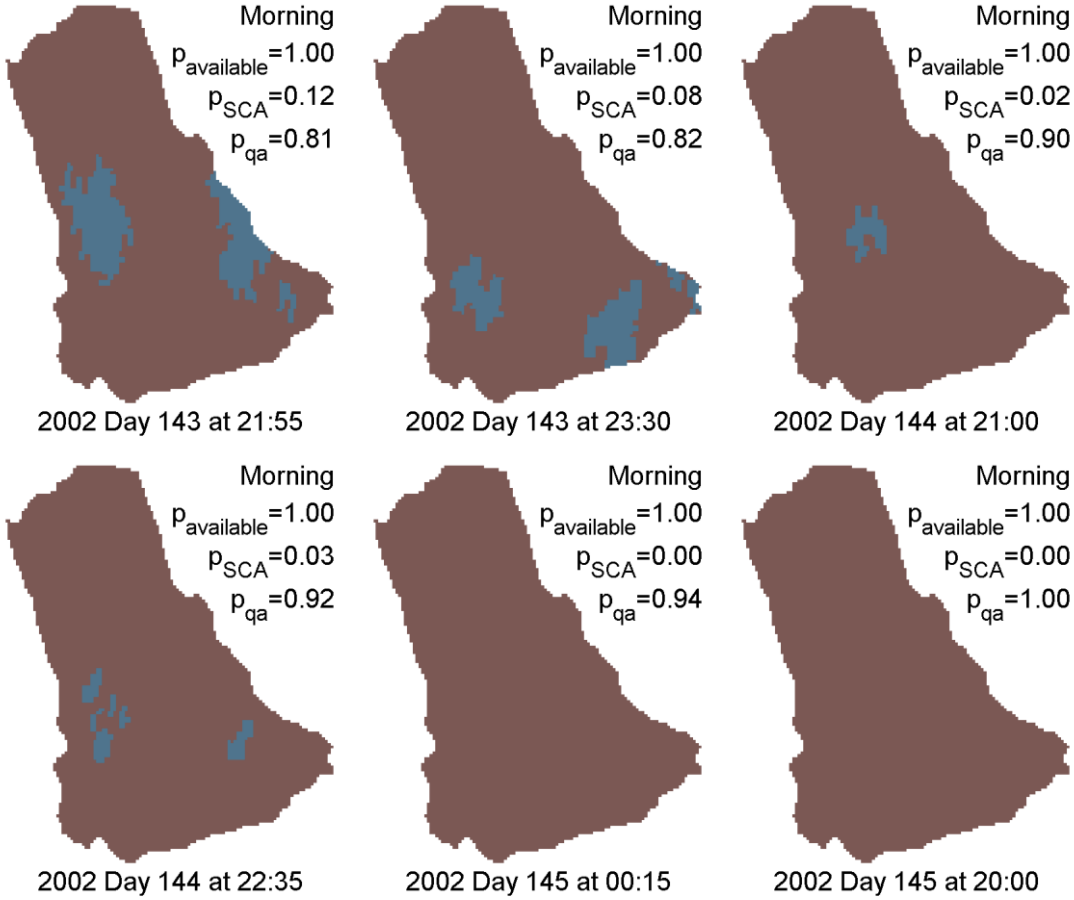

Figure 4-6 2002 Select MODIS Scenes Continued from Previous Page

Extending the time periods in Figure 4-4, Figure 4-5, and Figure 4-6 to days both before and after their respective melt periods reveal some scenes that have high data availability, but unrealistic coverage. MODIS reports near complete SCA, for example, on day 144 of the year 2000 and almost no SCA on the local evening of day 145 at 5:25 UTC. The sensor, subsequently, reports almost 100% SCA later in the day after a period of low availability due to cloud coverage. The time that a given measurement was collected explains the poor quality of this scene, and many others like it. Figure 4-7, Figure 4-8, and Figure 4-9 show the effect of measurement time and quality on SCA for all the unfiltered scenes from 2000, 2001, and 2002. The first plot in each of these figures (a) shows the proportion of four supporting quality assurance measures at each swath point cropped by the model area in the Global Coordinate System (GCS). The second plot in each of these figures (b) shows the data from data on an hourly basis in relationship to sunset, sunrise, and solar noon. These plots define two measurement time periods — morning, which is close to solar noon and evening, which extends past sunset. The third plot in each of these figures (c) summarizes plot a, plot b, and SCA reports. The larger, bluer, circles in these plots represent increasing proportions of good quality swath points. Note that the evening data in the second plot of each figure includes night scenes even though all the DAAC queries in this study included the request to ignore night data. See Figure 4-7 for this description of the three plots specific to year 2000.

The 2000 data in Figure 4-7 shows MODIS collected the highest quality measurements (> 0.90) before and after the three days of quick snow melt. During the melt, almost all the scenes with 50% or higher quality assurance are morning scenes.

Figure 4-8 shows 2001 data in the same types of plots described in Figure 4-7. Figure 4-8a shows a high proportion of abnormal quality points during the melt period which are reflected by the gray areas in Figure 4-4 maps. Figure 4-8b shows that while MODIS reports the highest cloud coverage after sunset, it also reports many good quality points. This could suggest that MODIS could mistake low-lit ground for clouds after sunset. In each day during the beginning of the melt shown in Figure 4-8c, the points that deviate from the upper SCA envelope the most are all evening points. The quality of these points, however range from 0% good quality points to over 50% good quality points. The scenes on day 148 and 149 with the lowest SCA and medium-good quality, for example, both occur in the evening. These points, therefore, are probably invalid due to poor measurement capabilities of MODIS in the evening.

Figure 4-6a, which plots supporting quality assurance information versus the time of year 2002, shows the proportion of good quality points scattered across the month of May starting on day 121. Abnormal points are also scattered over the month. The proportion of cloud obscured points remains consistently below 0.3 or over 0.9 with the exception of four outliers, half of which contain mostly invalid points of data among the remaining cloud free points. The other two outliers contain mostly good points of data among remaining cloud free points. Figure 4-6a shows that the fourteen scenes with a proportion of invalid points greater than 0.01 all occur before day 133 with the exception of one scene occurring on day 139 with a proportion of invalid points under 0.05. The apparent drop off of invalid points later in the month cannot easily be explained by this figure alone. Figure 4-6b shows there

are exactly 47 scenes in the morning set and 47 scenes in the evening set. Looking at the proportion of quality assurance information in Figure 4-6b in relationship to apparent sunset, the set of data collected later in the evening includes many invalid points after sunset between hour seven and hour nine UTC. Based on the apparent association between invalid points and time after apparent sunset, the drop off of the proportion of invalid points on day 133 (unexplained by Figure 4-6a alone) may be due to DAAC results successfully limiting night scenes starting on day 133. Also, in the evening period, the median of the good quality points in the model interest area above 0.10 at night is higher than the median of all other proportions of good quality points above 0.10. In other words, at night, MODIS reports that measurements are either very poor quality or very high quality. There is no proportion of good quality points between 0.20 and 0.80 at night and this study has not found an explanation for this result in the literature. This study can, however, attribute the lack of "abnormal" points and increase of "invalid points" at night to the poor reflectance of snow in low light. The evening points, in summary, contain less trustworthy information based on the night scenes with a high proportion of invalid points. Finally, the frequency of the proportion of cloud-covered points in the model area during the morning times and the evening times is compared: There are no points in the morning time interval with more than a 0.05 proportion of cloud coverage while every hour in the evening time interval has at least one scene with a 0.15 proportion of cloud coverage. Based on both these observations and conclusions made by Hall et al. (2001) (Section 2.2.2.1), the map comparison in this study uses the set of measurement scenes captured in the morning instead of set of measurement scenes captured in the evening.

Given the results described above, and the availability of TOPLATS input parameters for 2000, 2001, and 2002, the remainder of this study discusses the morning scenes for the year 2002, and focuses in particular, on the filtered observations in Figure 4-6. Of the three years discussed, this study has the most confidence in the measurements from the year 2002. The MODIS data from the year 2000 contains too many invalid scenes (Figure 4-4 and Figure 4-7). Data from 2001 does not contain any scenes in the middle third of the melt period. Although scenes like the one on day 143 at 20:15 in 2002 shown in Figure 4-6 look out of place in context with the two filtered scenes occurring before and after it, the number of available (including cloud-free) scenes in the year 2002 outnumbers the available scenes in the other two years. The 2002 measurements show two areas of persistent snow, that get progressively smaller (Figure 4-2b and Figure 4-6) more clearly than in 2000 and 2001. MODIS observations for the year 2002, therefore, can most appropriately be used to evaluate model output.

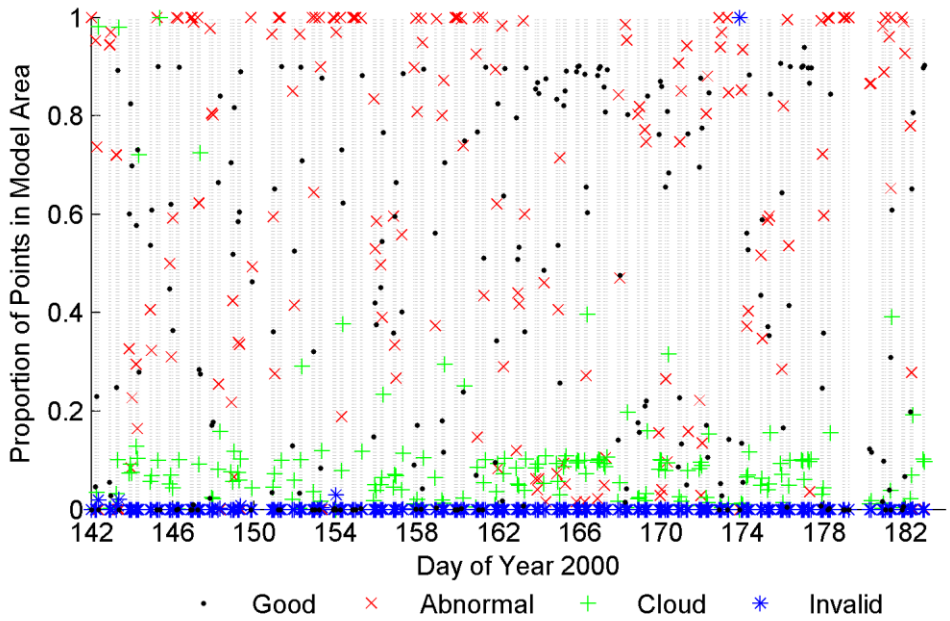

Figure 4-7a. Supporting Quality Assurance Information Versus Day of Year

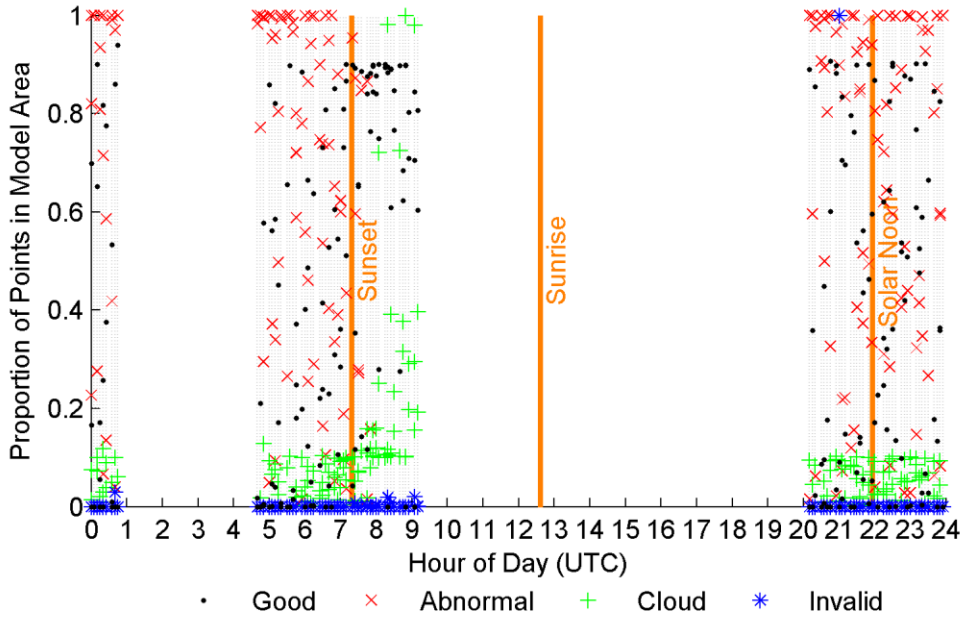

Figure 4-7b. Supporting Quality Assurance Information Versus Hour of Day

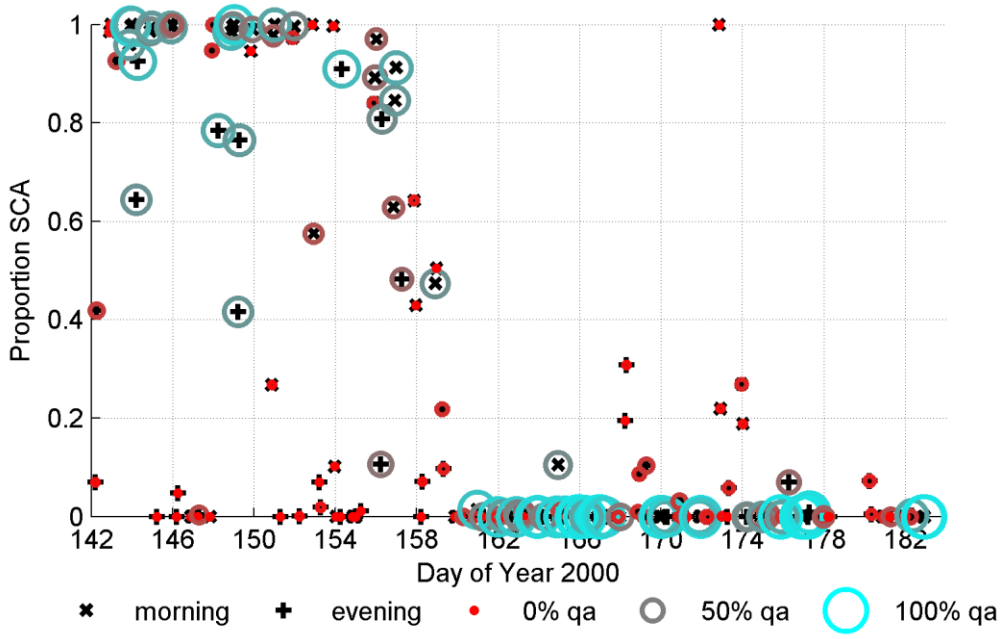

Figure 4-7c. SCA Versus Day of Year, Morning or Evening, and Quality Assurance

Figure 4-7 Year 2000 Quality Assurance, Collection Time, and Proportion SCA
MODIS reports four supporting quality assurance measures at each swath point. Figure 4-7a shows the proportion of each of these measures in every scene cropped by the model area in the GCS. Figure 4-7b shows the data from Figure 4-7a on an hourly basis in relationship to sunset, sunrise, and solar noon. The plot defines two measurement time periods — morning, which is close to solar noon and evening, which extends past sunset. Figure 4-7c combines Figure 4-7a, Figure 4-7b, and SCA reports. In Figure 4-7c, the larger, bluer, circles represent increasing proportions of good quality swath points within a model area scene. Figure 4-7a and Figure 4-7c share the same x-axis scale and range.

Good quality scenes during the year 2000 melt are almost all morning scenes. Read more about this figure in Section 4.1.2.

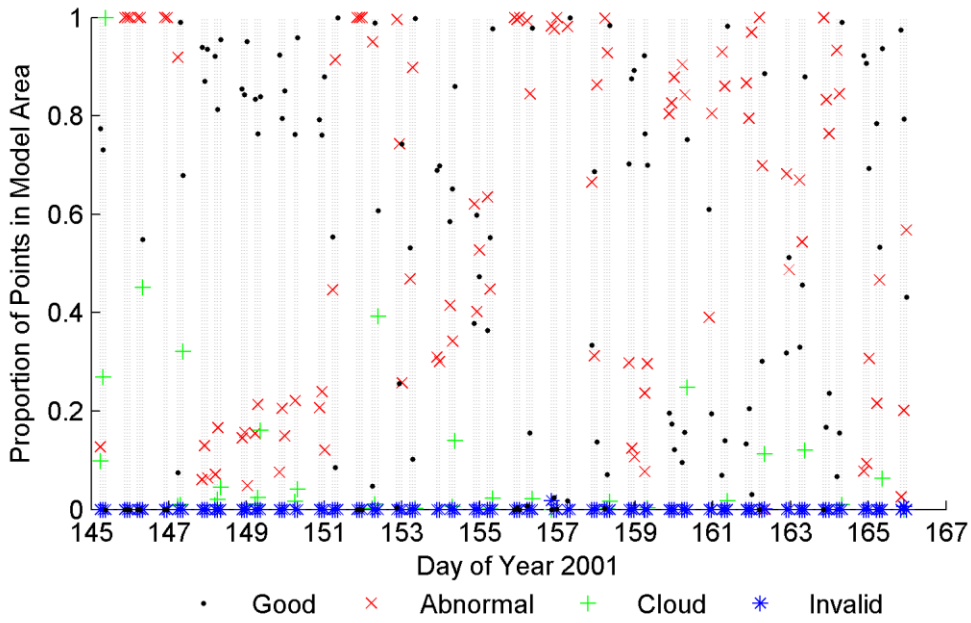

Figure 4-8a. Supporting Quality Assurance Information Versus Day of Year

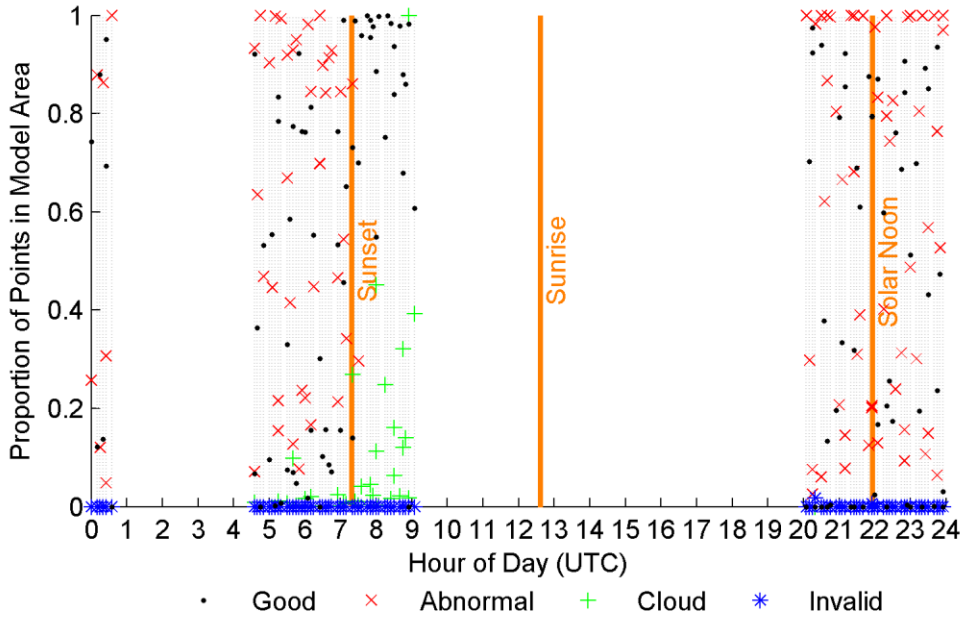

Figure 4-8b. Supporting Quality Assurance Information Versus Hour of Day

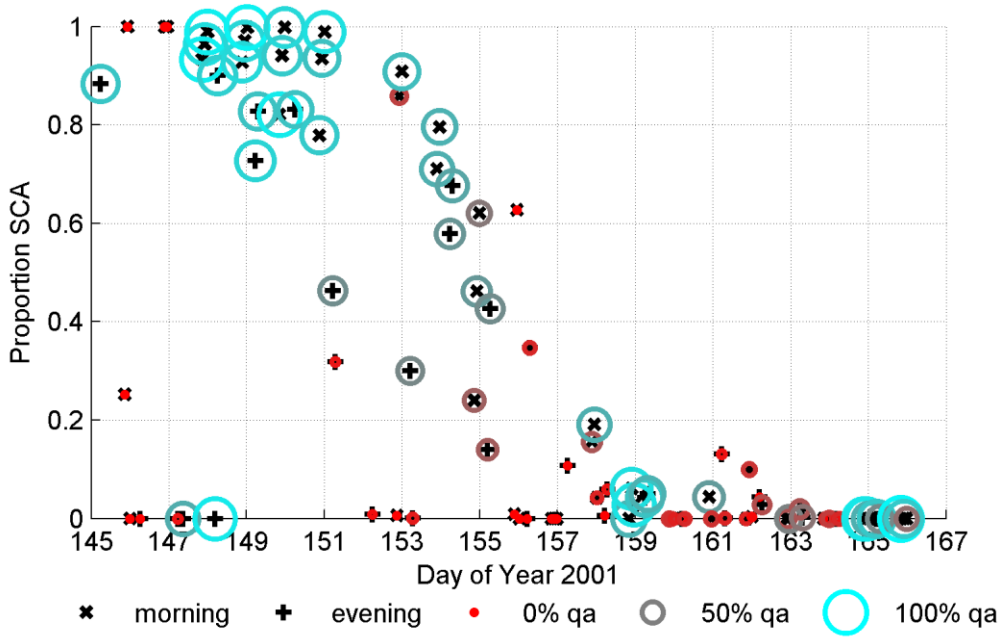

Figure 4-8c. SCA Versus Day of Year, Morning or Evening, and Quality Assurance

Figure 4-8. Year 2001 Quality Assurance, Collection Time, and Proportion SCA
This figure shows 2001 data in the same types of plots described in Figure 4-7. This study suspects evening points, like one with the medium-good quality but no SCA during the beginning of the melt on day 148, report invalid information due to the poor ability of MODIS to detect snow at times of the day far from solar noon. Section 4.1.2 analyzes this figure further.

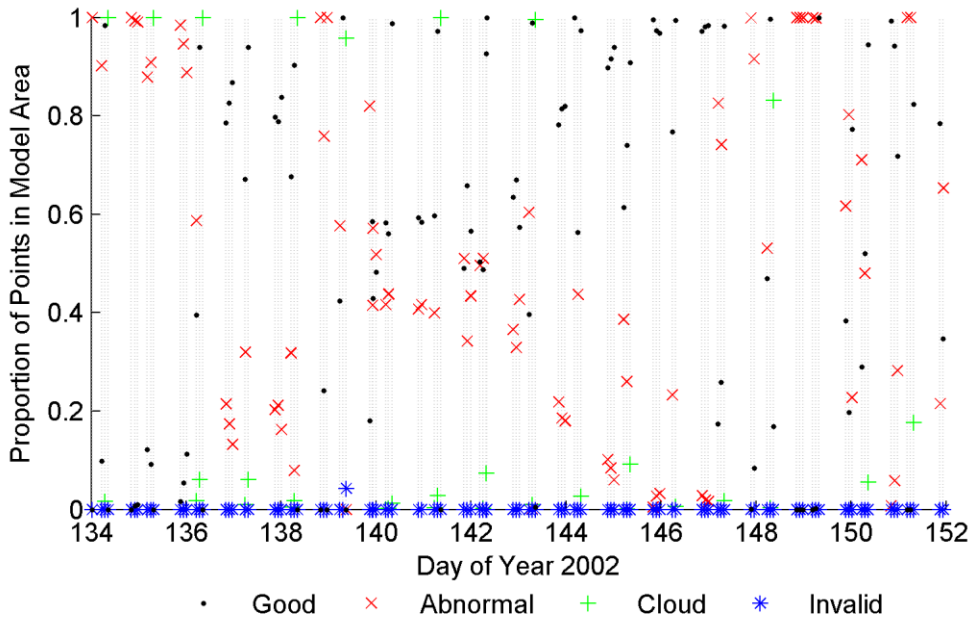

Figure 4-9a. Supporting Quality Assurance Information Versus Day of Year

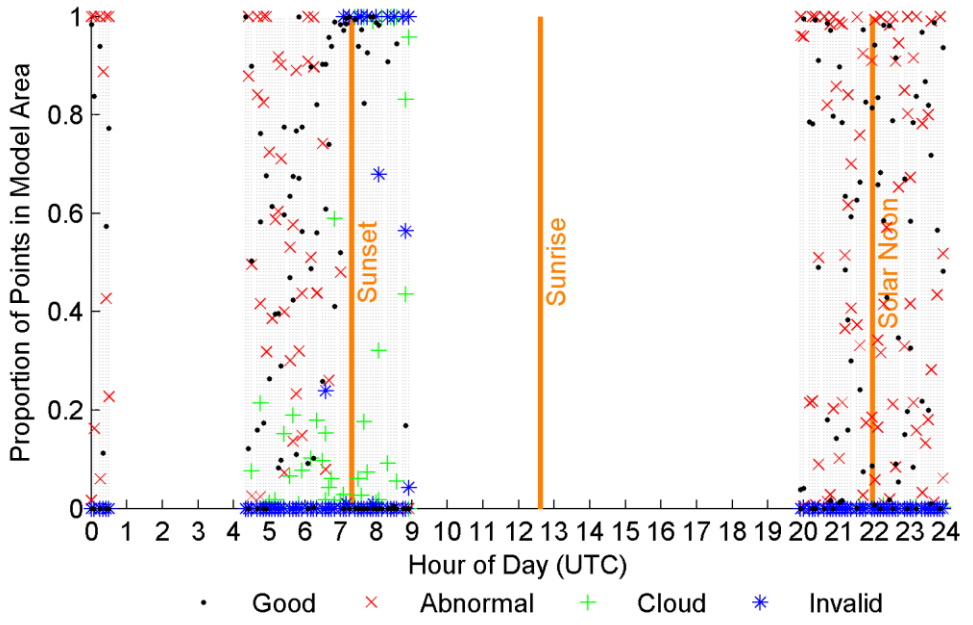

Figure 4-9b. Supporting Quality Assurance Information Versus Hour of Day

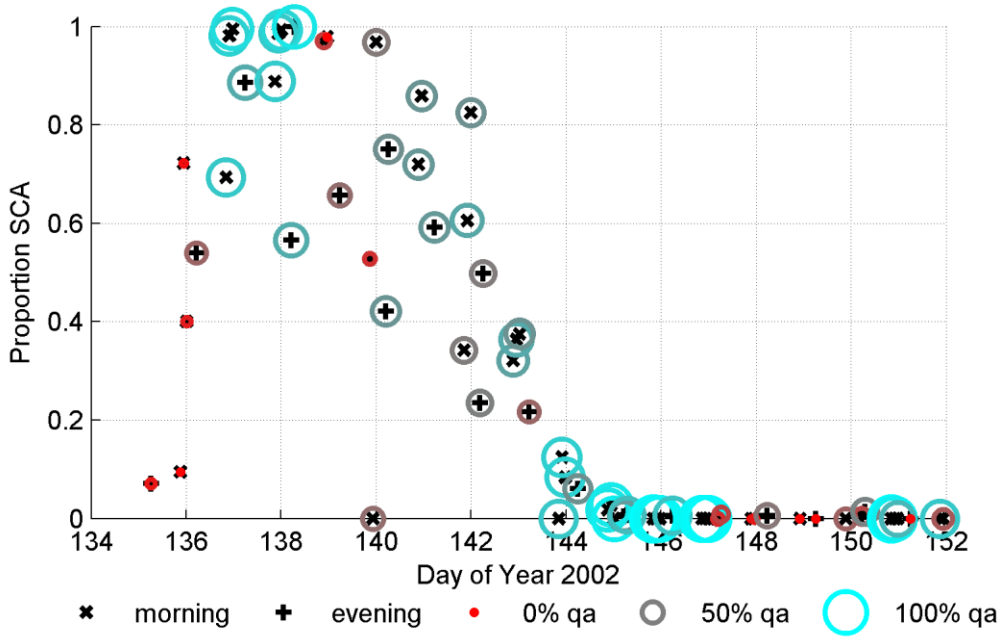

Figure 4-9c. SCA versus Day of Year, Morning or Evening, and Quality Assurance

Figure 4-9. Year 2002 Quality Assurance, Collection Time, and Proportion SCA
This figure shows 2002 data in the same types of plots described in Figure 4-8. Section 4.1.2 analyzes this figure further.

Figure 4-10 plots the minimum, likely, and maximum proportion SCA values that define the triangle-shaped probability density (PD) distributions described in Section 2.4.3.2. Plots are shown for (a) all scenes, (b) all morning scenes, and (c) all morning scenes with a 0.50 or greater proportion of good quality swath points. The figure reinforces the conclusion that a combination of measurement availability, collection time information, and supporting quality assurance information determines the overall usefulness of a series of measurements. The black circles in each scene represent the most likely proportion of SCA and the black lines represent the probability distribution. The red x points represent the least likely proportion of SCA and the green cross points represent the maximum proportion of SCA. In cloud-free scenes with 100% availability, the maximum and minimum proportion of SCA values are equal. Figure 4-10 marks these scenes with overlapping red x points and green + points; but for clarity, does not include black PDF lines which would extend infinitely on the PD axis. Additionally, Figure 4-10 hides the black PDF lines for scenes with 100% unavailable (in-part cloud obscured) pixels. The figure does show, however, the opposing minimum (0) and maximum (1) proportion of SCA values for these scenes. The PDF lines in these scenes, if they were shown, would form the apex of a triangle at a PD equal to 2 and at a proportion of SCA equal to 0.50, making the figure hard to read.

Figure 4-11 show the proportion of SCA for all morning scenes. Figure 4-12 shows the proportion of SCA for only morning scenes with a 0.50 or greater proportion of good quality swath points (Figure 4-10). Bothe figures show SCA for the whole watershed and each elevation zone. The plots show more scatter in the

higher elevation zones. The scatter, however, is likely due to the smaller sample sizes. (Figure 4-3 explains that zone one covers 3,015 pixels, zone two covers 4,173 pixels, zone three covers 1,184 pixels, and zone four covers 185 pixels.)

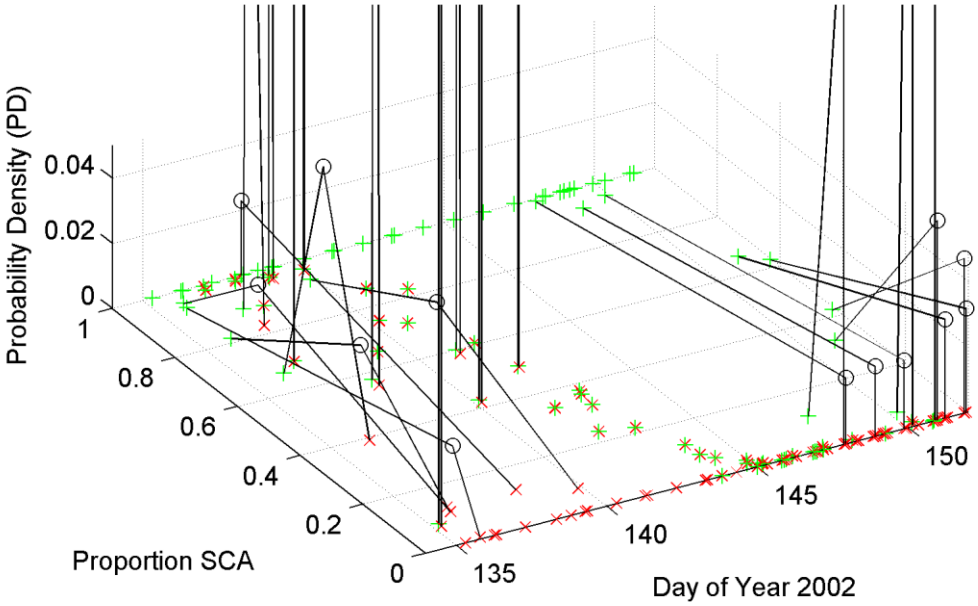

Figure 4-10a. All Scenes

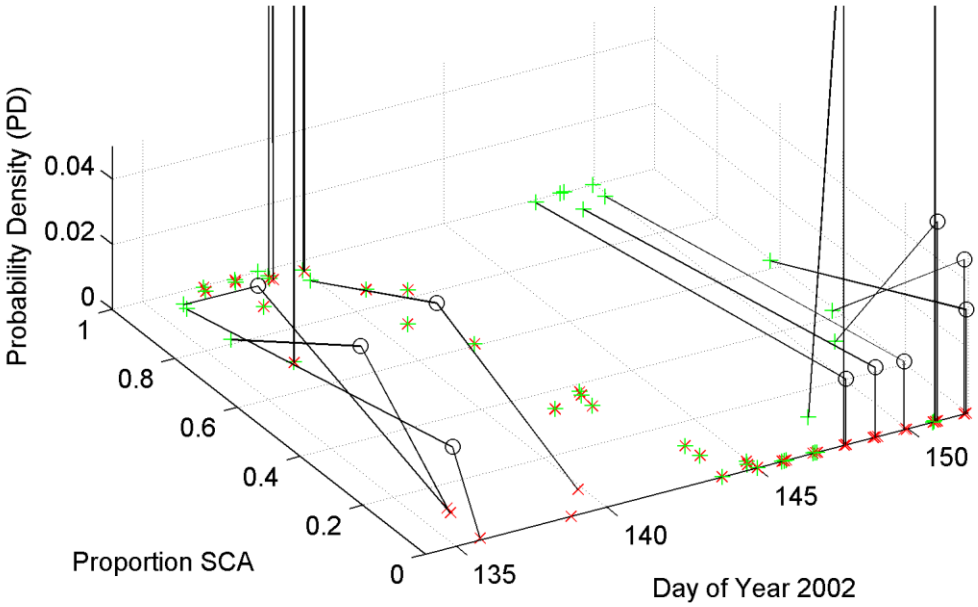

Figure 4-10b. Morning Scenes

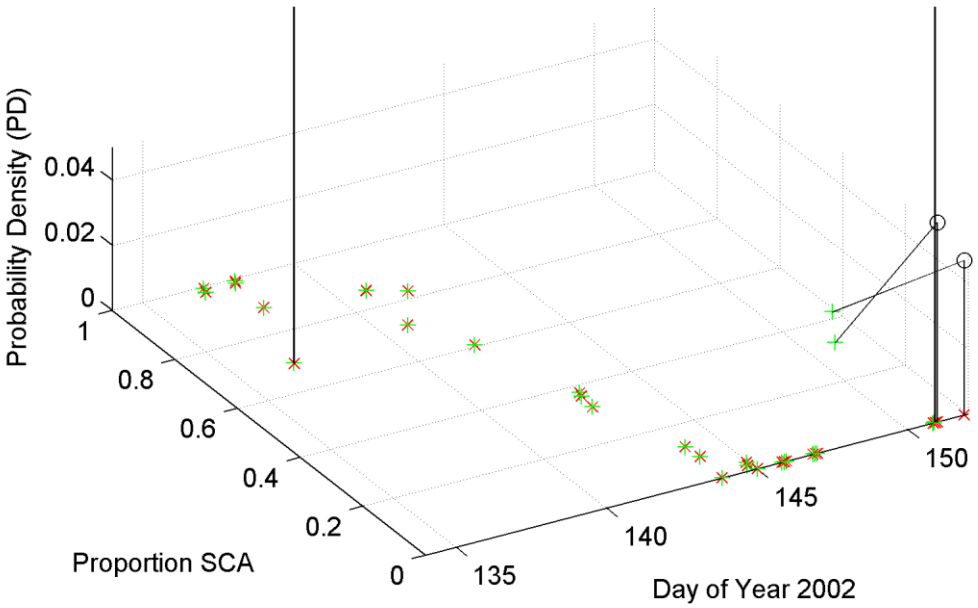

Figure 4-10c. Morning Scenes with a 0.50 or Greater Proportion of Good Quality Points

Figure 4-10. 2000 Probability as a Measure of Uncertainty
Probability density (PD) plots indicate increasing certainty of measurements from (a) all scenes to (b) morning scenes to (c) morning scenes with a 0.50 or greater proportion of good quality swath points. In each figure, the black lines represent the triangular proportion of SCA distribution, the red x points represent the minimum proportion of SCA and the green cross points represent the maximum proportion of SCA. The black circles represent the most likely proportion of SCA for scenes with any available points or scenes where the maximum proportion of SCA does not equal the minimum proportion of SCA.

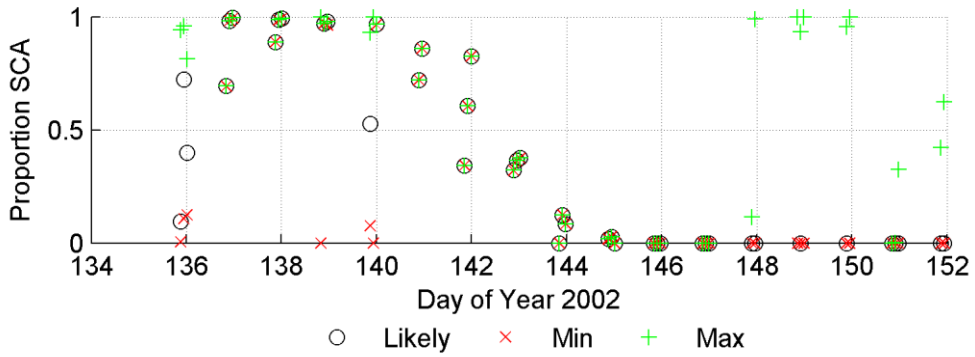

Figure 4-11a. Watershed

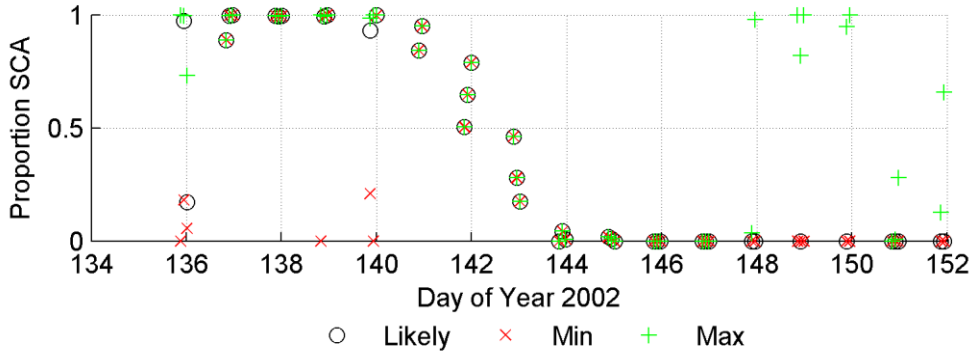

Figure 4-11b. Zone One

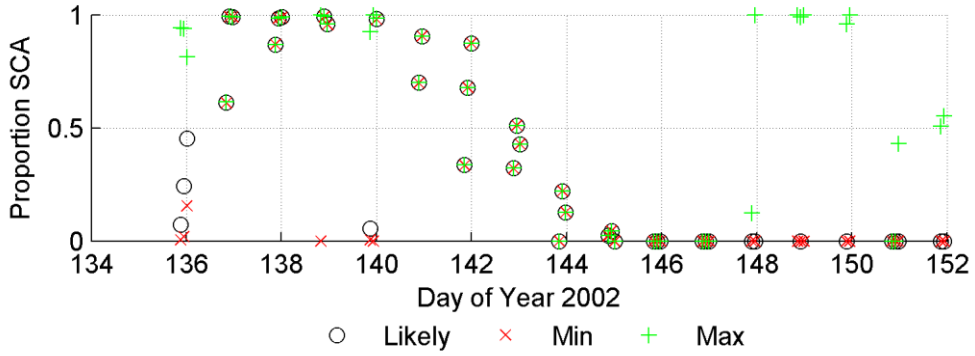

Figure 4-11c. Zone Two

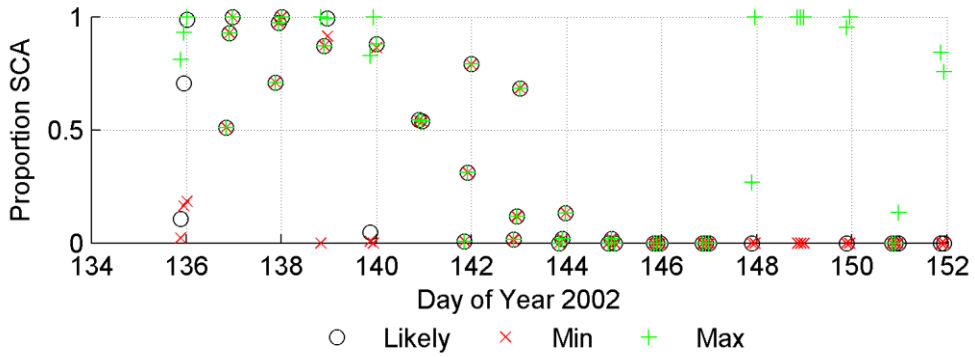

Figure 4-11d. Zone Three

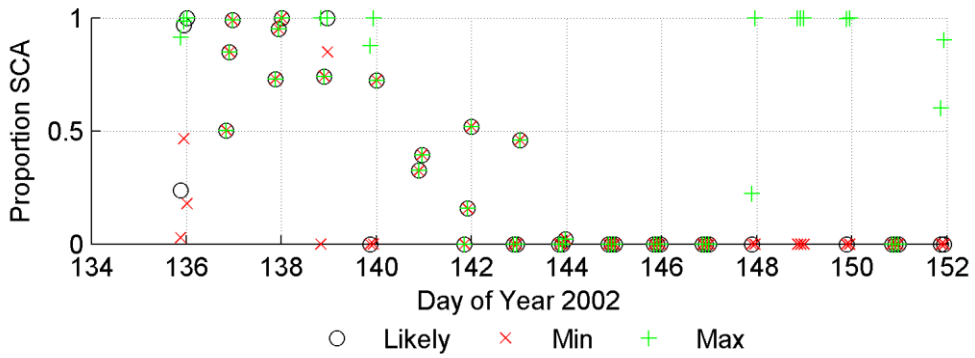

Figure 4-11e. Zone Four

Figure 4-11. 2002 Morning Scenes Across The UKRW and Four Elevation Zones
The proportion minimum, likely, and maximum SCA shown in Figure 4-10b are plotted for (a) the entire watershed and four elevation zones (b-e). Only, and all, morning scenes are shown.

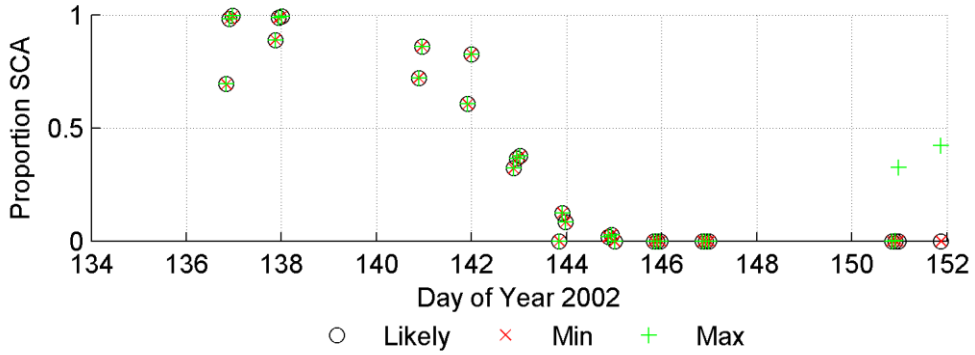

Figure 4-12a, Watershed

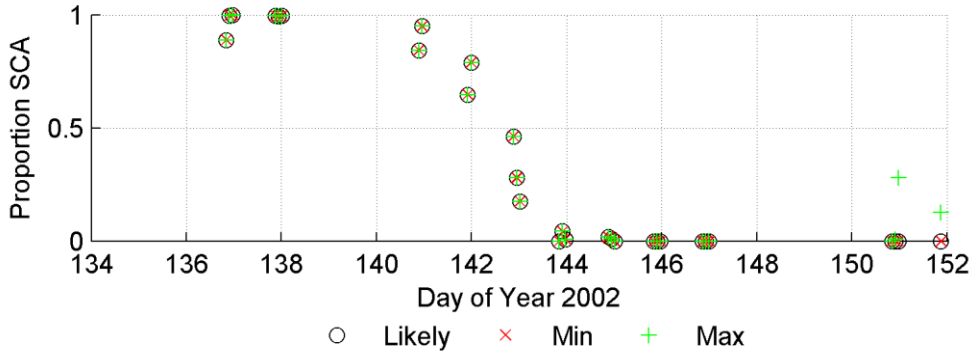

Figure 4-12b. Zone One

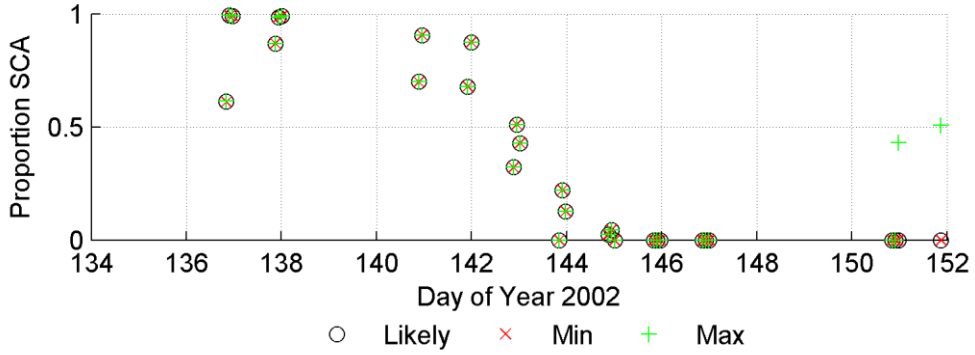

Figure 4-12c. Zone Two

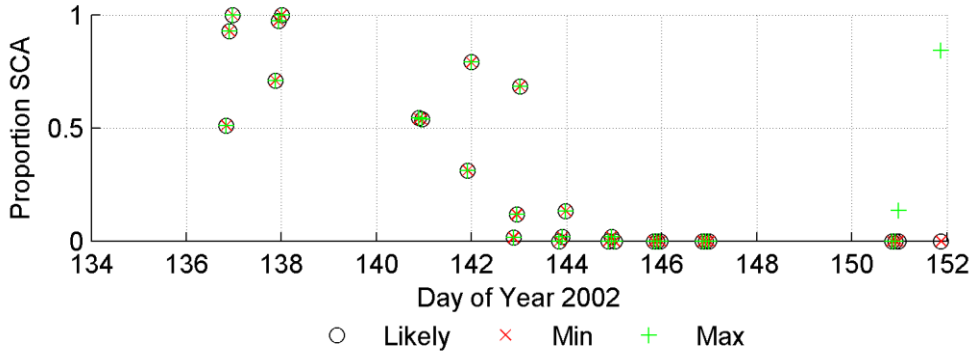

Figure 4-12d. Zone Three

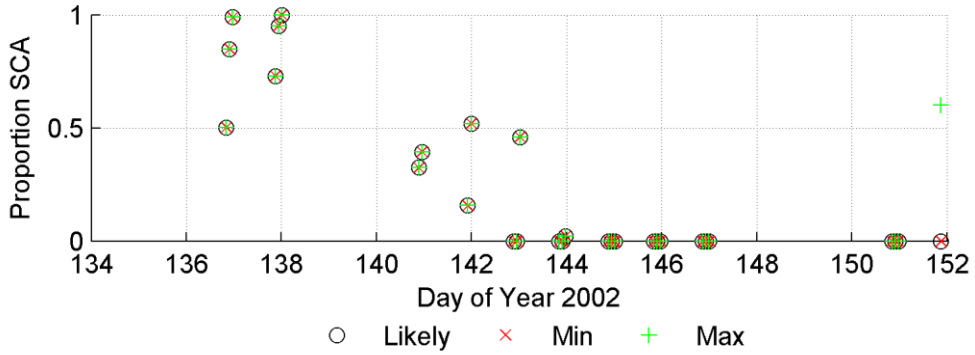

Figure 4-12e. Zone Four

Figure 4-12. 2002 Morning Scenes with a Proportion of 0.50 or Greater Good Quality Swath Points Across The UKRW and Four Elevation Zones
The proportion minimum, likely, and maximum SCA shown in Figure 4-10c are plotted for (a) the entire watershed and four elevation zones (b-e). Only, and all, morning scenes with a proportion of 0.50 or greater good quality swath points are shown.

4.2 MODEL SNOW MAPS

The USDA ARS at the Hydrology and Remote Sensing Lab helped perform the model runs to provide this study with model output maps at selected times corresponding to the MODIS scenes. Two parameters, in addition to DEM and adiabatic lapse rate (discussed in Section 2.3.1), drive model %SCA results: (a) the snow albedo, measured in a percentage of light reflected by the snow surface, and (b) the SWE threshold, which indicates the minimum millimeters of SWE to consider a model cell snow-covered. The model predicts a continuous SWE value in each pixel, whereas MODIS snow or snow-free categories. In order to make a comparison between these measures, a new parameter — SWE threshold — defines the value of SWE at a model pixel where that pixel is considered snow covered.

In a sensitivity study where snow albedo varies between trials, the model produced two simulated SWE maps for each trial: an overstory map and an understory map. This study uses the sum of the overstory SWE and the understory SWE. Raising the snow albedo lengthens the melt period by causing the snow to reflect more, and absorb less, of the incoming energy. In some trials, raising the snow albedo led TOPLATS to irrationally simulate snow accumulation during the melt period.

Section 4.2.1 discusses TOPLATS results independent of MODIS measurements and independent of any SWE threshold. It maps three TOPLATS scenes corresponding to the select 2002 scenes from Figure 4-6, and shows the effect of elevation on SWE results in the model. Section 4.2.3 shows the effect of three

SWE thresholds on SWE results in conjunction with MODIS SCA results. This section only discusses results from the year 2002.

4.2.1 Snow Water Equivalent

Figure 4-13 shows TOPLATS SWE maps for snow albedo values of 0.75, 0.80, and 0.85 for the (a) first, (b) middle (seventh), and (c) last scene of the select 2002 MODIS scenes shown in Figure 4-6. Figure 4-14, Figure 4-15, Figure 4-16, Figure 4-17, and Figure 4-18 show SWE means, SWE standard deviations, and box plots grouped by day for the entire watershed and each of four elevation zones during the 2002 melt period.

Figure 4-13 shows the effect of elevation on model results. Snow in the higher elevation zones, framed by Figure 4-3, depletes most quickly. The whitest areas in both Figure 4-13b for a 0.80 albedo and Figure 4-13c for a 0.85 albedo show that snow remains the longest along the river path. Figure 4-13 also indicates the model with the 0.80 albedo, without consideration to a SWE threshold, best predicts the 2002 MODIS measurements because the other two scenarios show complete snow melt on day 142 (albedo = 0.75) and incomplete snow depletion at the end of the melt period (albedo = 0.85). The mean watershed SWE and daily SWE boxplots shown in Figure 4-14 confirm this result.

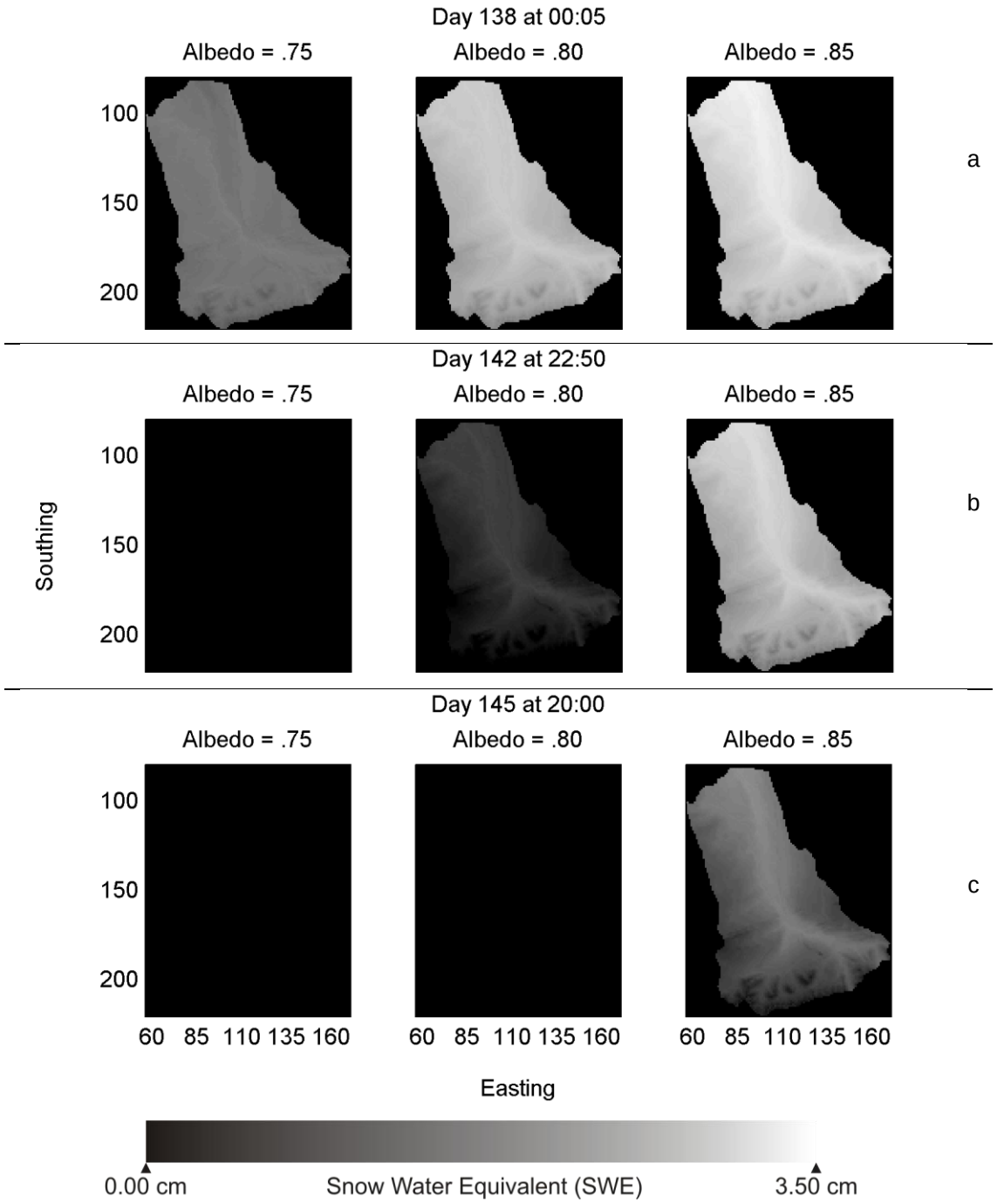

Figure 4-13 Select TOPLATS SWE Scenes for Albedo Values 0.75, 0.80, and 0.85
(a) On day 138, TOPLATS blankets each watershed with snow. (b) On day 142, the 0.75 albedo watershed has no snow and the 0.80 watershed has very little snow. (c) On day 151, after the measured melt, TOPLATS shows snow on the 0.85 map. Southing and easting coordinates reference the model coordinate system and interest area. Figure 4-6 shows respective MODIS scenes.

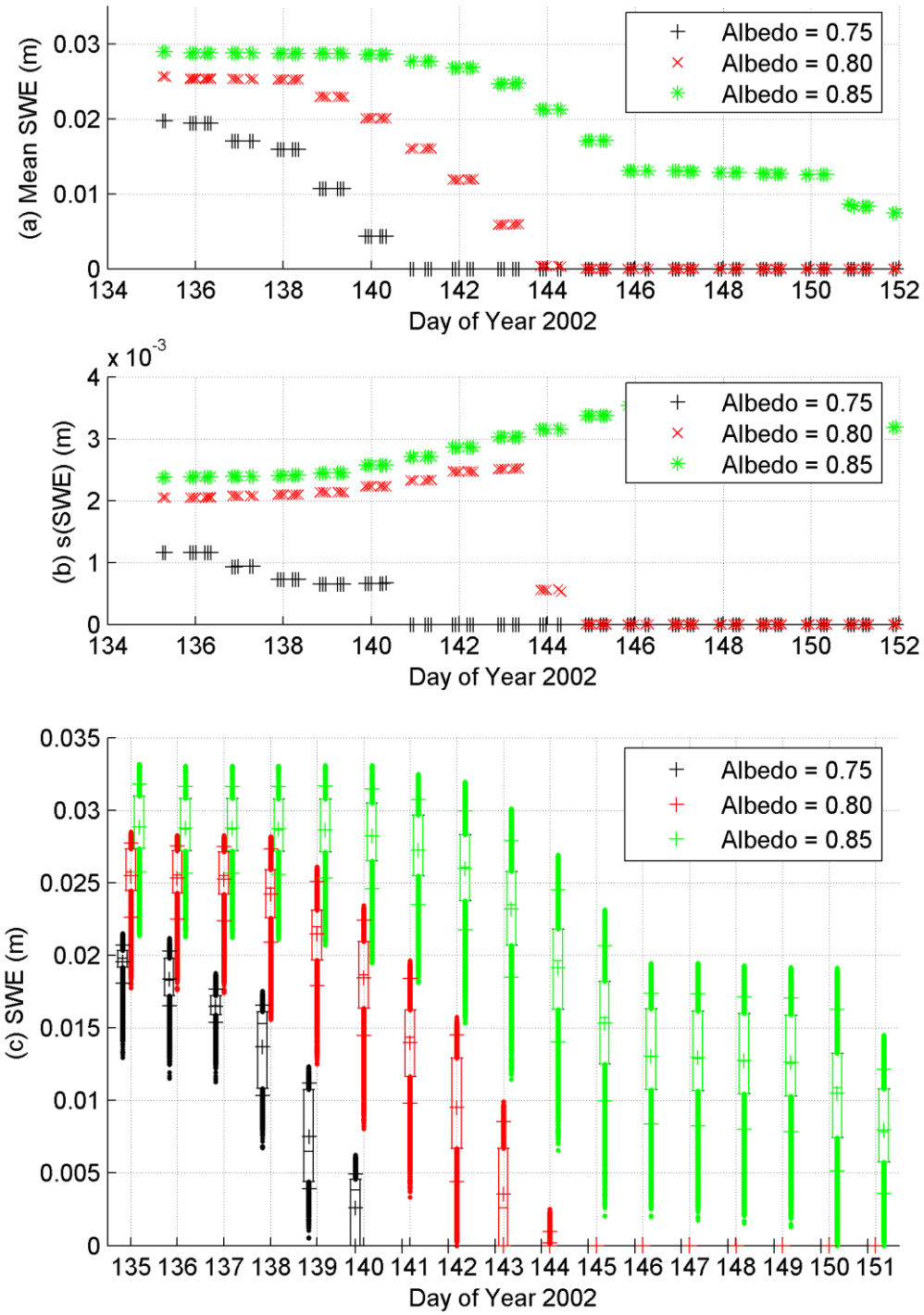

Figure 4-14 TOPLATS Watershed SWE (8,557 pixels)
(a) 8,557 SWE pixel values averaged over the watershed versus time confirm that the time for snow to melt increases with albedo. (b) The slope of the standard deviation of SWE for all pixels increases with albedo. (c) Box and whisker plots grouped by day show that the distribution is skewed with a relatively long tail below the twenty-fifth percentile. For each box, the line in the box is the median and the "+" in the box is the mean. The box encloses points above the twenty-fifth percentile and points below the seventy-fifth percentile. (The "+" whisker lines outside the box are the tenth and ninetieth percentile.)

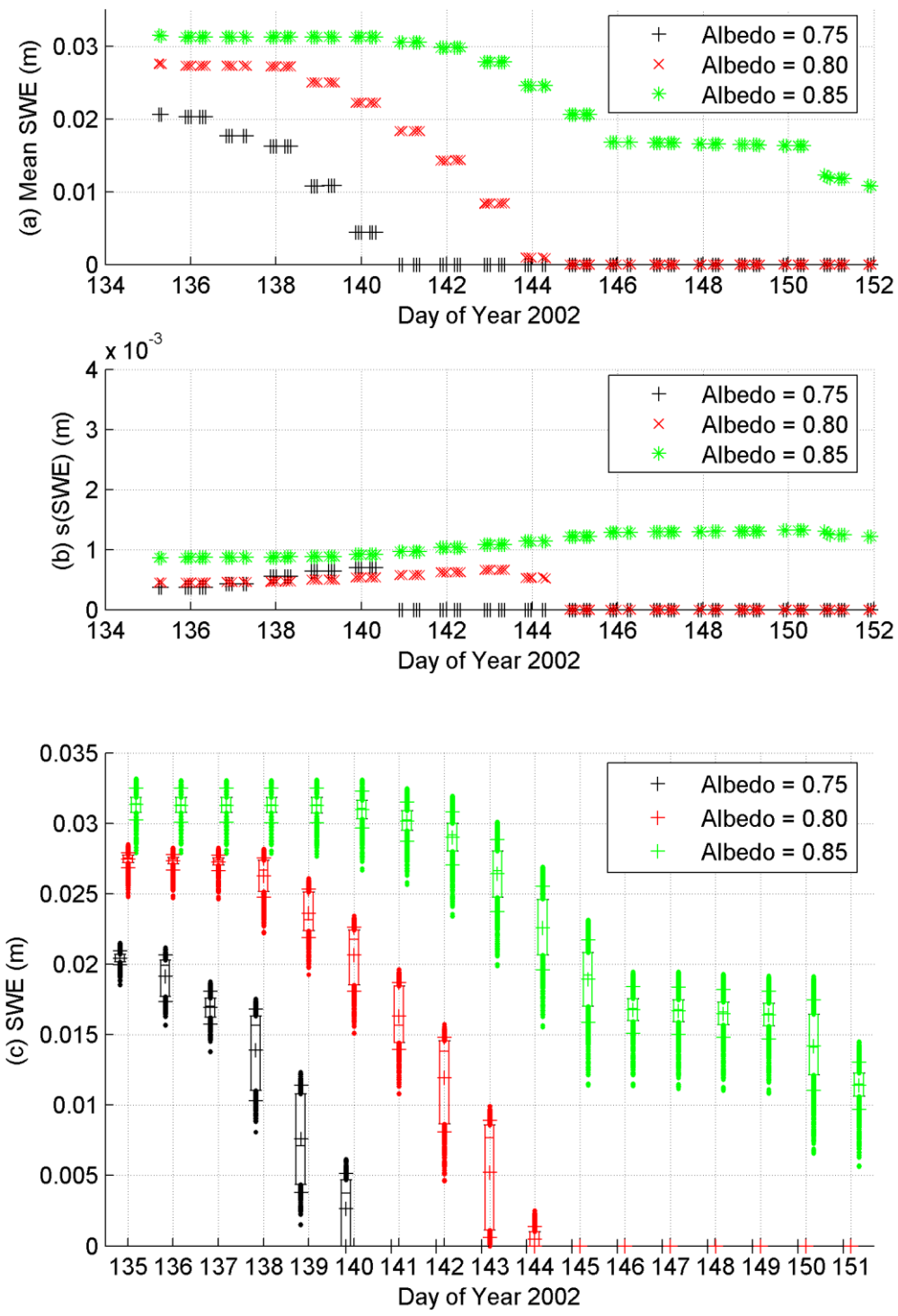

Figure 4-15 TOPLATS Zone One SWE (3,015 pixels)
Zone one pixels have the lowest elevation and reach the farthest north compared to the other two zones. (a) 3,015 zone one SWE pixel values start higher and end lower than the watershed SWE values for an albedo of 0.85. (b) Standard deviation values are lower than those for the entire watershed. (c) The range of SWE at each day in zone one is smaller than that shown in the entire watershed. See Section 4.2.1 for further analysis.

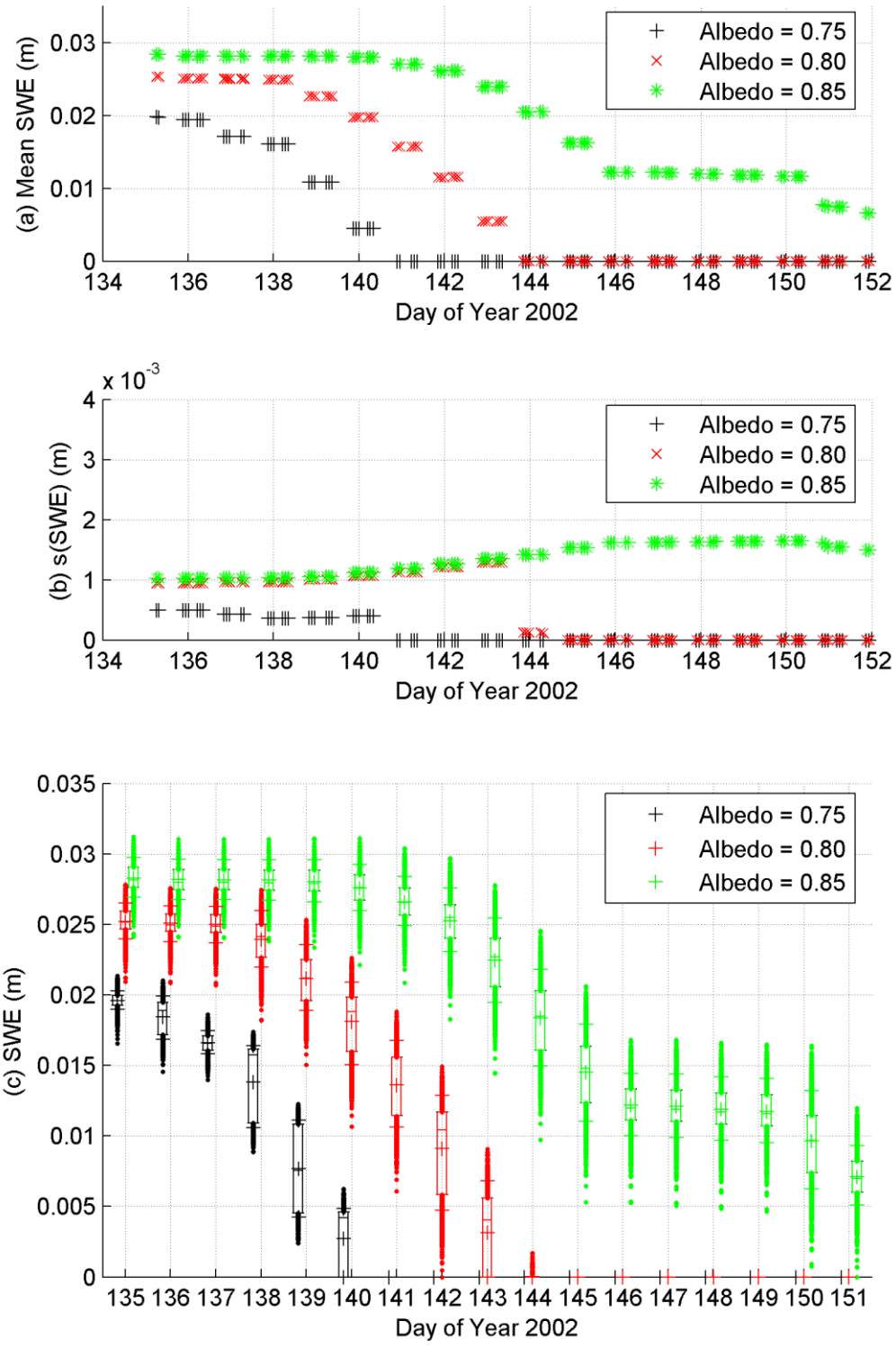

Figure 4-16 TOPLATS Zone Two SWE (4,173 pixels)
4,173 zone two SWE pixel values are overall lower than zone one values. The shorter melt causes the standard deviation values for the 0.80 albedo simulation and 0.85 albedo simulation to rise above standard deviation values in the zone one simulation.

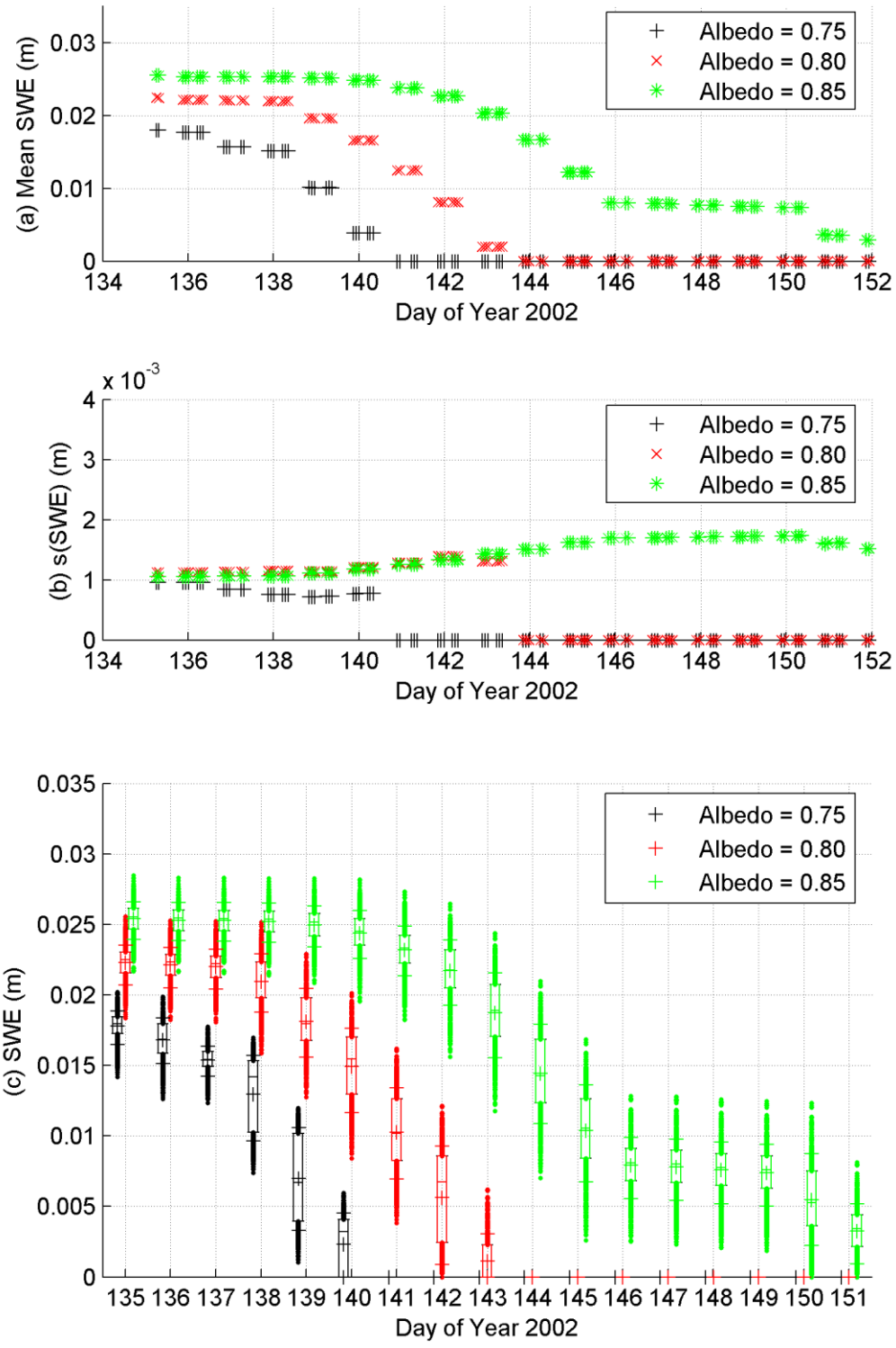

Figure 4-17 TOPLATS Zone Three SWE (1,184 pixels)
Zone three SWE values decrease faster than the lower elevation zones.

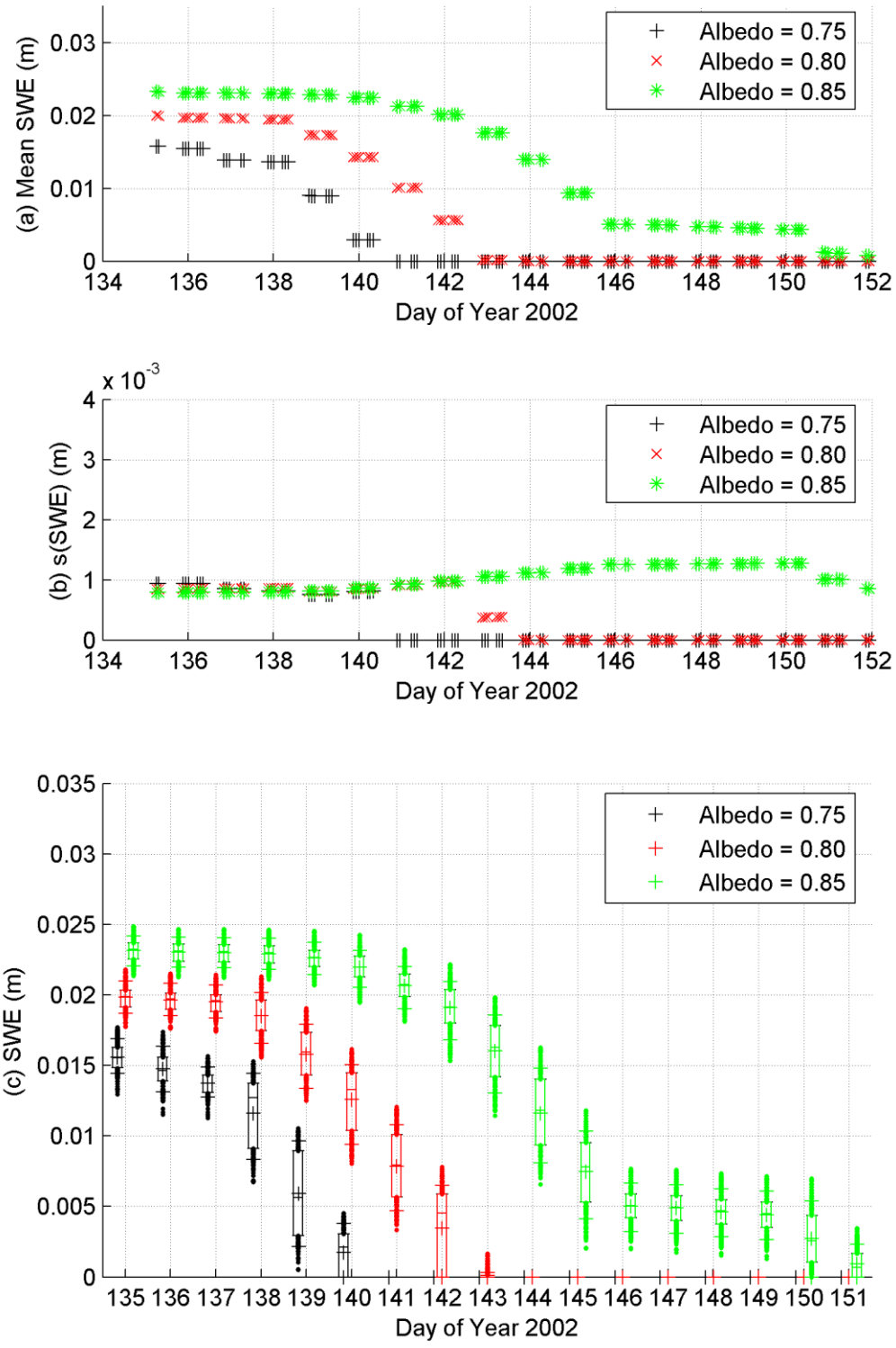

Figure 4-18 TOPLATS Zone Four SWE (185 pixels)
Zone four pixels have the highest elevations and are the farthest south compared to the other three zones. The SWE in the 185 pixels in zone four are the lowest compared to the other four zones. The time to melt, therefore, is the shortest compared to the other zones.

Figure 4-14, additionally, shows (a) a period of relatively constant SWE from day 146 to day 150 given an albedo of 0.85, (b) a decreasing SWE standard deviation in the 0.75 albedo series compared to an increasing SWE standard deviation in the 0.80 albedo series and the 0.85 albedo series, and (c) SWE values further below the 25% quartile than above the 75% quartile. The shape of the simulated SWE curve appears to match that of an arc more than the decreasing logistic function referenced by McCuen (2003) (Section 2.1.2).

In the 0.75 albedo series, the snow melts relatively quickly compared to the other two albedo series. The model reports no snow at the end of day 140. The mean SWE plot reveals snow melting in downward "steps" that each, shown in a zoom view, incline upward slightly with time. The mean SWE starts at 1.97 cm. In the 0.80 albedo series, snowmelt completes exactly four days (96 hours) after the melt completes with an albedo of 0.75 and the total SWE starts at 2.56 cm. During this time period, the SWE standard deviation and range increase over the melt period. In the 0.80 albedo series snowmelt completes well after the expected time period. The range and standard deviation of the SWE values increase throughout the simulation. The mean SWE starts at 2.89 cm and exceeds 1 cm through day 150.

Mean SWE model results for an albedo of 0.85 start higher and end lower in elevation zone one (Figure 4-15a) compared to watershed values (Figure 4-14a). Standard deviation values for zone one (Figure 4-15b) are lower than those for the entire watershed (Figure 4-14b) and increase during the beginning of the melt defined by the mean values. Box plots for zone one (Figure 4-15c) show that the range of SWE at each day in zone one is smaller than that shown in the entire watershed

(Figure 4-14c). The zone one boxes, whiskers, and minimum values are all larger than those in the entire watershed. The maximum values are close to those in the watershed. Zone two through four SWE values, therefore, should have lower SWE values than zone one. The time to melt in zone one appears to mirror that of the watershed.

Zone two SWE values shown in Figure 4-16a and Figure 4-16c are lower than zone one values shown in Figure 4-15a and Figure 4-15c. Given the 0.80 albedo box-plots in zone one and zone two, while melt completes in both series at day 145, the mean SWE value approaches zero more quickly (day 144) in zone two. The magnitude of the spread and standard deviation of the SWE values in zone two is close to that of zone one because they have similar sample sizes compared to the watershed. A shorter melt period in zone two compared to zone one causes the standard deviation of the 0.80 series to increase more rapidly from the beginning of the melt period through day 143 where it drops down to close to zero at the end of the 0.80 albedo melt on day 144. The standard deviation of the 0.75 series, conversely, decreases in zone two during the melt period compared to the increase in zone one.

Figure 4-17 shows that zone three SWE values decrease faster than the lower zones. Unlike zone one and zone two, during end melt for both the 0.80 albedo and the 0.85 albedo, on day 142, the standard deviation of the SWE values for the 0.80 albedo series is higher than that of the 0.85 albedo series. Also unlike lower zones, the 0.80 albedo series completely melts at day 144 compared to day 145. At the top of the watershed, SWE values shown in Figure 4-18 are the lowest and the melt period is the shortest. There is still snow on the ground, however, on the last simulated day

(day 151). The standard deviation values for all three albedo values in zone four are all almost the same until day 141 when the 0.75 albedo series melts. On day 143, the 0.80 series standard deviation series diverges from the 0.85 series standard deviation series because TOPLATS, at this time, completely depletes the snow in some partial areas of zone four.

4.2.2 Comparison with MODIS Maps

Two plots in Figure 4-19 compare SWE values from Figure 4-14a with MODIS SCA values on a second, overlapping axis. The first plot (Figure 4-19a) shows mean SWE values and the second plot (Figure 4-19b) shows the mean SWE values normalized by the minimum mean and maximum mean SWE values in the series. In each plot, blue circles mark the likely MODIS proportion SCA for each scene. Blue lines, capped with blue points, connect the minimum and maximum possible proportion SCA values (Section 2.4.3.2). Figure 4-20 shows a subset of the information in Figure 4-19 filtered by the morning scenes with a proportion of 0.50 good quality swath points. The MODIS measurements in this figure are the same as those plotted in Figure 4-12a. The uncertainty of MODIS measurements in this figure are the same as those plotted in Figure 4-10c. Fewer uncertainty lines in Figure 4-20 compared to Figure 4-19 confirm the finding described in Section 4.1 that morning scene measurements are less ambiguous than evening scene measurements. The two figures also confirm that the 0.75 albedo series depletes too quickly and the 0.85 series, even when it is normalized, depletes too slowly. Figure 4-20 suggests that the 0.85 series, normalized by the maximum mean SWE at the start of the series (2.89 cm) and the minimum

mean SWE at the end of the apparent MODIS melt period, around day 145, could be more comparable to the 0.80 series. Figure 4-21 tests this idea and reveals that if the normalized SWE series were used to indicate proportion SCA, the 0.85 albedo series would overestimate the MODIS proportion SCA more than the 0.80 albedo series would underestimate it.

In summary, plots of SWE and SCA show that the 0.75 albedo series time to melt is too short. The 0.80 albedo series and 0.85 albedo series, however, could both predict MODIS SCA depending on both the spatial variability of SWE values (shown in Figure 4-14 through Figure 4-18) and a SWE threshold.

Section 4.1 reviewed the MODIS measurements in terms of filters including collection time of day and quality assurance information. The section shows that measurements from the year 2002 can be trusted more than those from the year 2000 and 2001. In Section 4.2.1 and in Section 4.2.2, the SCA measurements from 2002 are compared with TOPLATS SWE model results in a sensitivity study for values of varying albedo. This section shows that while the 0.80 albedo simulation or the 0.85 albedo simulation could possibly predict the measured data, at least on a time-to-melt basis, the 0.75 simulation produces a brief melt time that under-predicts the observed melt time.

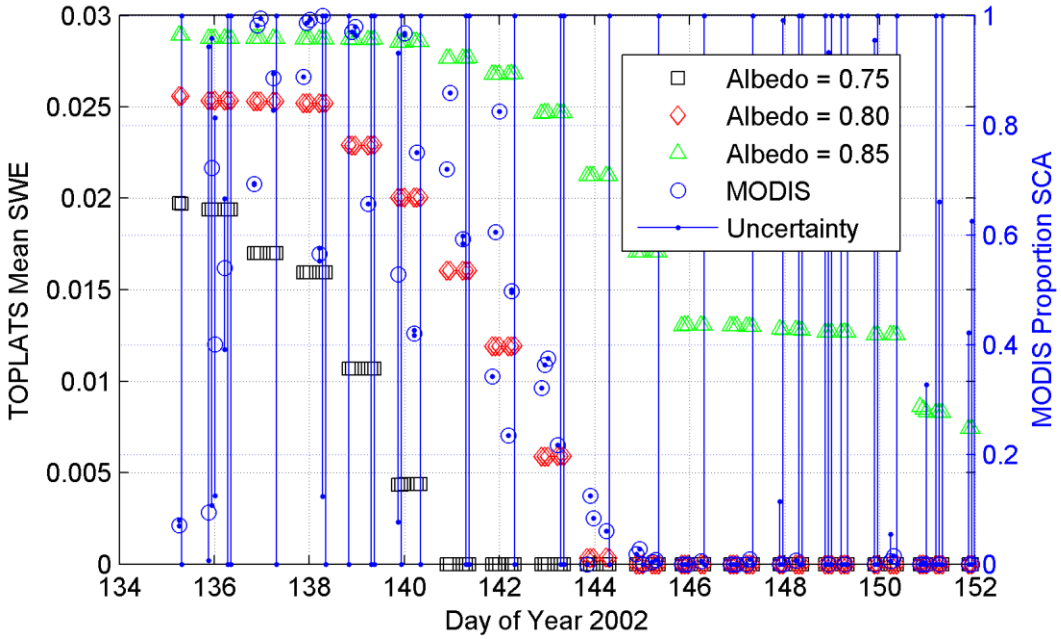

Figure 4-19a. Mean SWE (m)

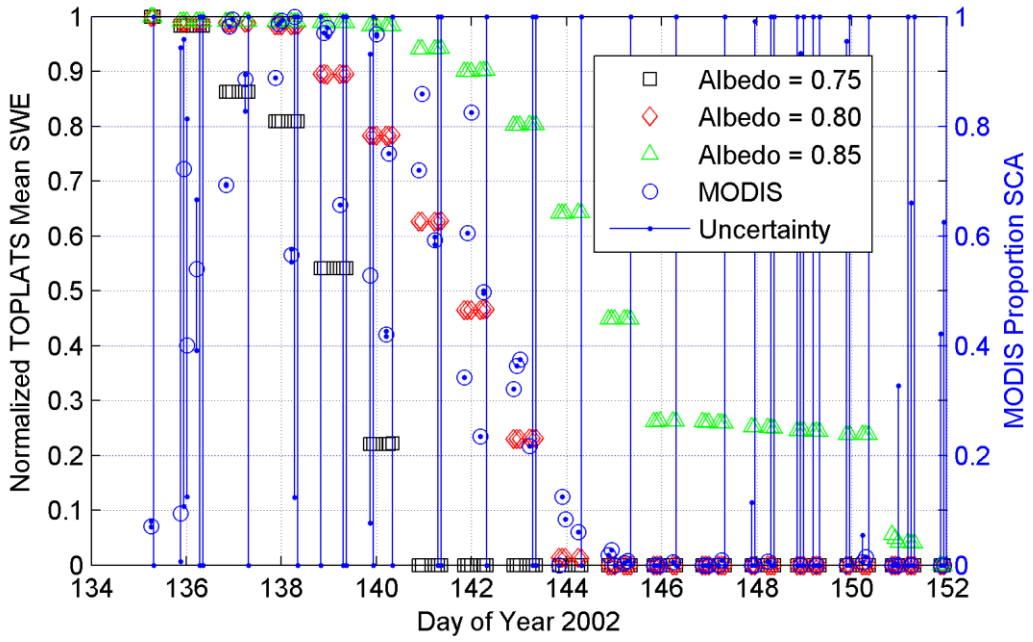

Figure 4-19b. Mean SWE Normalized by the Minimum, Mean, and Maximum Mean SWE

Figure 4-19 2002 Effect of the Albedo Parameter on SWE Model Results
TOPLATS pixel SWE values, averaged over the watershed, for snow albedo values 0.75, 0.80, and 0.85 (left axes) are shown with MODIS SCA (right axis, blue circles) from day 134 through 152. Plot b shows the SWE values normalized by the minimum, mean, and maximum mean SWE values in the watershed area.

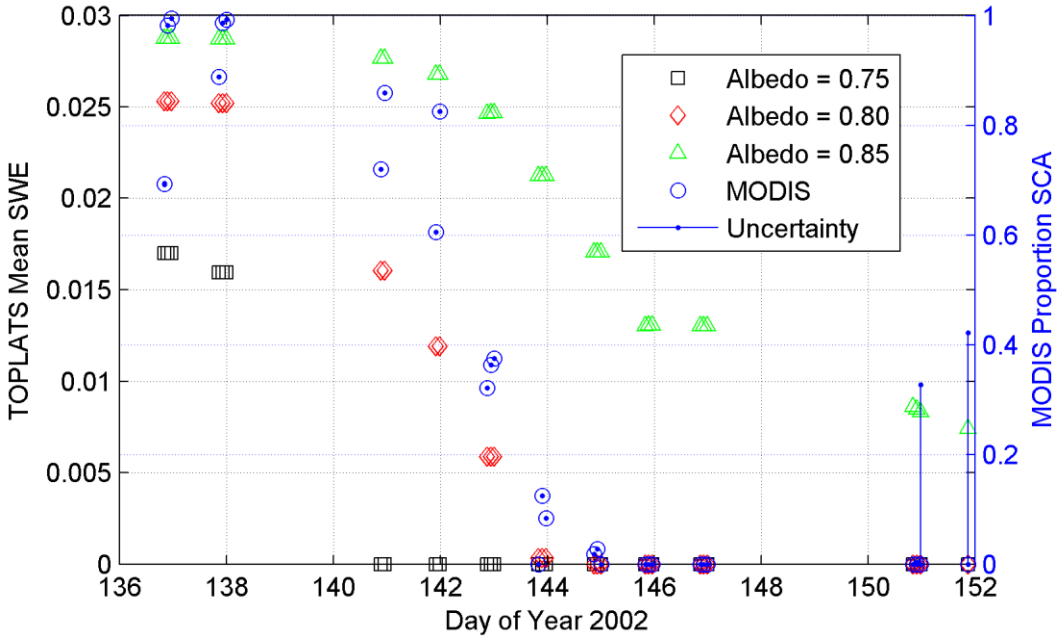

Figure 4-20a. Mean SWE (m)

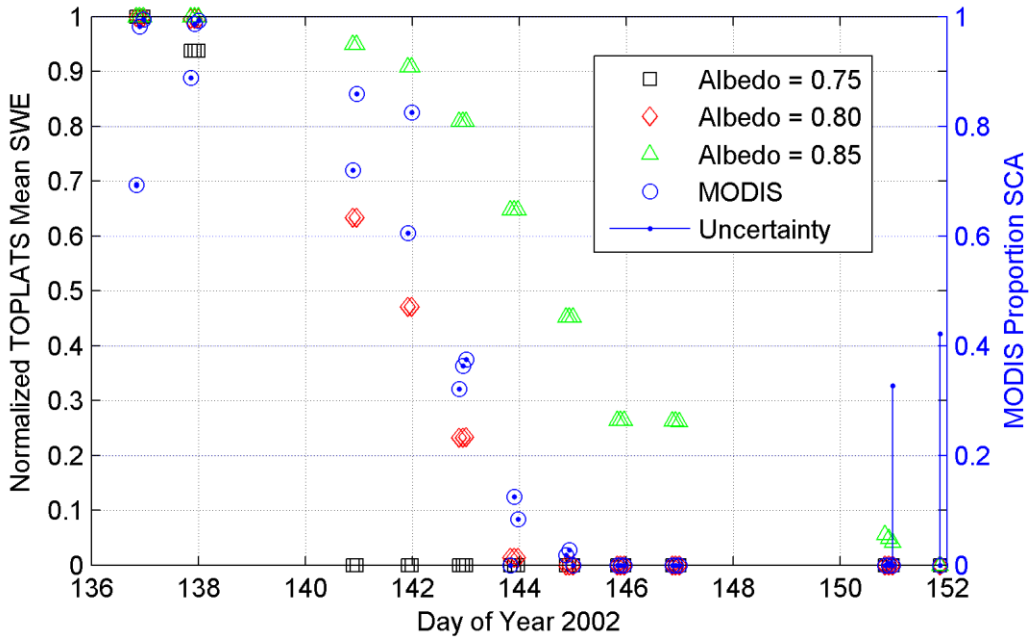

Figure 4-20b. Mean SWE Normalized by the Minimum, Mean, and Maximum Mean SWE

Figure 4-20 2002 Effect of the Albedo Parameter on SWE Model Results for Good Quality Morning Points
The morning scenes with a 0.50 or greater proportion of good quality swath points are shown on the same types of plots described in Figure 4-19.

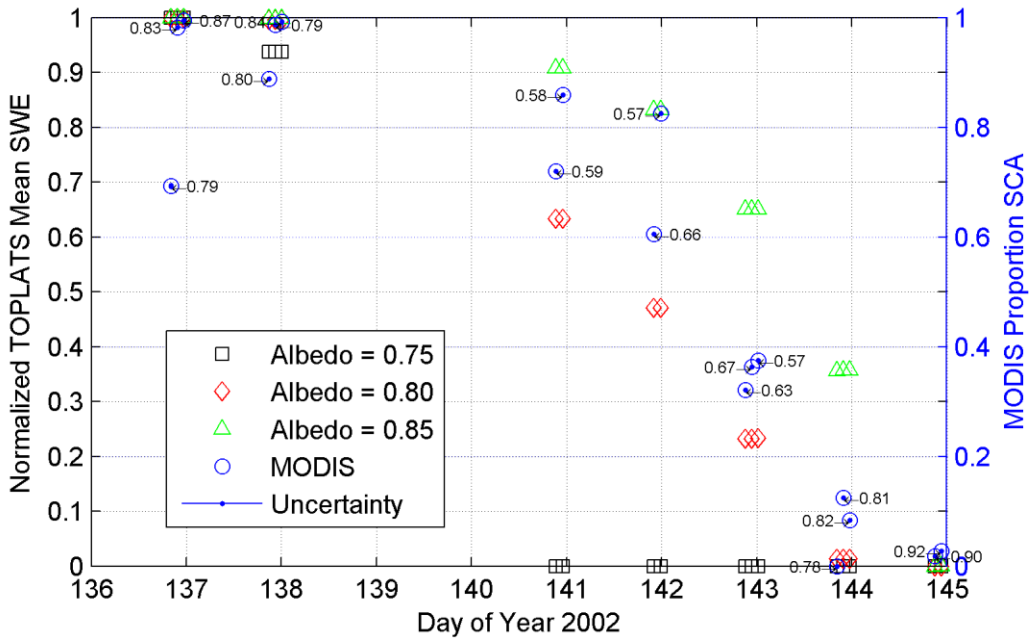

Figure 4-21 2002 Effect of the Albedo Parameter on SWE Model Results for Good Quality Morning Points Ending for All Scenes Measured Before The Apparent End of Melt on Day 146.

Compared to Figure 4-20, normalizing the 0.85 series over the shorter time interval makes the 0.85 series more comparable to the 0.80 series. The proportion of good quality swath points at each scene, labeled with black text, however, shows that higher quality scenes lie closer to the 0.80 series than the 0.85 series.

4.2.3 Snow Covered Area Threshold

Converting the continuous SWE values from the model output to binary snow/snow-free values is necessary for comparing model maps to the MODIS maps. The SWE threshold parameter (Section 3.2.1) determines the minimum SWE for any pixel in any scene for this study to consider that pixel snow covered. The mean SWE and normalized mean SWE plots help seed the selection of this SWE threshold: Figure 4-20a suggests the SWE threshold seed for the 0.80 albedo series starts at 0 m because the mean SWE series depletes before the MODIS SCA series does; raising the threshold for this series would lower the mean SWE values yielding an even earlier time of depletion at some locations. For the 0.85 albedo series, Figure 4-20a suggests seeding the SWE threshold between 1 cm and 1.5 cm where the snow melts at day 145. The SWE distributions marked with box-plots in Figure 4-14c, however, shows that these thresholds need to be expanded to consider the distribution of SWE values about the mean. Therefore, given these seed values and box-plots, a fair comparison between the 0.80 albedo series and the 0.85 albedo series considers SWE thresholds from 0.00 cm to 3.00 cm in 0.25 cm increments.

With the TOPLATS SWE maps converted to TOPLATS categorical maps using the SWE threshold, quantitative map comparison analysis, using the methods of Section 3.2, is possible. The first two plots in Figure 4-22a through Figure 4-22f (i) compare MODIS and TOPLATS proportion SCA and (ii) show the proportion of agreement between the two maps, both due their initial arrangement and in consideration of a random relocation of cells, for a 0.80 albedo. The first two plots in Figure 4-23a through Figure 4-23f show similar information for a 0.85 albedo

simulation. Both Figure 4-22 and Figure 4-23 only show select plots relevant to their respective albedo values.

The proportion SCA comparison in Figure 4-22a, which employs the 0.00 cm SWE threshold seed value inferred from Figure 4-20a shows the 0.80 albedo TOPLATS series over predicting for the MODIS observations. In Figure 4-22b, the 0.75 cm SWE threshold model data gets closer to the TOPLATS data, especially at the beginning and end of day 141. The modeled proportion of SCA at the end of day 141 in Figure 4-22c, for a 1.00 cm SWE threshold, lies the closest to the measured SCA data than that in any marker shown in Figure 4-22 – but the prediction of SCA on day 143 is too close to zero compared to a measurement of 0.40 proportion SCA. Therefore, based on the SCA and proportion of agreement plots alone, the 0.75 cm SWE threshold series shown in Figure 4-22b best predicts the MODIS measurements for the 0.80 albedo. Figure 4-23, similarly, shows that the 2.50 cm SWE threshold series (Figure 4-23d) best predicts the MODIS observations for the 0.85 albedo. Figure 4-24 shows the absolute maximum error in the 0.80 series is higher than then the 0.85 series on every day except for day 142. Overall, the 0.85 albedo series with a 2.50 cm SWE threshold best matches the MODIS measurement scenes.

This section focuses on SCA and proportion of agreement results. The following section discusses the Kappa statistics for the 0.80 albedo results (Figure 4-22) and 0.85 albedo results (Figure 4-23).

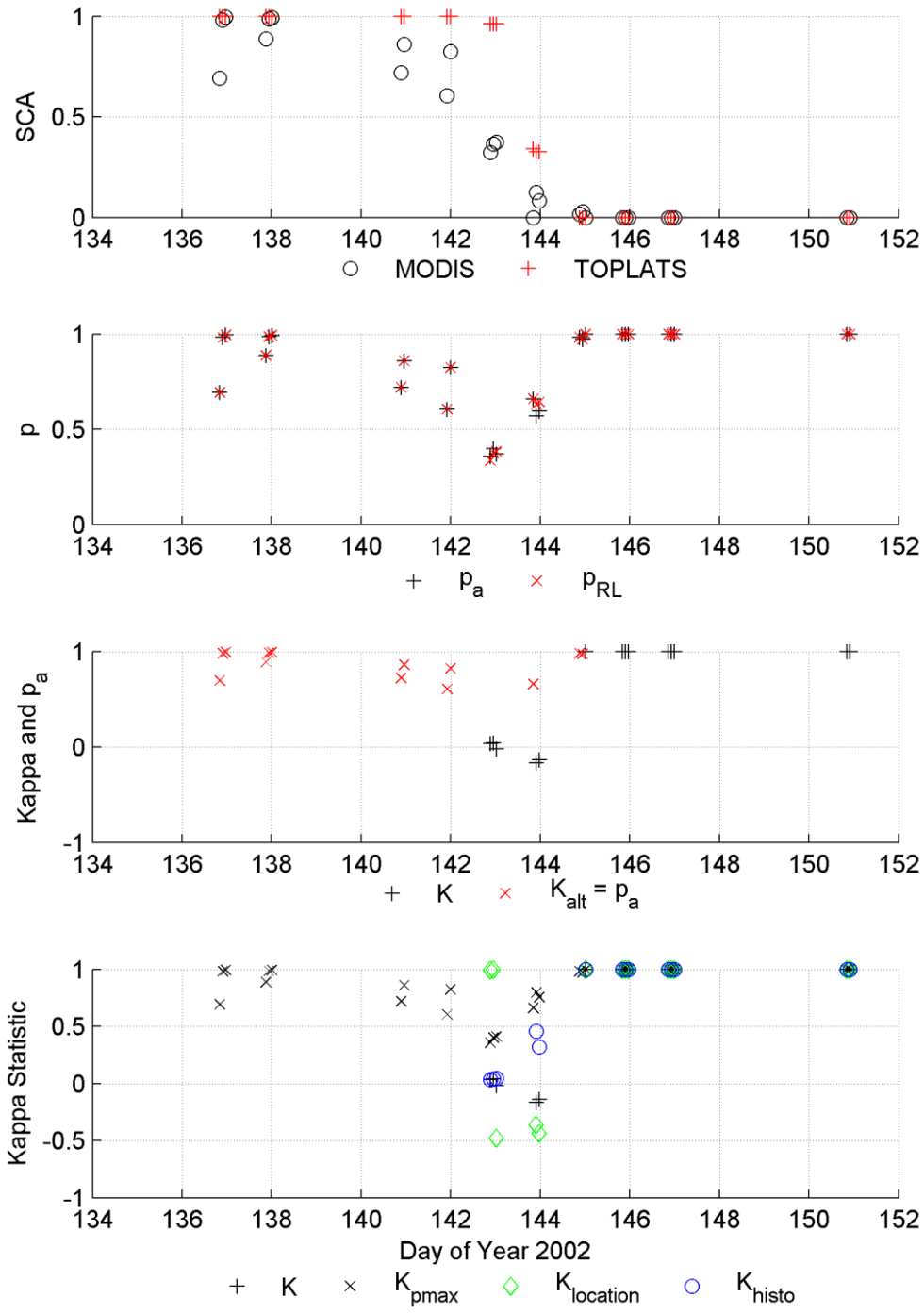

Figure 4-22a 0.00 cm SWE Threshold (Year 2002, 0.80 Albedo)

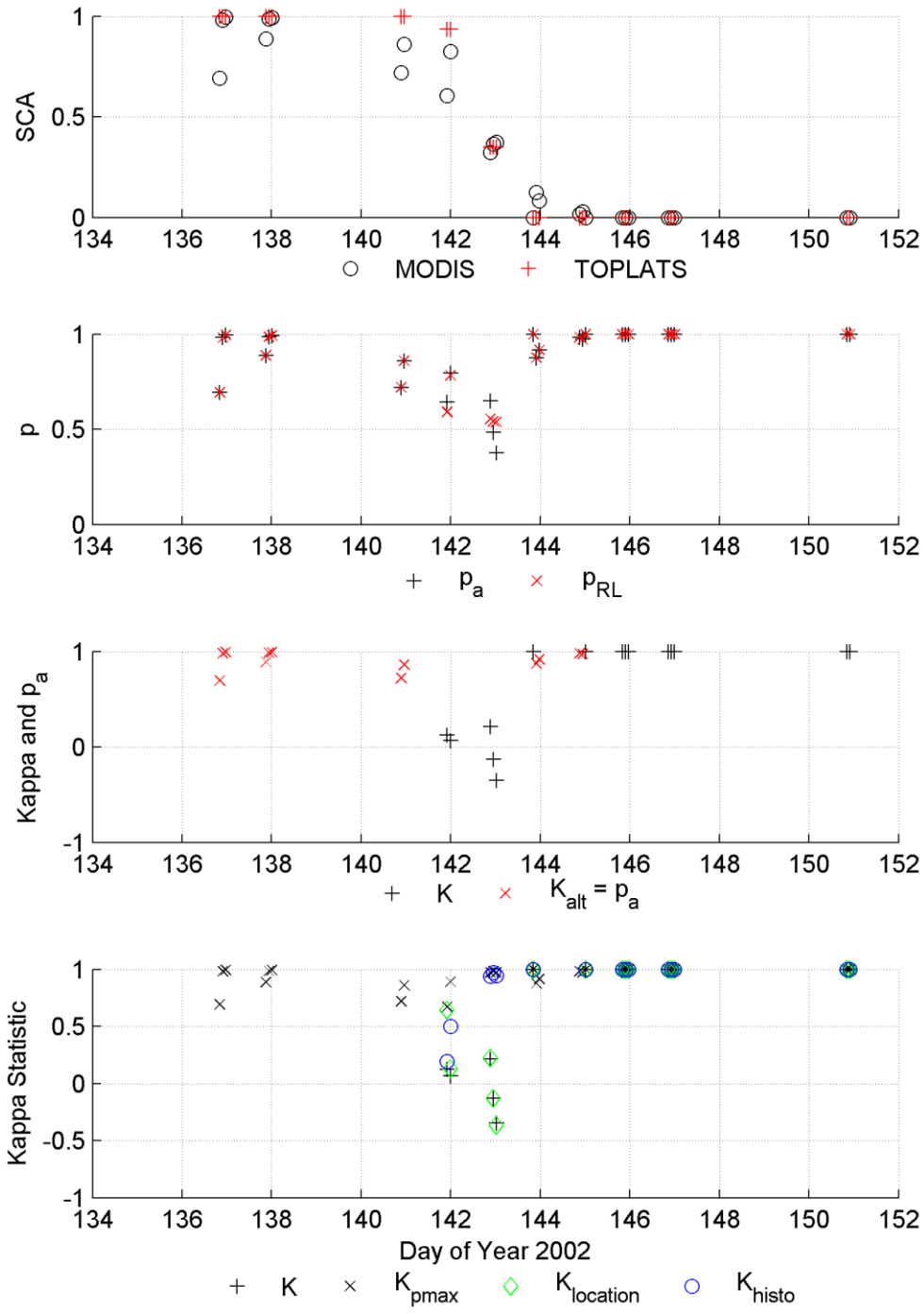

Figure 4-22b 0.75 cm SWE Threshold (Year 2002, 0.80 Albedo)

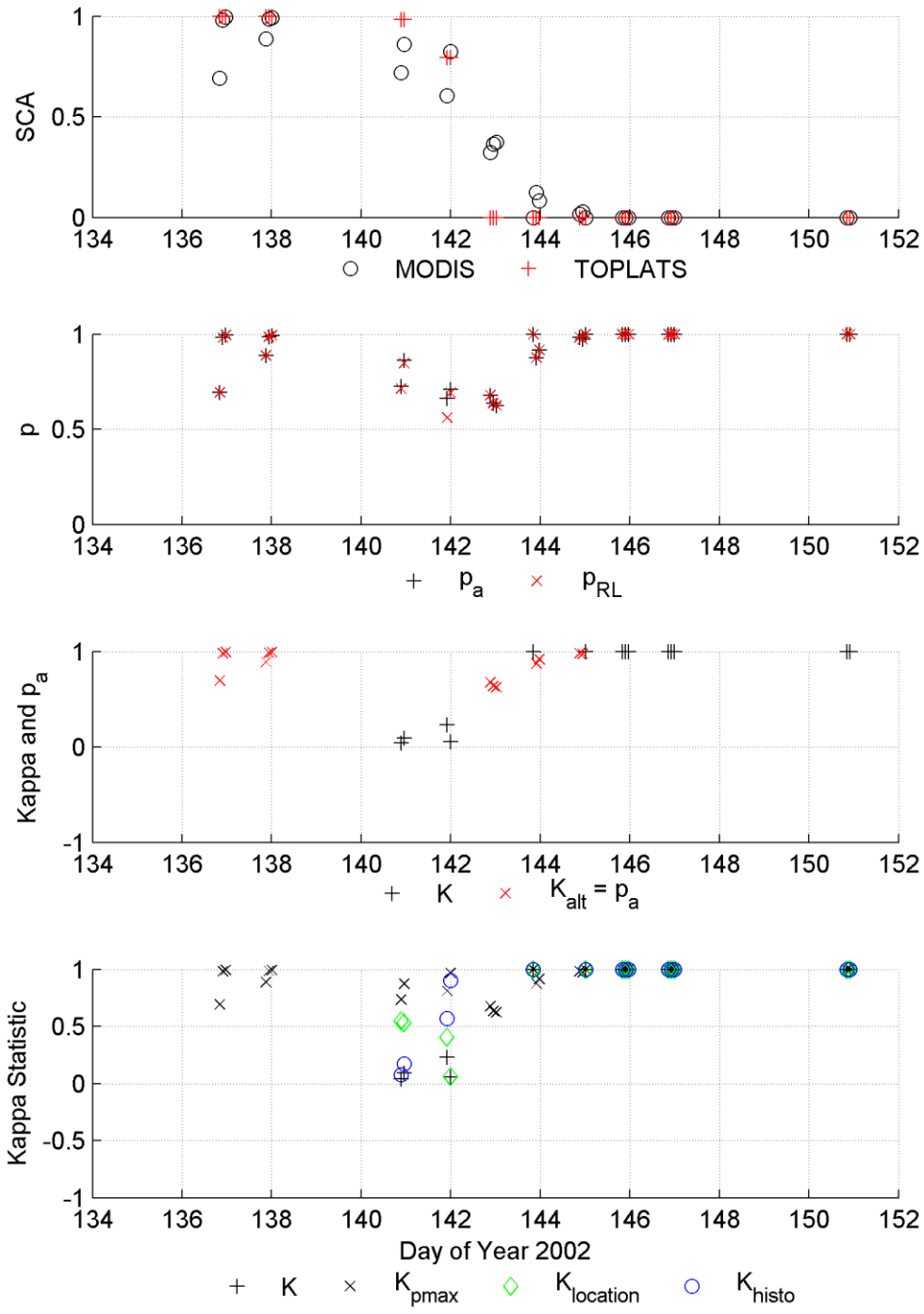

Figure 4-22c cm 1.00 SWE Threshold (Year 2002, 0.80 Albedo)

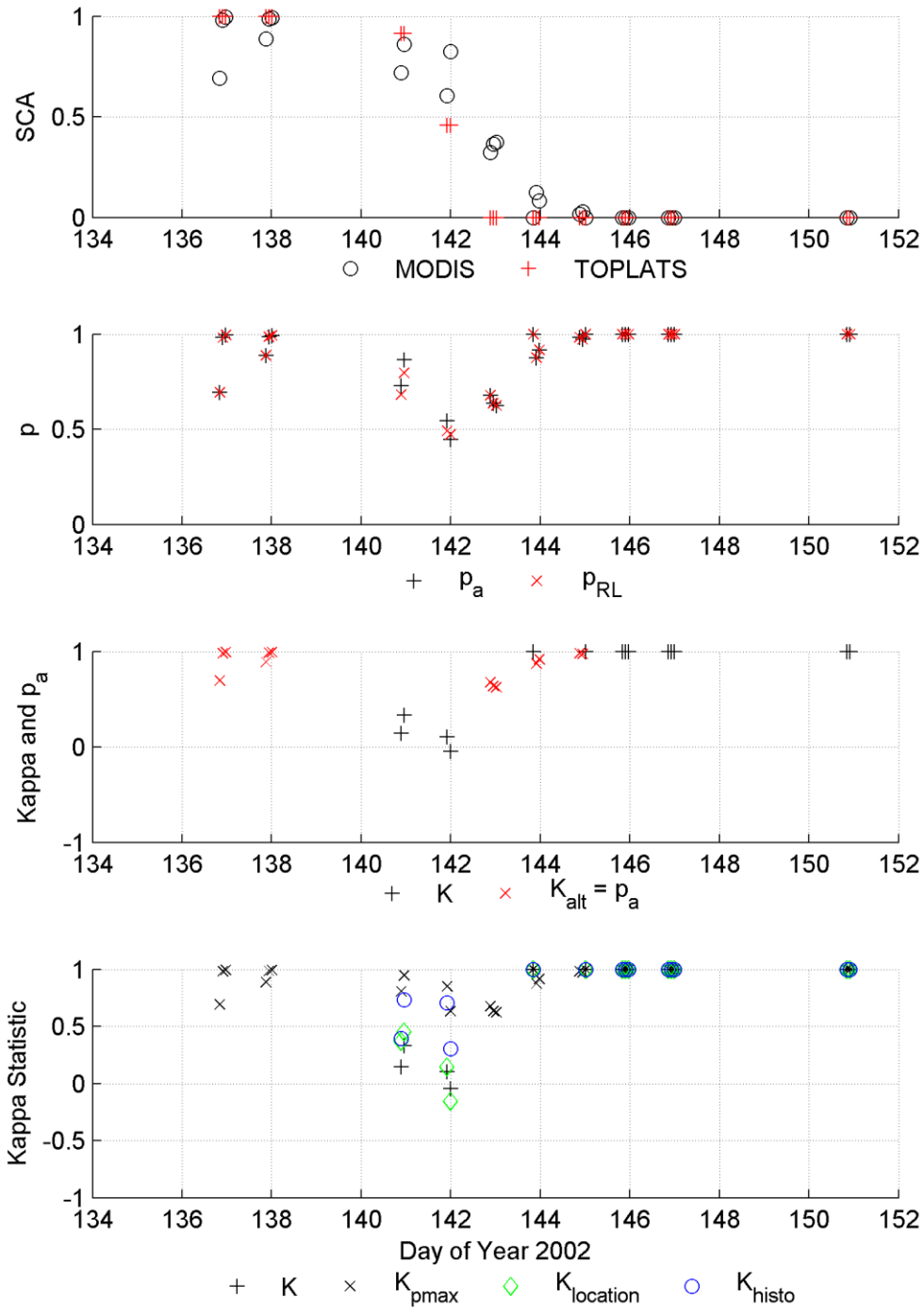

Figure 4-22d 1.25 cm SWE Threshold (Year 2002, 0.80 Albedo)

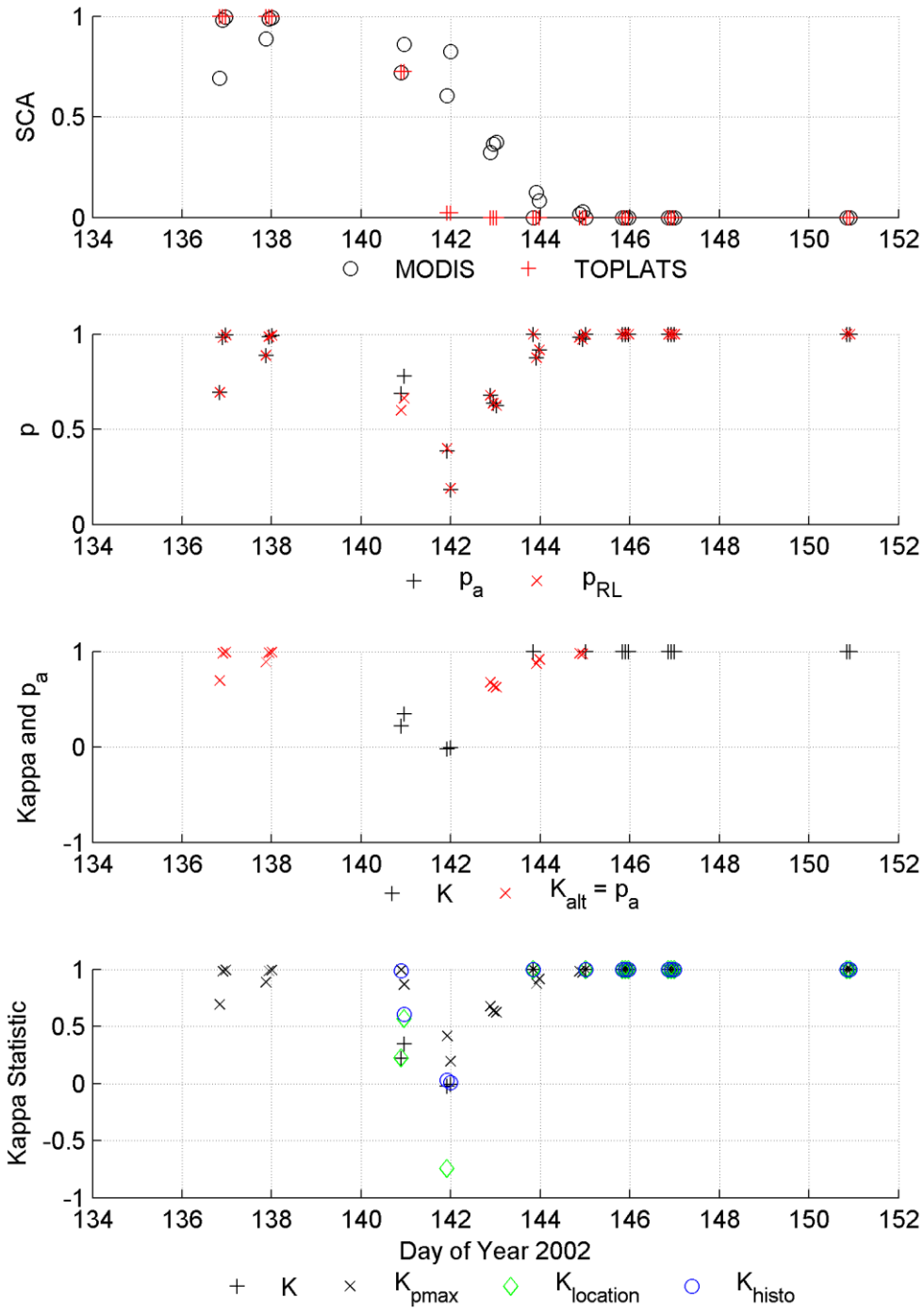

Figure 4-22e 1.50 cm SWE Threshold (Year 2002, 0.80 Albedo)

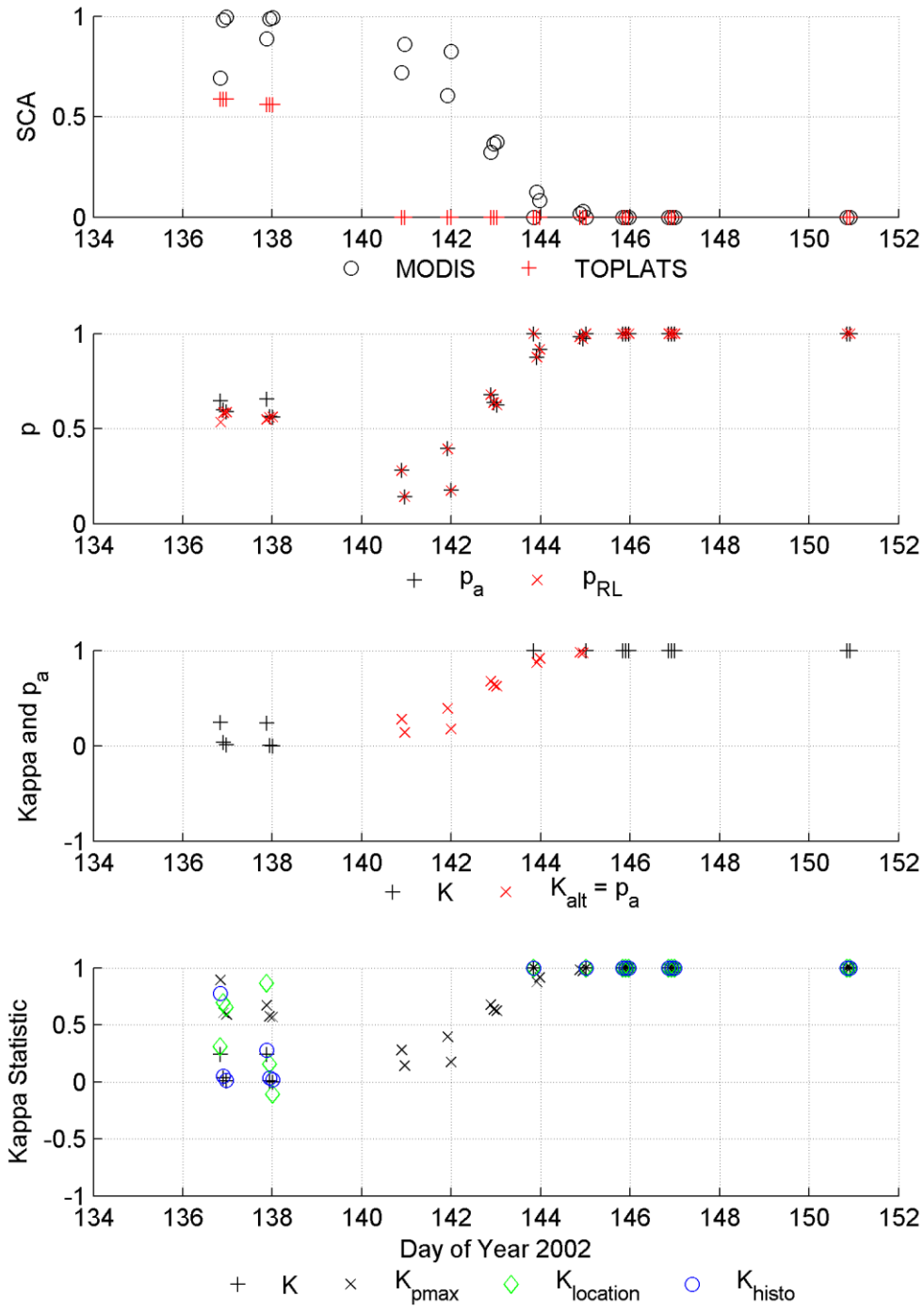

Figure 4-22f 2.50 cm SWE Threshold (Year 2002, 0.80 Albedo)

Figure 4-22 Year 2002 0.80 Albedo Map Comparison for the Entire Watershed (Zone 0)
Select plots from a complete set of plots for SWE thresholds from 0.00 to 3.00 cm.

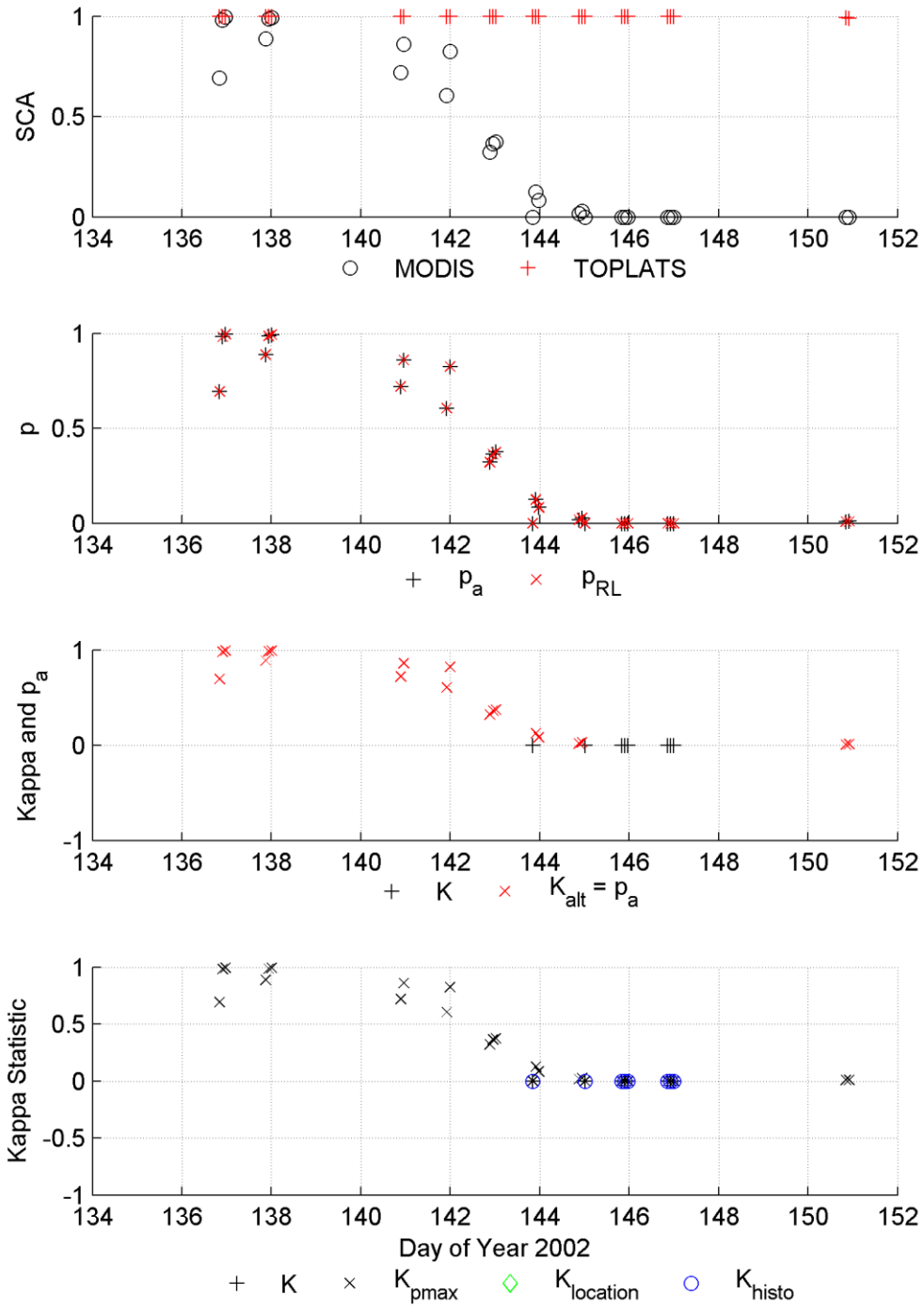

Figure 4-23a 0.00 cm SWE Threshold (Year 2002, 0.85 Albedo)

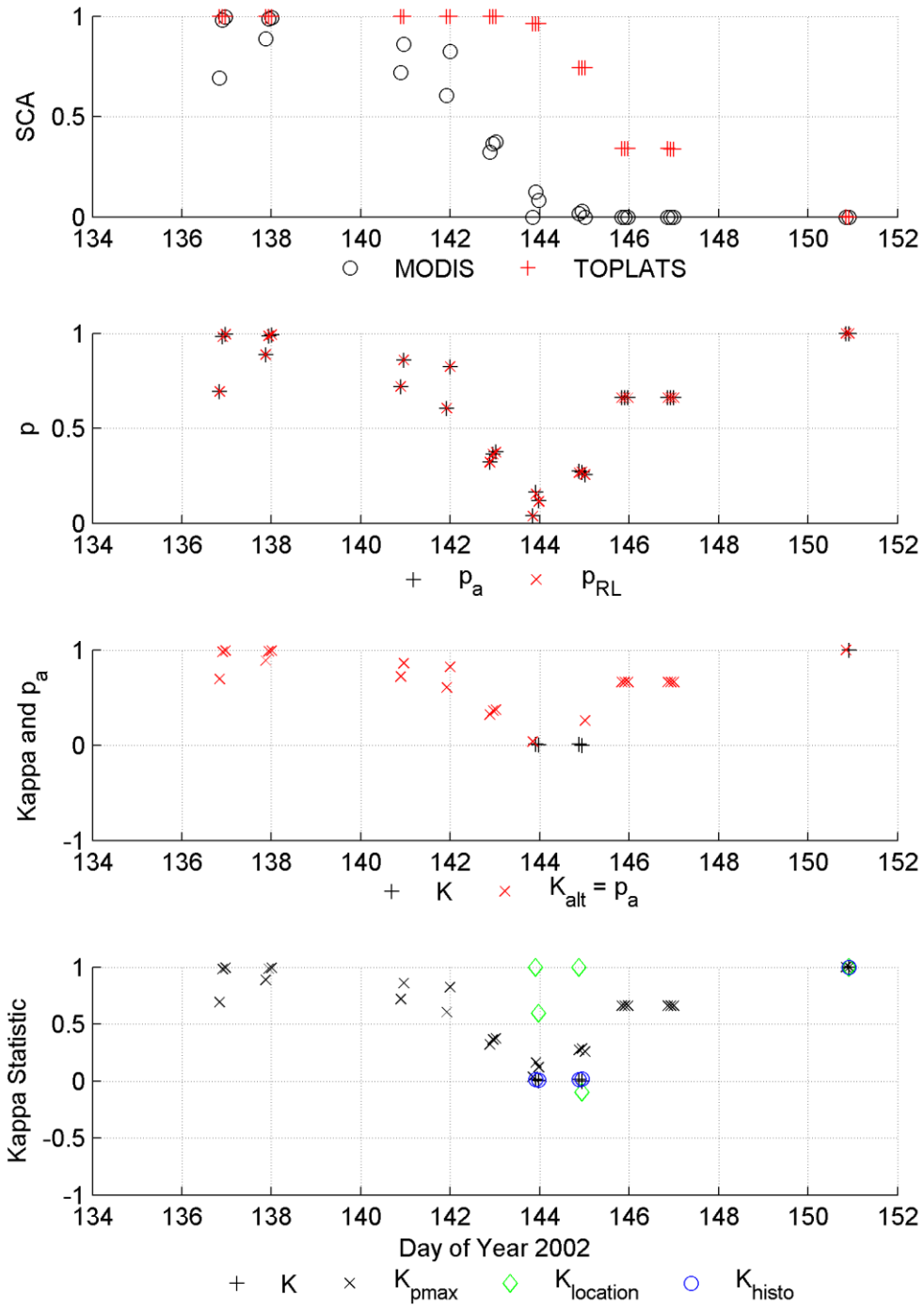

Figure 4-23b 1.50 cm SWE Threshold (Year 2002, 0.85 Albedo)

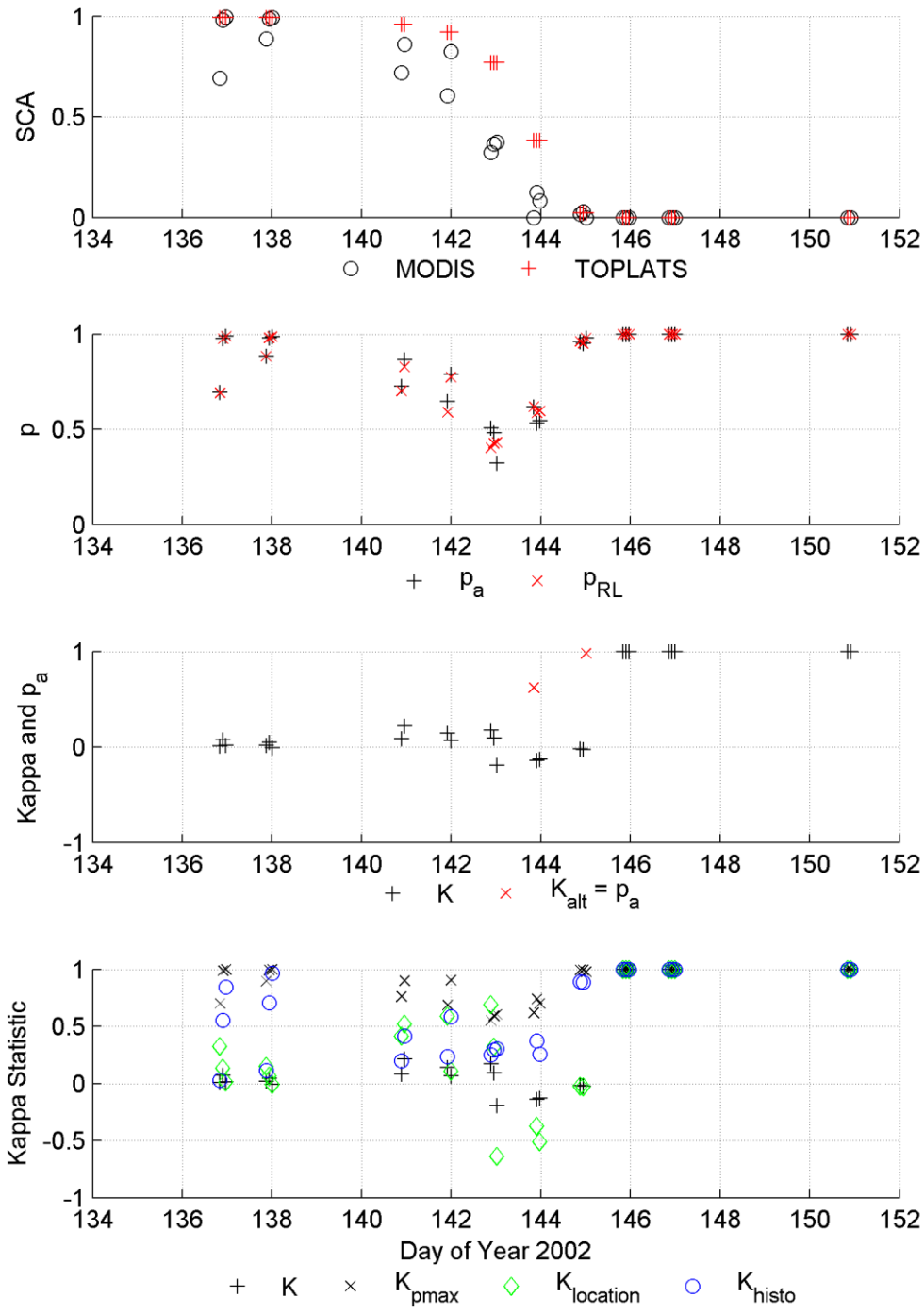

Figure 4-23c 2.25 cm SWE Threshold (Year 2002, 0.85 Albedo)

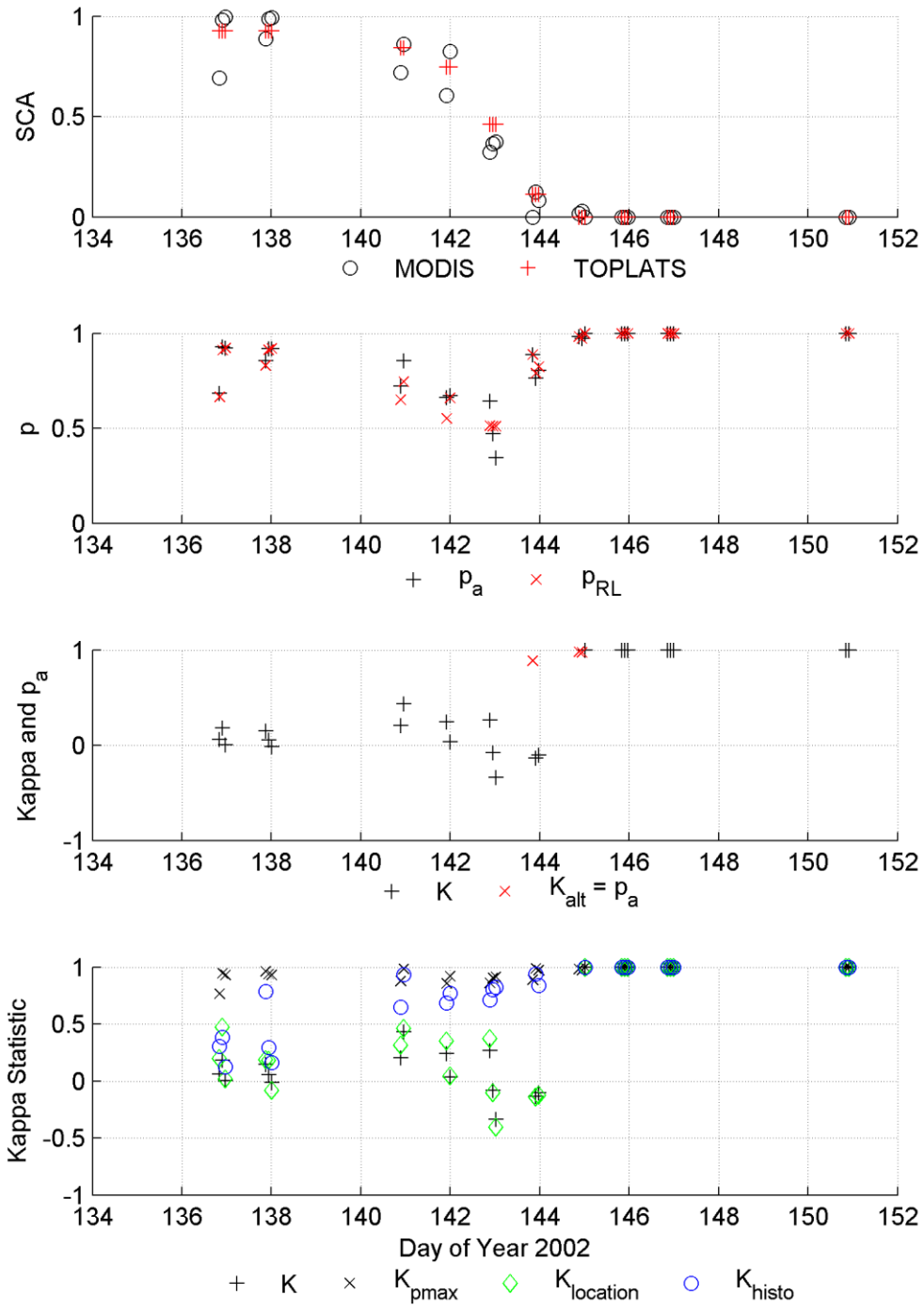

Figure 4-23d 2.50 cm SWE Threshold (Year 2002, 0.85 Albedo)

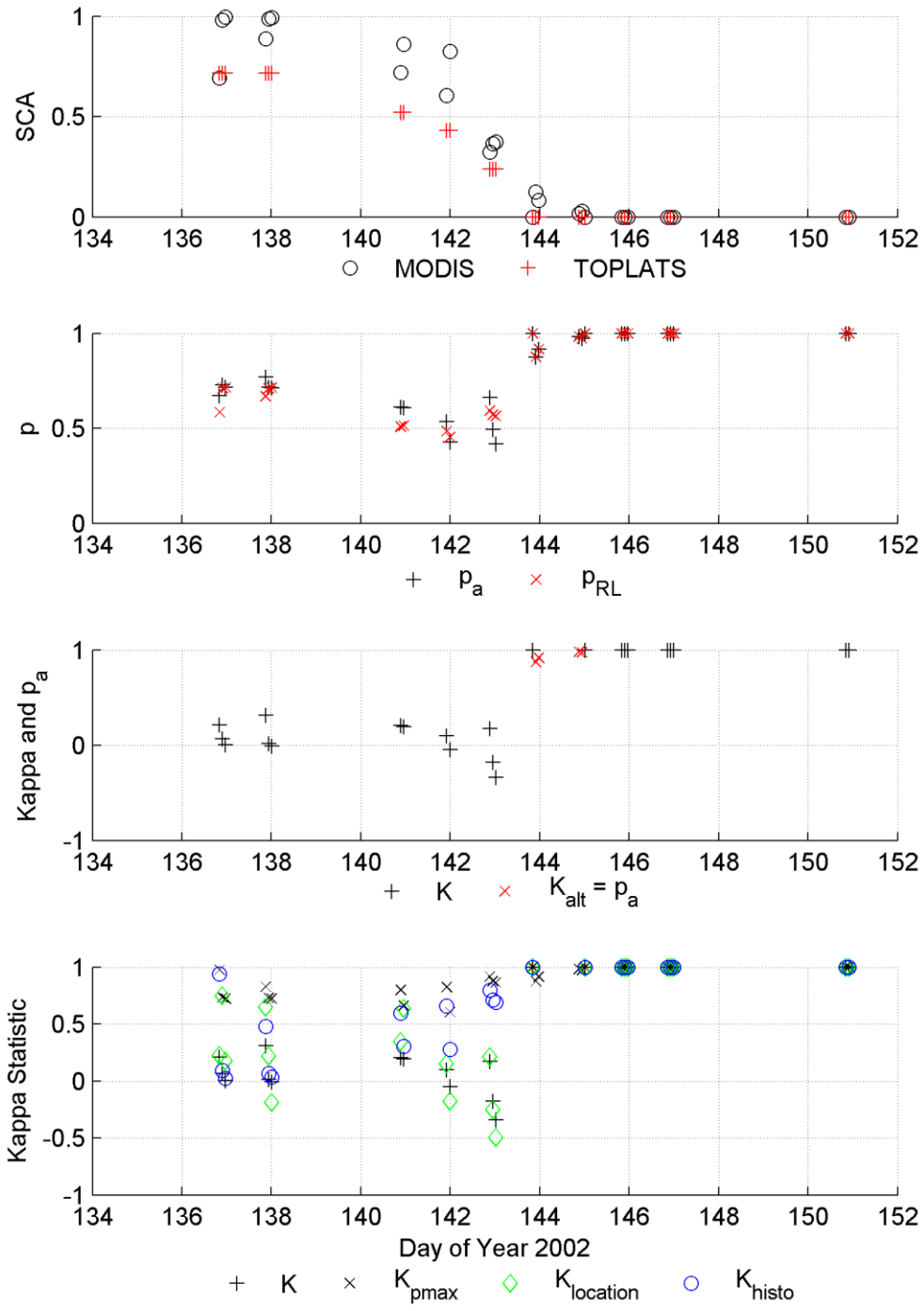

Figure 4-23e 2.75 cm SWE Threshold (Year 2002, 0.85 Albedo)

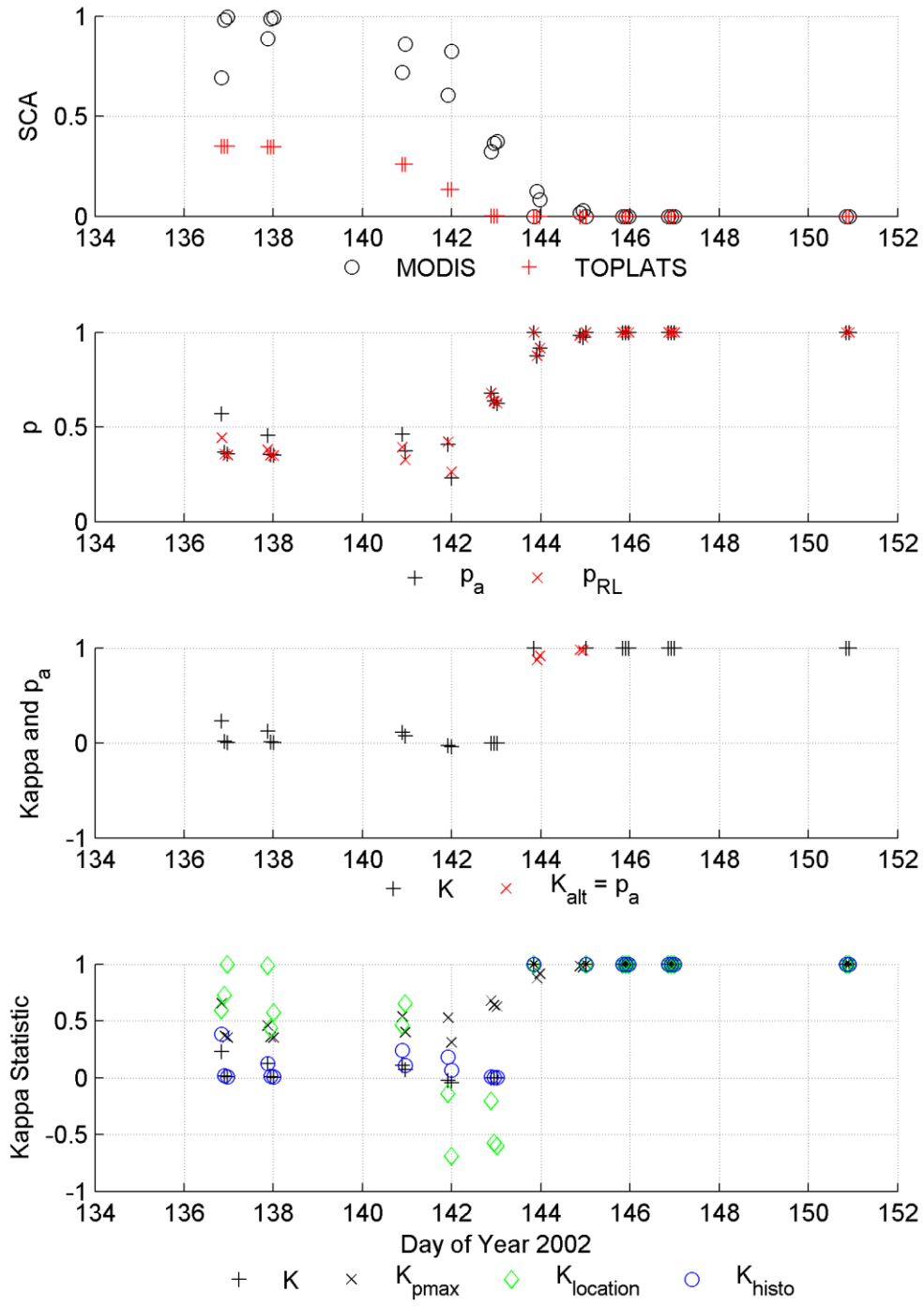

Figure 4-23f 3.00 cm SWE Threshold (Year 2002, 0.85 Albedo)

Figure 4-23 Year 2002 0.85 Albedo Map Comparison for the Entire Watershed (Zone 0)
Select plots from a complete set of plots for SWE thresholds from 0.00 to 3.00 cm.

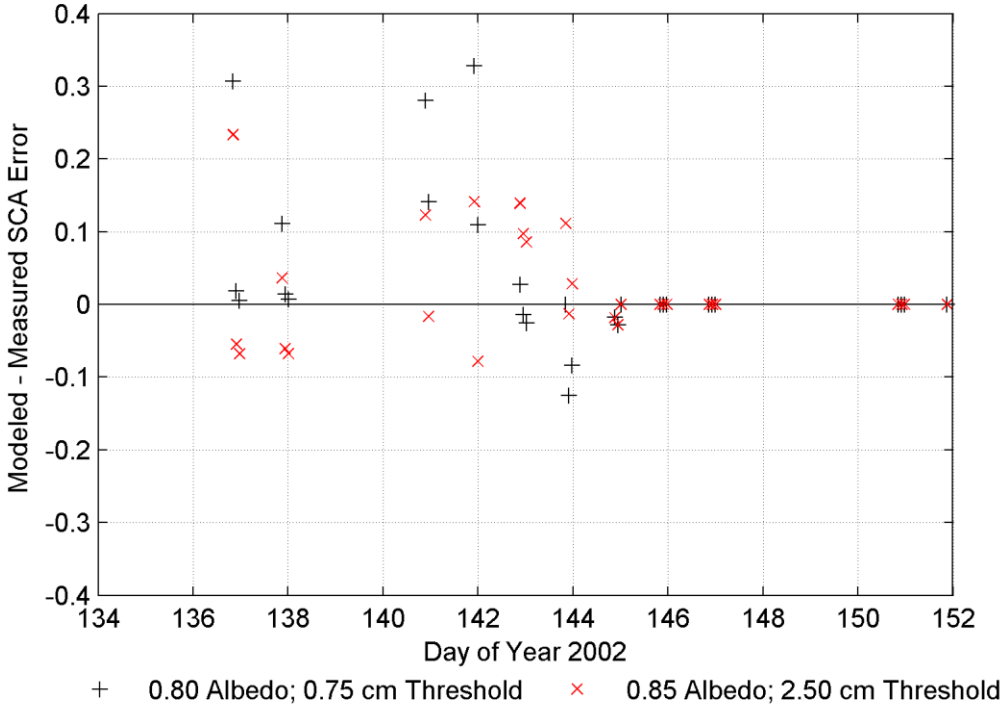

Figure 4-24 Year 2002 0.80 Albedo and 0.85 Albedo SCA Error
SCA error from both the 0.80 albedo 0.75 SWE Threshold series and the 0.85 albedo 2.50 SWE Threshold series.

4.3 MODEL CONFIRMATION

Section 4.2 describes results from selecting a SWE threshold for each of two snow albedo values using only (a) overlaying, filtered model and measurement SCA plots and (b) plots of the proportion of agreement between the two map series to confirm the best quality observed scenes shown in Figure 4-21. This study should consider (c) the Kappa statistics, (d) the effect of elevation on the overall map comparison, and (e) the uncertainty in the MODIS measurements for scenes with less than 100% coverage in order to both calibrate the model and use the best MODIS measurements to evaluate the model performance. This section completes item c and item d for the select series from Section 4.2.3, plots filtered, modeled, and measured maps side by side, and shows the zone-specific comparison statistics all in order to determine if a time series of MODIS scenes can be used to evaluate the TOPLATS model performance. The section skips item e because the given filters based on QA and collection time in the 2002 reduced the series of measurement scenes to those with only 100% available coverage. This completely cloud-free series raises this study's overall confidence in the measurement series to report truth and leaves confirmation subjective to the QA information in each scene, which ranges from 0.50 to 0.92 (Figure 4-21), side-by-side maps, and elevation information.

Figure 4-25 and Figure 4-26 separate the series of statistics in Figure 4-22b and Figure 4-23d into four elevation zones. The SCA plots in these series show SCA agreement across the watershed as a whole agrees much better than the SCA on a zone-basis. This explains the poor Kappa and $K_{location}$ values in Figure 4-22b and Figure 4-23d showing the watershed composite results. Even though the proportion of

agreement on a watershed basis is good; the Kappa statistics reveal poor agreement in by pixel-pixel comparisons. The zone statistics in Figure 4-25 and Figure 4-26 show the Kappa values are best for zone one at the beginning of the melt period and that the 0.80 simulation confirms the start and middle of the melt period across zones two through four better than the 0.85 series.

Figure 4-27 shows the two series side by side with MODIS observations. The maps illustrate the result from Kappa statistics, both across the watershed and separated into zones, that TOPLATS poorly confirms MODIS results. Further, the figure reiterates that TOPLATS relies primarily on DEM information and shows that additional physical processes should be incorporated, or further emphasized, in order for TOPLATS to well confirm MODIS results.

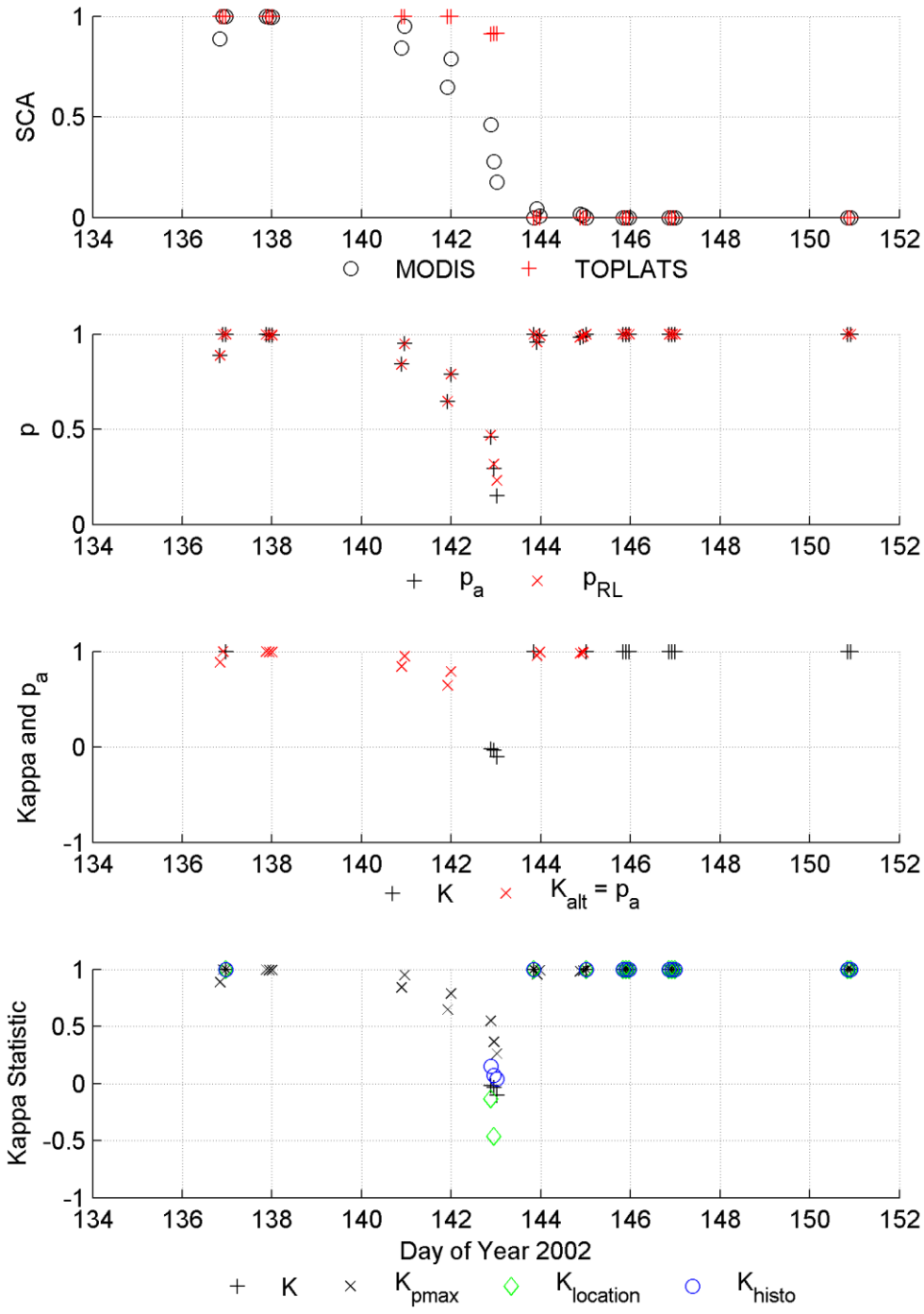

Figure 4-25a Zone One (year 2002, 0.80 albedo, 0.75 cm threshold)

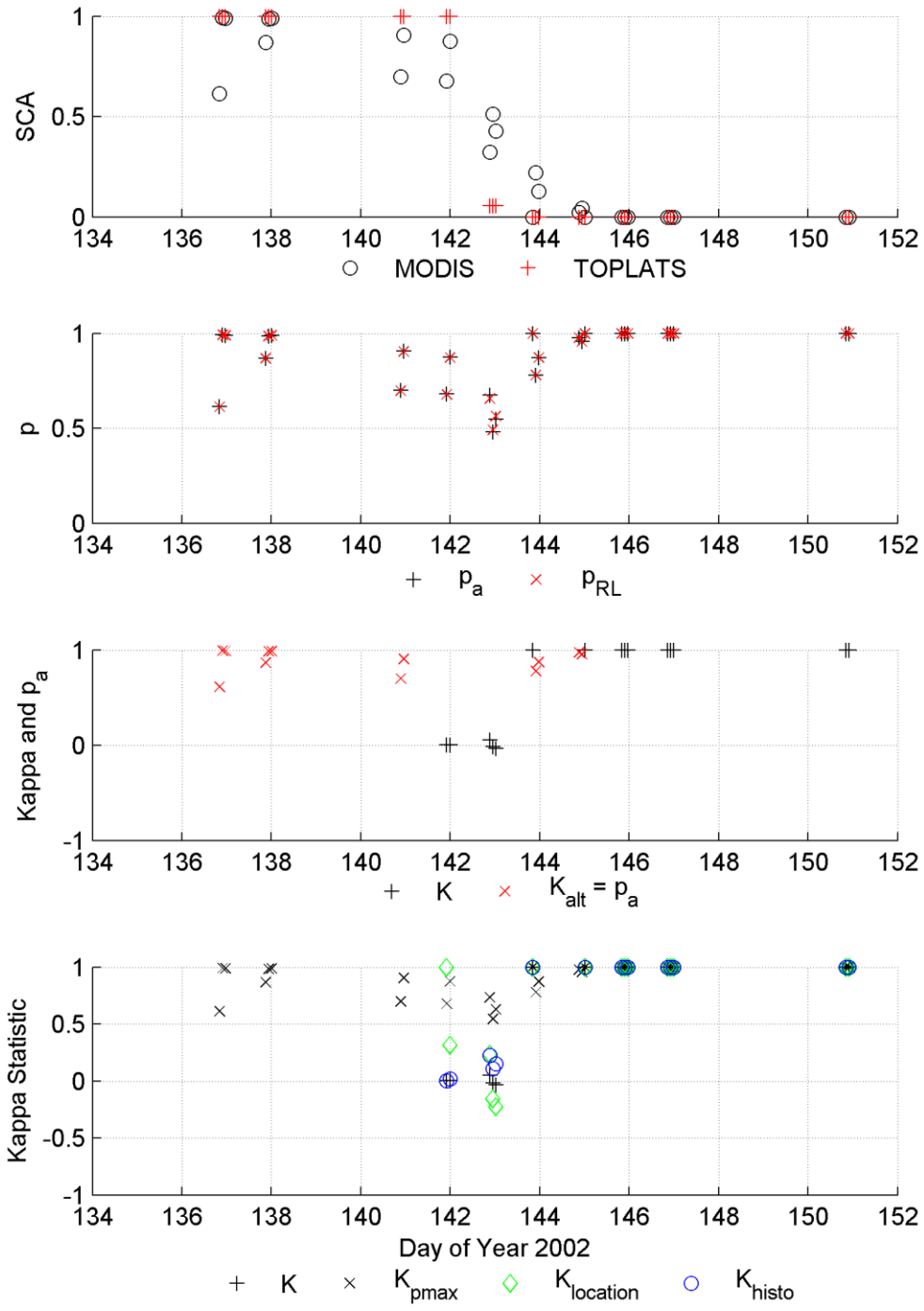

Figure 4-25b Zone Two (year 2002, 0.80 albedo, 0.75 cm threshold)

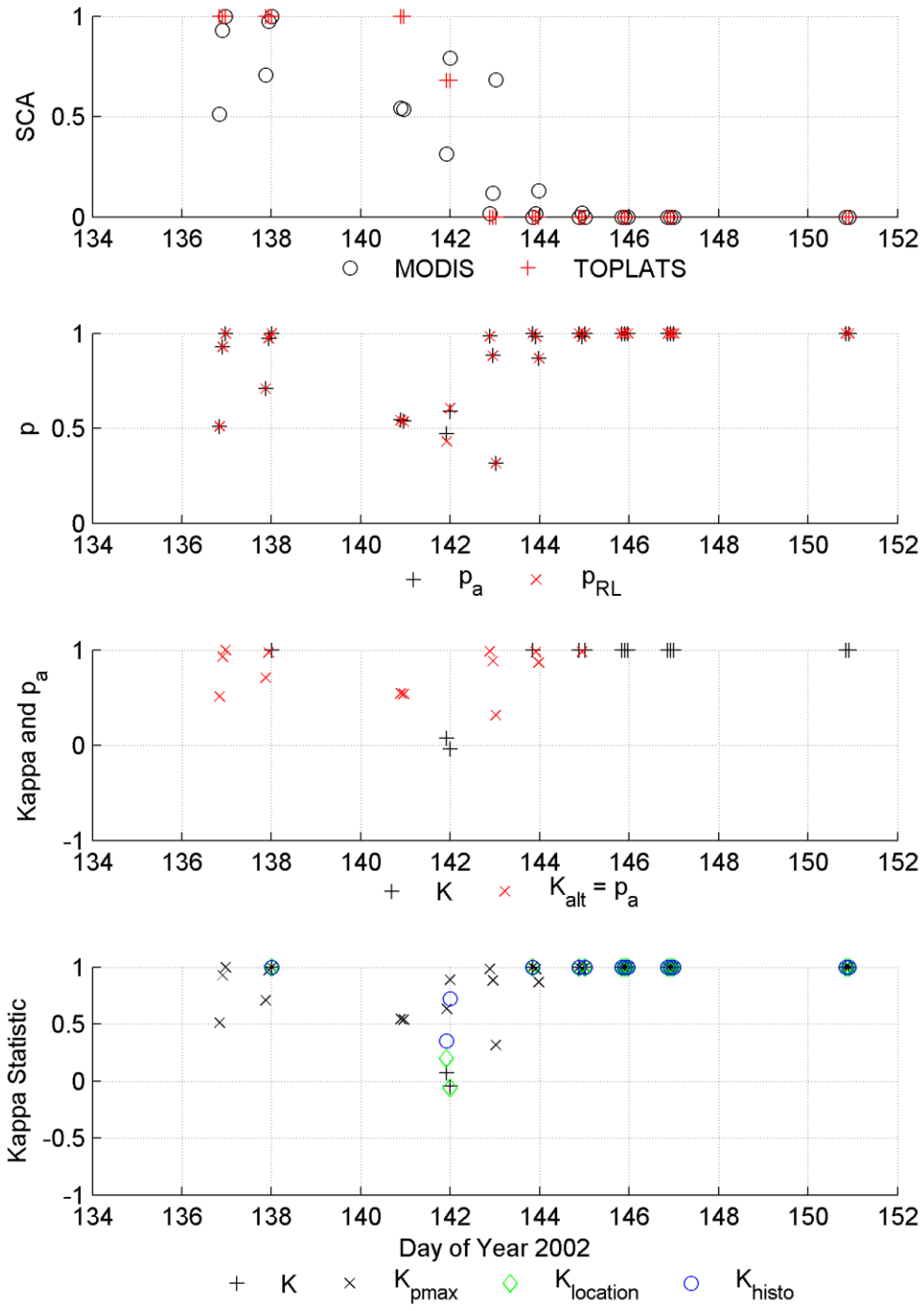

Figure 4-25d Zone Three (year 2002, 0.80 albedo, 0.75 cm threshold)

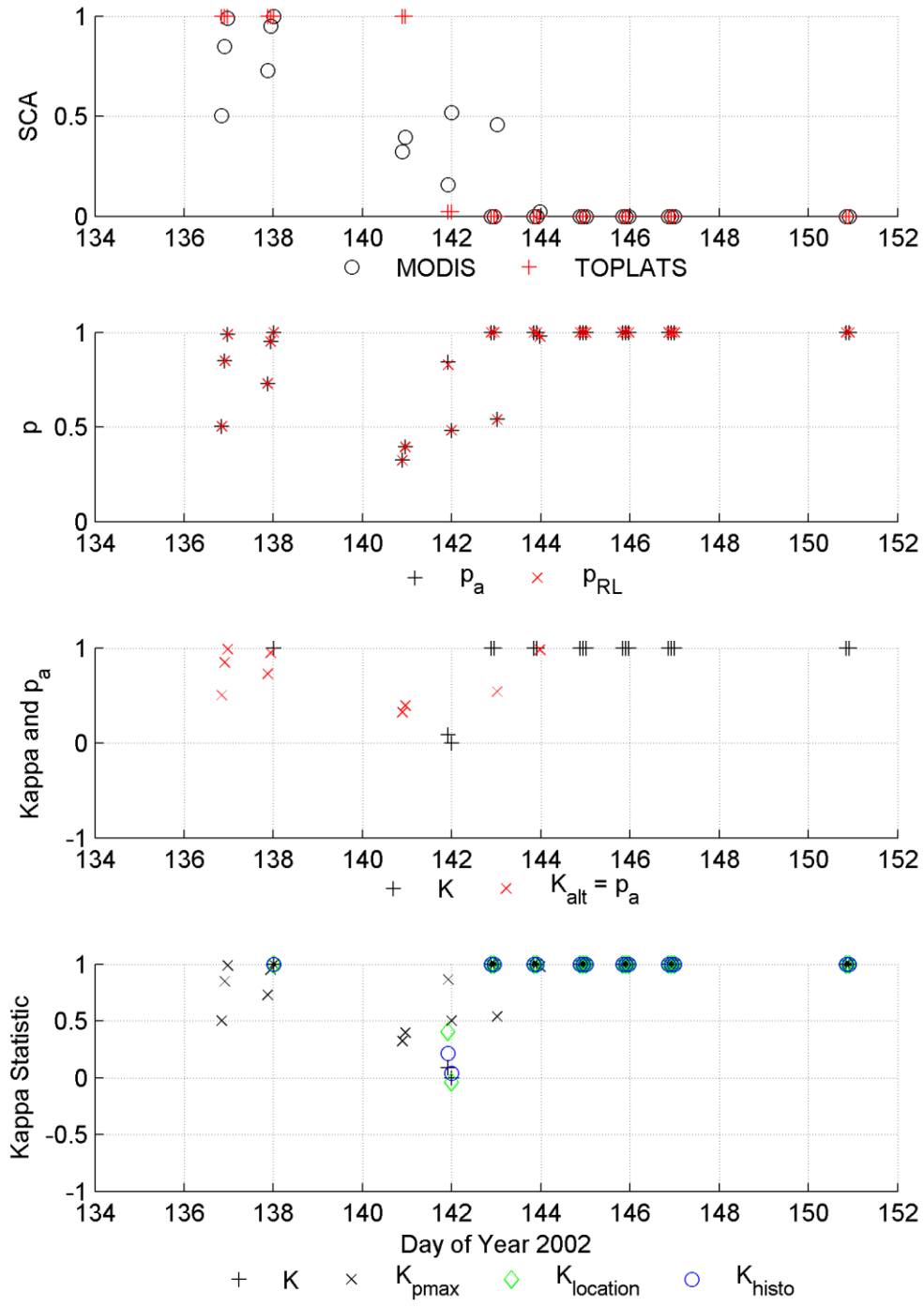

Figure 4-25d Zone Four (year 2002, 0.80 albedo, 0.75 cm threshold)

Figure 4-25 Year 2002 0.80 Albedo, 0.75 cm SWE Threshold for Four Elevation Zones
Select plots from a complete set of plots for SWE thresholds from 0.00 to 3.00 cm.

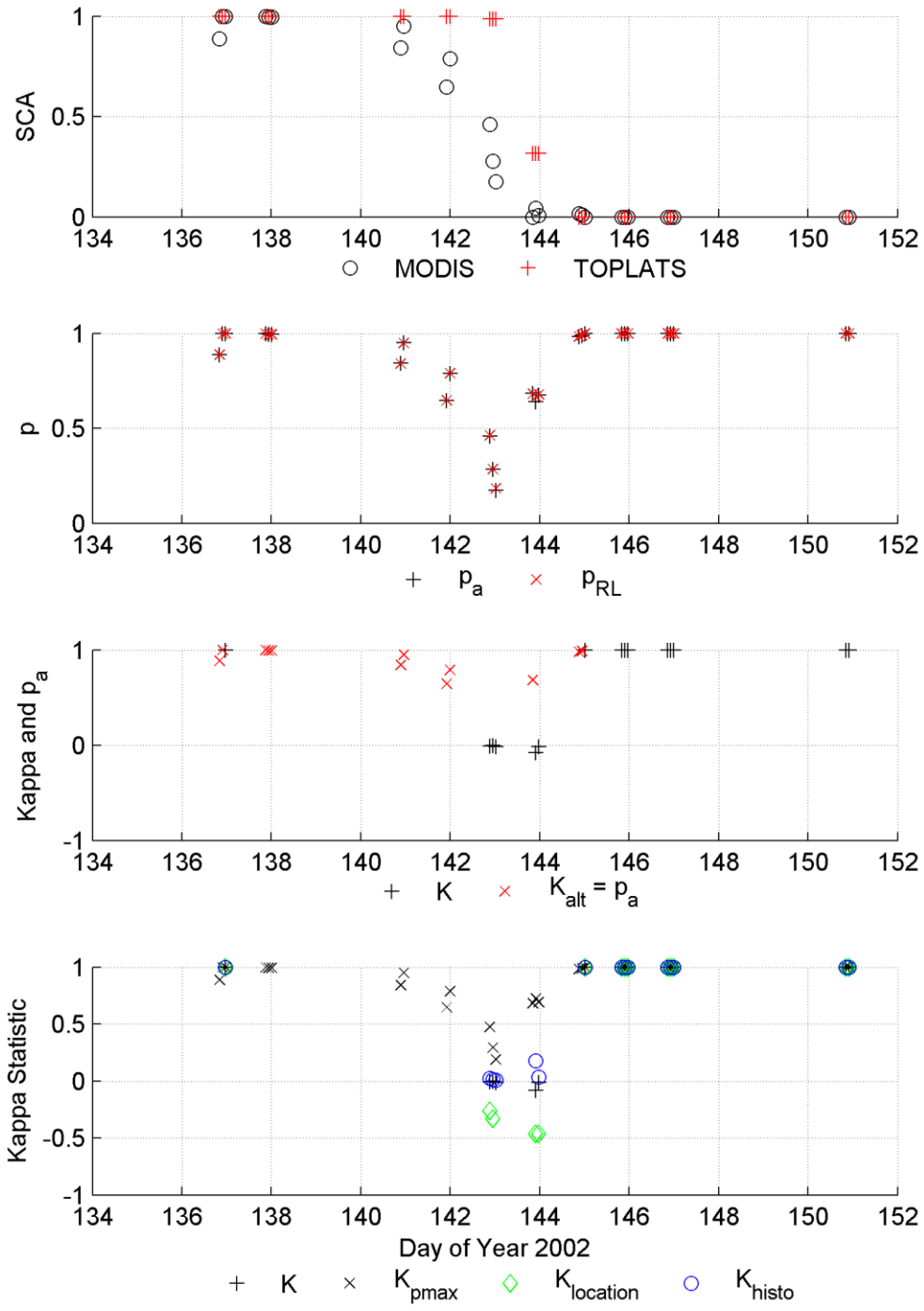

Figure 4-26a Zone One (year 2002, 0.85 albedo, 2.50 cm threshold)

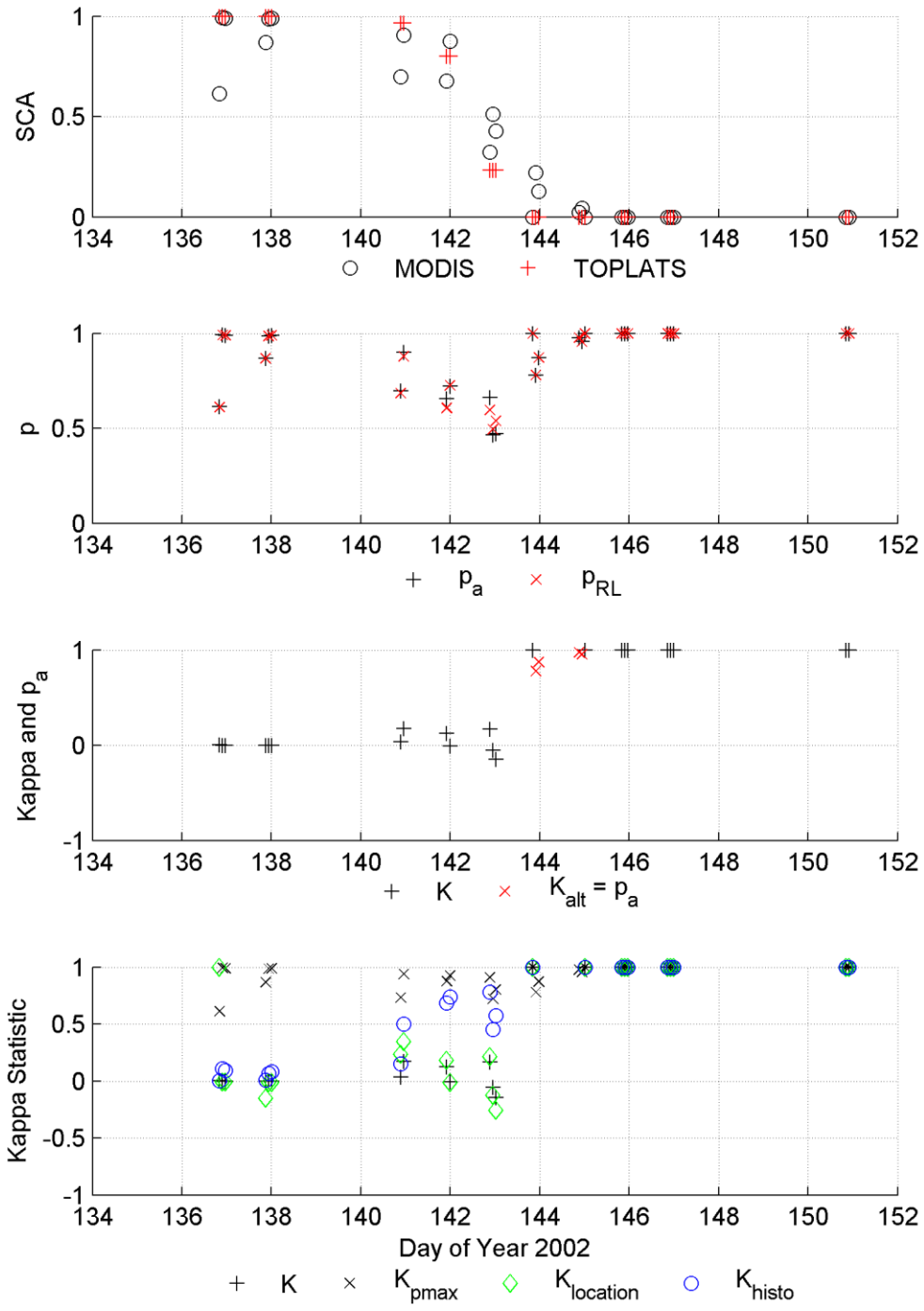

Figure 4-26b Zone Two (year 2002, 0.85 albedo, 2.50 cm threshold)

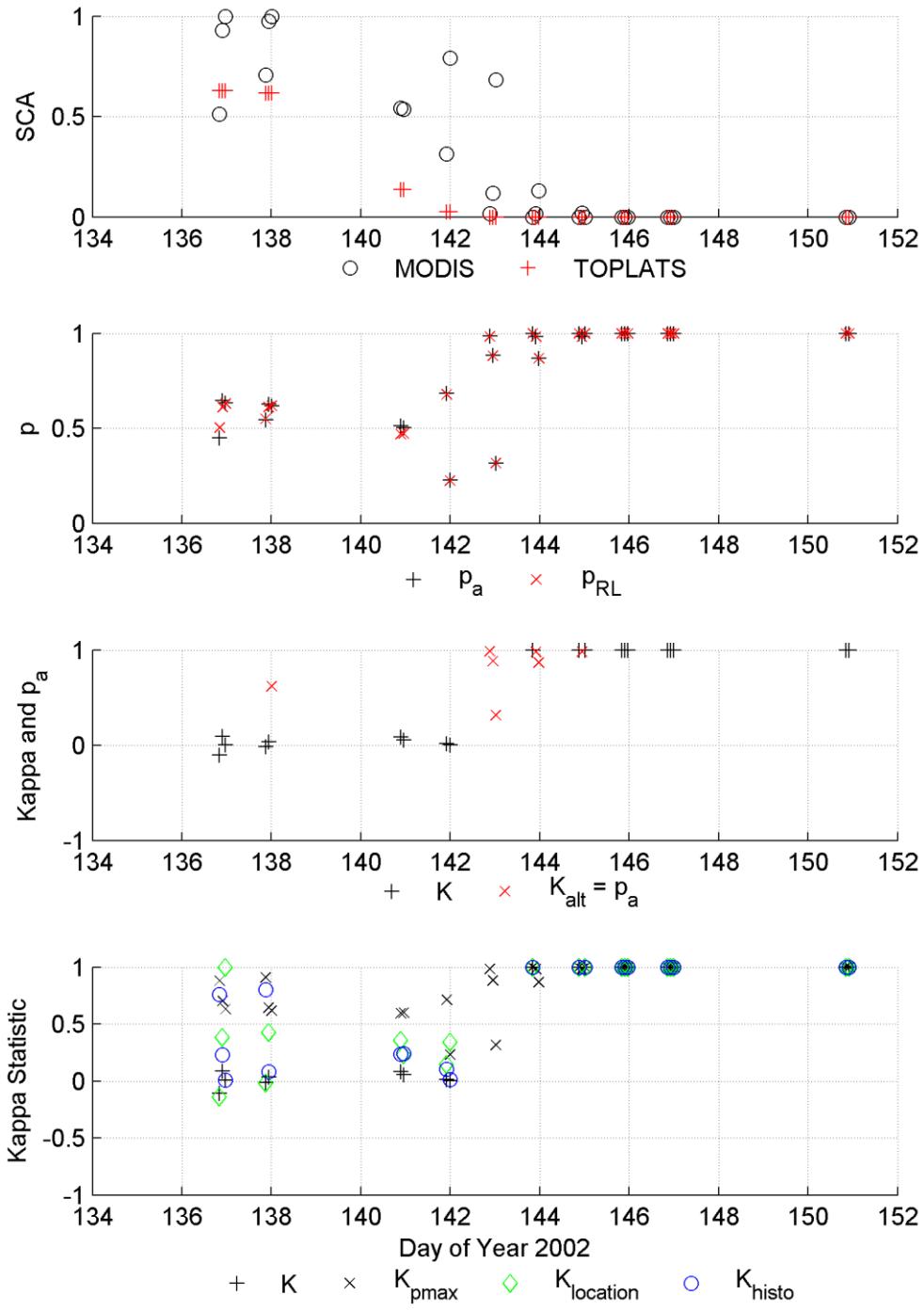

Figure 4-26d Zone Three (year 2002, 0.85 albedo, 2.50 cm threshold)

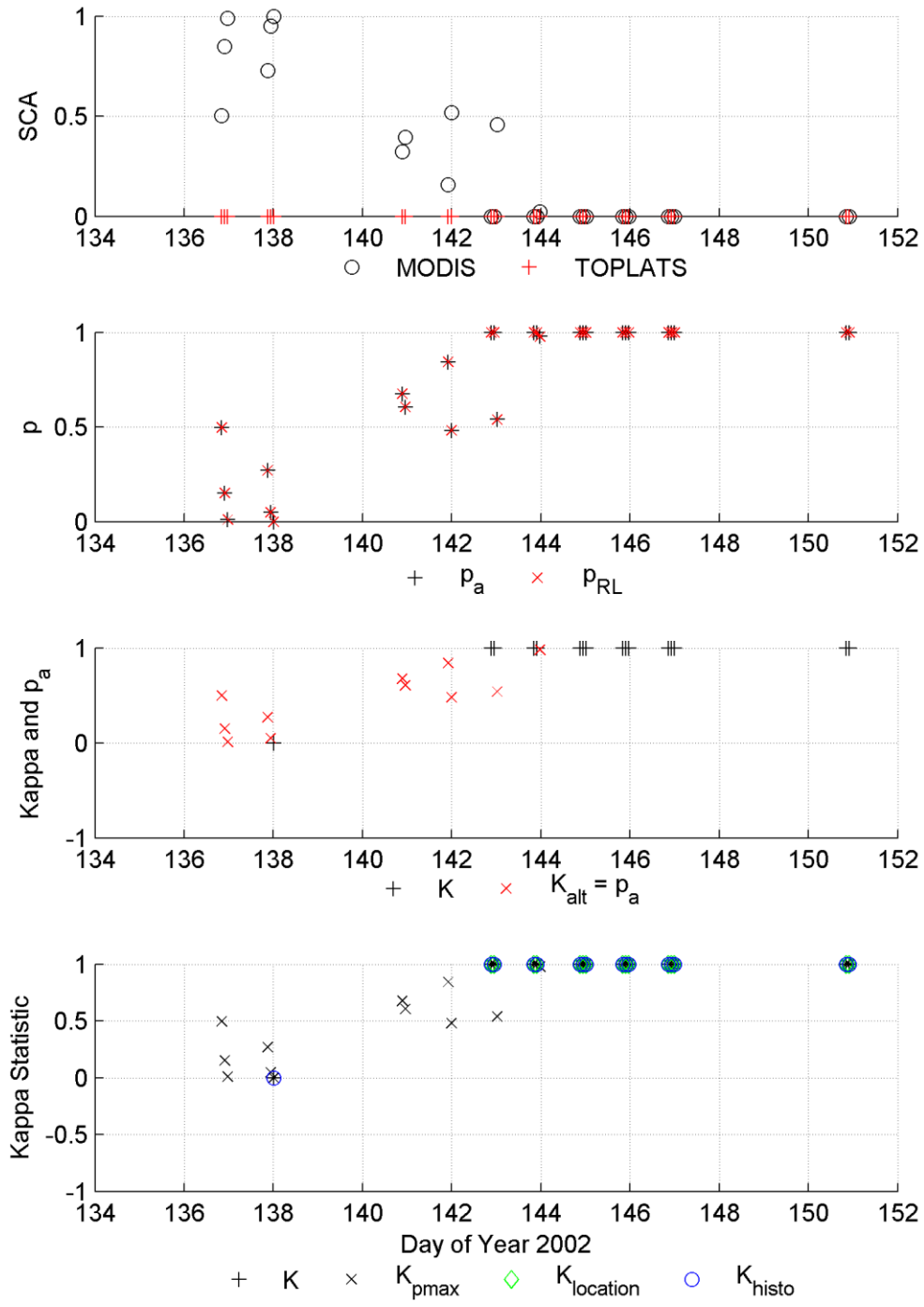

Figure 4-26d Zone Four (year 2002, 0.85 albedo, 2.50 cm threshold)

Figure 4-26 Year 2002 0.85 Albedo, 2.50 SWE Threshold for Four Elevation Zones
Select plots from a complete set of plots for SWE thresholds from 0.00 to 3.00 cm.

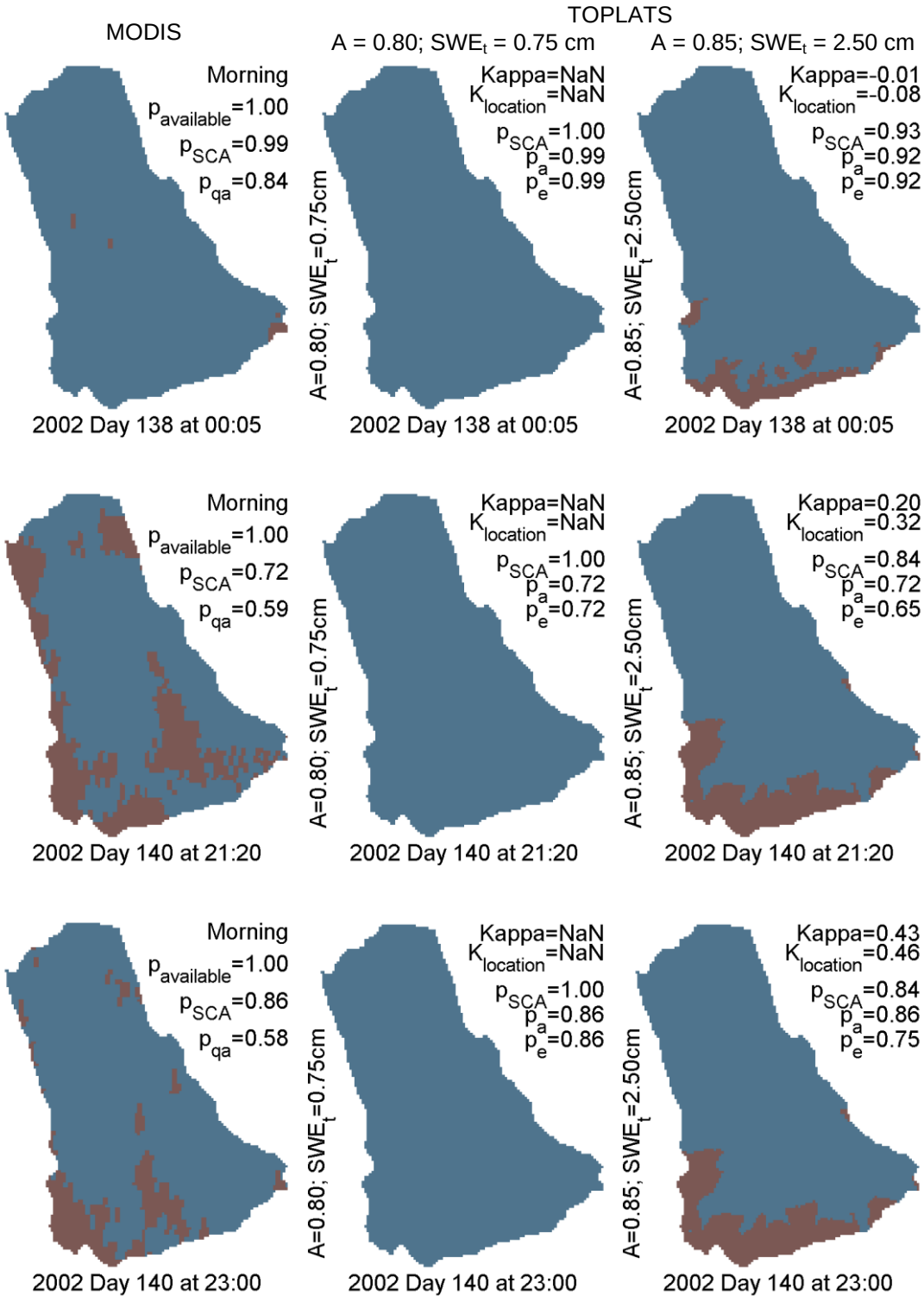

Figure 4-27 SCA Maps for Measured, and Two Sets of Model SCA Results
Continued on the following pages, the 15 MODIS scenes selected for 2002 in Figure 4-6 (column one) are shown to the left of TOPLATS results for an albedo (A) of 0.80 and a SWE threshold (SWE_t) of 0.75 cm (column two) and the TOPLATS results for an albedo of 0.85 and a SWE threshold of 2.50 cm (column three).

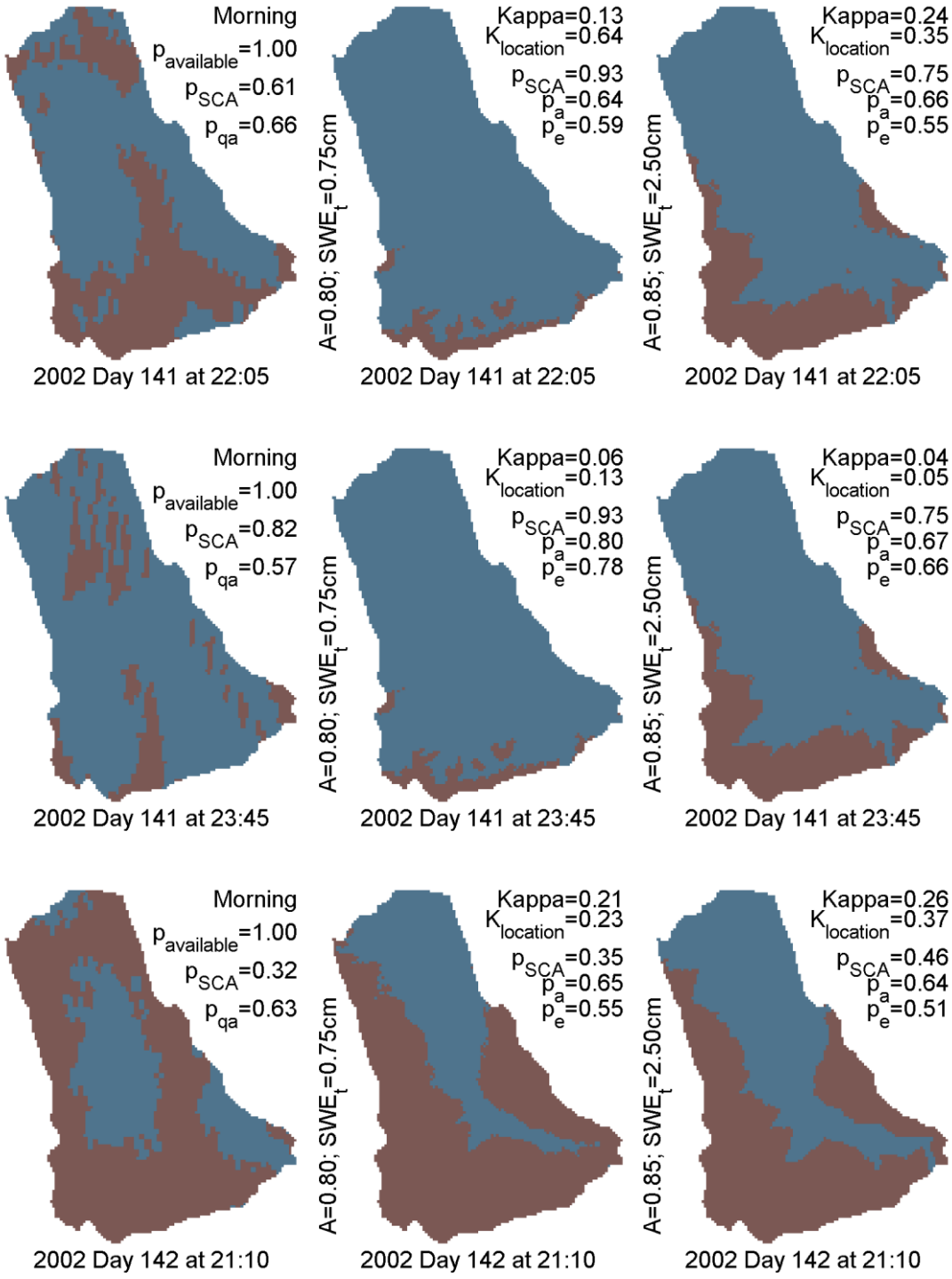
Morning
p_available=1.00
p_SCA=0.61
p_qa=0.66
Kappa=0.13
K_location=0.64
p_SCA=0.93
p_a=0.64
p_e=0.59
A=0.80; SWE_t=0.75cm
Kappa=0.24
K_location=0.35
p_SCA=0.75
p_a=0.66
p_e=0.55
A=0.85; SWE_t=2.50cm
2002 Day 141 at 22:05
2002 Day 141 at 22:05
2002 Day 141 at 22:05
Morning
p_available=1.00
p_SCA=0.82
p_qa=0.57
Kappa=0.06
K_location=0.13
p_SCA=0.93
p_a=0.80
p_e=0.78
A=0.80; SWE_t=0.75cm
Kappa=0.04
K_location=0.05
p_SCA=0.75
p_a=0.67
p_e=0.66
A=0.85; SWE_t=2.50cm
2002 Day 141 at 23:45
2002 Day 141 at 23:45
2002 Day 141 at 23:45
Morning
p_available=1.00
p_SCA=0.32
p_qa=0.63
Kappa=0.21
K_location=0.23
p_SCA=0.35
p_a=0.65
p_e=0.55
A=0.80; SWE_t=0.75cm
Kappa=0.26
K_location=0.37
p_SCA=0.46
p_a=0.64
p_e=0.51
A=0.85; SWE_t=2.50cm
2002 Day 142 at 21:10
2002 Day 142 at 21:10
2002 Day 142 at 21:10

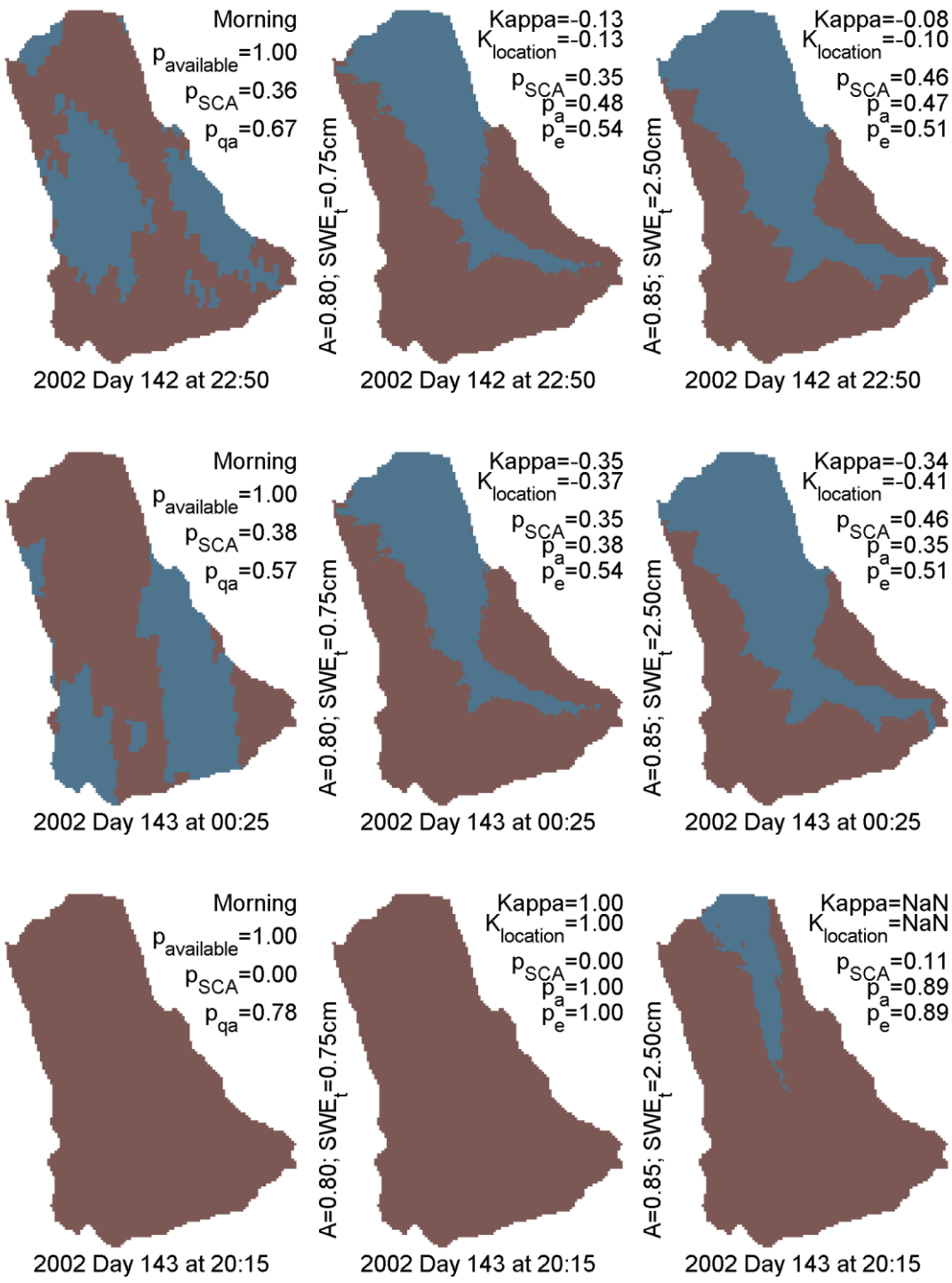
Morning
$p_{available}$=1.00
p_{SCA}=0.36
p_{qa}=0.67
2002 Day 142 at 22:50
A=0.80; SWE_t=0.75cm
Kappa=-0.13
$K_{location}$=-0.13
p_{SCA}=0.35
p_a=0.48
p_e=0.54
2002 Day 142 at 22:50
A=0.85; SWE_t=2.50cm
Kappa=-0.08
$K_{location}$=-0.10
p_{SCA}=0.46
p_a=0.47
p_e=0.51
2002 Day 142 at 22:50
Morning
$p_{available}$=1.00
p_{SCA}=0.38
p_{qa}=0.57
2002 Day 143 at 00:25
A=0.80; SWE_t=0.75cm
Kappa=-0.35
$K_{location}$=-0.37
p_{SCA}=0.35
p_a=0.38
p_e=0.54
2002 Day 143 at 00:25
A=0.85; SWE_t=2.50cm
Kappa=-0.34
$K_{location}$=-0.41
p_{SCA}=0.46
p_a=0.35
p_e=0.51
2002 Day 143 at 00:25
Morning
$p_{available}$=1.00
p_{SCA}=0.00
p_{qa}=0.78
2002 Day 143 at 20:15
A=0.80; SWE_t=0.75cm
Kappa=1.00
$K_{location}$=1.00
p_{SCA}=0.00
p_a=1.00
p_e=1.00
2002 Day 143 at 20:15
A=0.85; SWE_t=2.50cm
Kappa=NaN
$K_{location}$=NaN
p_{SCA}=0.11
p_a=0.89
p_e=0.89
2002 Day 143 at 20:15

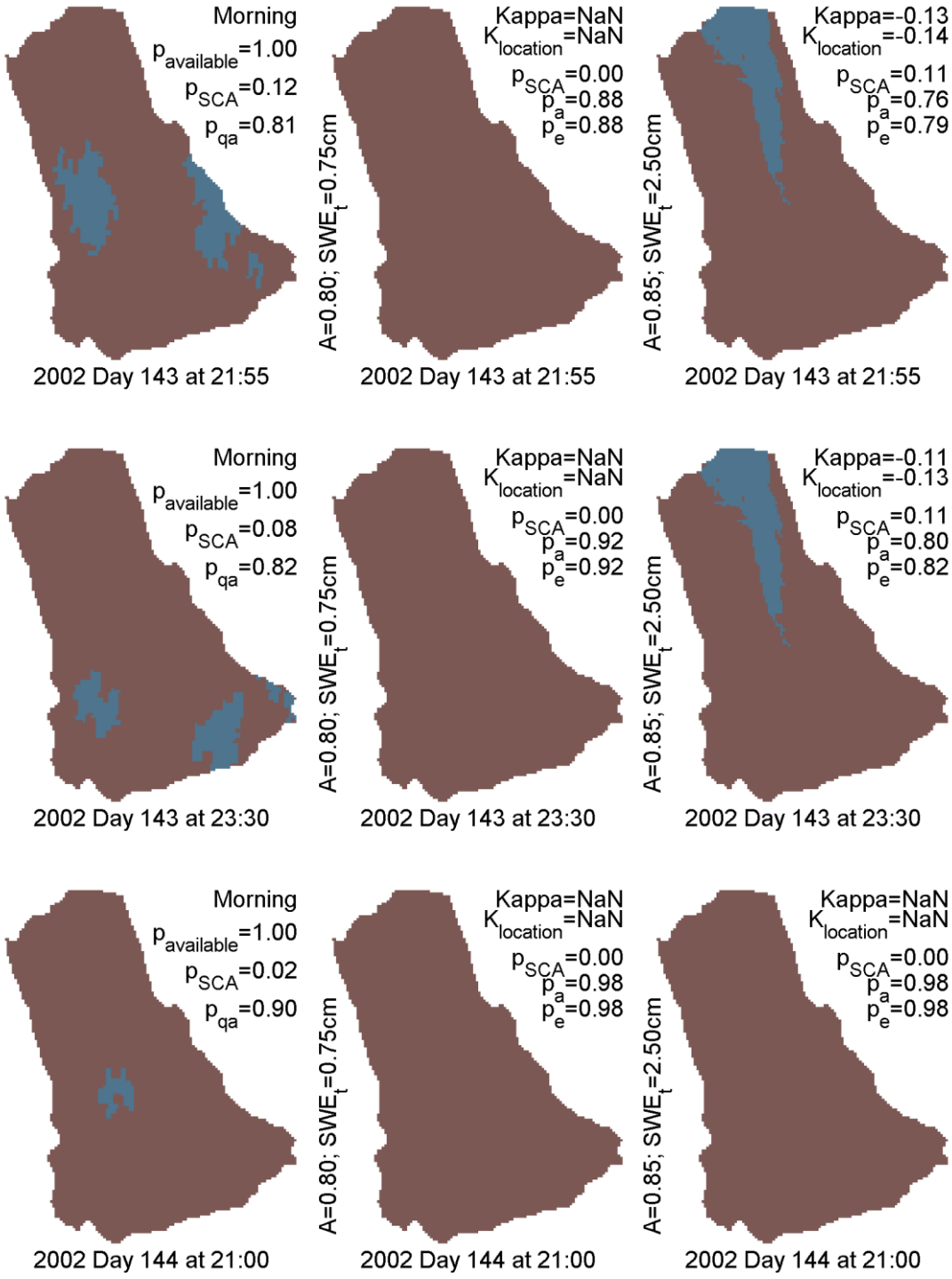
Morning
$p_{available}$=1.00
p_{SCA}=0.12
p_{qa}=0.81
Kappa=NaN
$K_{location}$=NaN
p_{SCA}=0.00
p_a=0.88
p_e=0.88
Kappa=-0.13
$K_{location}$=-0.14
p_{SCA}=0.11
p_a=0.76
p_e=0.79
A=0.80; SWE_t=0.75cm
A=0.85; SWE_t=2.50cm
2002 Day 143 at 21:55
2002 Day 143 at 21:55
2002 Day 143 at 21:55
Morning
$p_{available}$=1.00
p_{SCA}=0.08
p_{qa}=0.82
Kappa=NaN
$K_{location}$=NaN
p_{SCA}=0.00
p_a=0.92
p_e=0.92
Kappa=-0.11
$K_{location}$=-0.13
p_{SCA}=0.11
p_a=0.80
p_e=0.82
A=0.80; SWE_t=0.75cm
A=0.85; SWE_t=2.50cm
2002 Day 143 at 23:30
2002 Day 143 at 23:30
2002 Day 143 at 23:30
Morning
$p_{available}$=1.00
p_{SCA}=0.02
p_{qa}=0.90
Kappa=NaN
$K_{location}$=NaN
p_{SCA}=0.00
p_a=0.98
p_e=0.98
Kappa=NaN
$K_{location}$=NaN
p_{SCA}=0.00
p_a=0.98
p_e=0.98
A=0.80; SWE_t=0.75cm
A=0.85; SWE_t=2.50cm
2002 Day 144 at 21:00
2002 Day 144 at 21:00
2002 Day 144 at 21:00

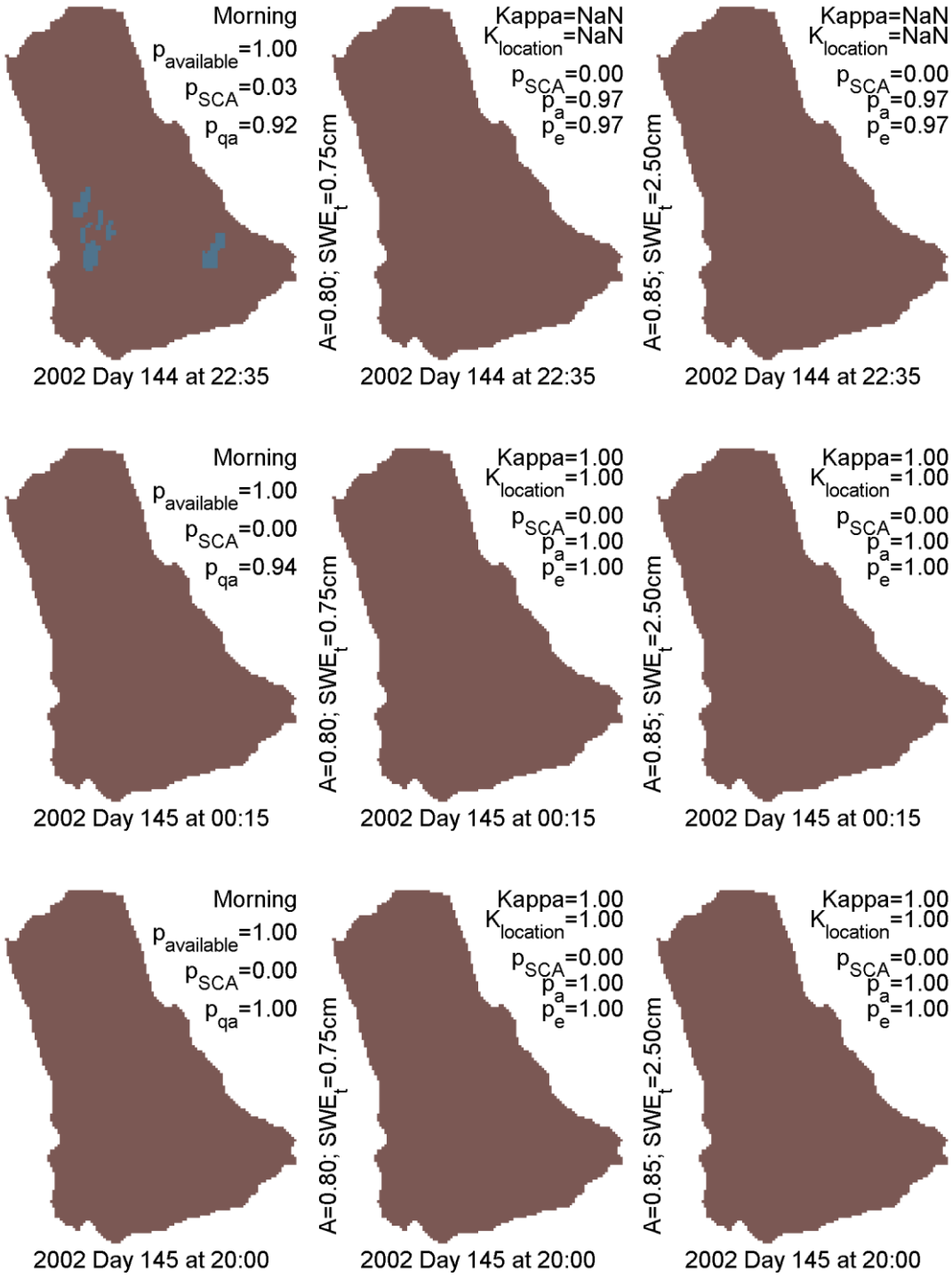
Morning
$p_{available}$=1.00
p_{SCA}=0.03
p_{qa}=0.92
2002 Day 144 at 22:35
A=0.80; SWE_t=0.75cm
Kappa=NaN
$K_{location}$=NaN
p_{SCA}=0.00
p_a=0.97
p_e=0.97
2002 Day 144 at 22:35
A=0.85; SWE_t=2.50cm
Kappa=NaN
$K_{location}$=NaN
p_{SCA}=0.00
p_a=0.97
p_e=0.97
2002 Day 144 at 22:35
Morning
$p_{available}$=1.00
p_{SCA}=0.00
p_{qa}=0.94
2002 Day 145 at 00:15
A=0.80; SWE_t=0.75cm
Kappa=1.00
$K_{location}$=1.00
p_{SCA}=0.00
p_a=1.00
p_e=1.00
2002 Day 145 at 00:15
A=0.85; SWE_t=2.50cm
Kappa=1.00
$K_{location}$=1.00
p_{SCA}=0.00
p_a=1.00
p_e=1.00
2002 Day 145 at 00:15
Morning
$p_{available}$=1.00
p_{SCA}=0.00
p_{qa}=1.00
2002 Day 145 at 20:00
A=0.80; SWE_t=0.75cm
Kappa=1.00
$K_{location}$=1.00
p_{SCA}=0.00
p_a=1.00
p_e=1.00
2002 Day 145 at 20:00
A=0.85; SWE_t=2.50cm
Kappa=1.00
$K_{location}$=1.00
p_{SCA}=0.00
p_a=1.00
p_e=1.00
2002 Day 145 at 20:00

CHAPTER 5: CONCLUSIONS

This chapter:

1. Summarizes accomplishments
2. Summarizes findings and implications
3. Critiques the methods and describes the value of the data
4. Suggests future work

5.1 ACCOMPLISHMENTS

In summary, the results of this study accomplished the objectives in Table 3-1 by developing and executing scripts and procedures to

1. Batch-manipulate MODIS granules for the UKRW in order to make MODIS data comparable, on a snow/snow-free basis, to categorical data in the TOPLATS coordinate system (Section 3.3). This data-management processes included developing a swath-to-grid data conversion procedure, which included a resamping algorithm with a modal decision (Section 3.3.1.2.3) used to assign categories with duplicate values.
2. Create visualizations of MODIS and model maps. These maps (frames of series) were displayed side-by-side and in overlays for visual comparison. The processes considered quality assurance information in the MODIS product itself and reviewed the association of quality information with the time of day and time of year measurements were collected.
3. Quantitatively compare maps, both spatially and temporally, using the simple proportion of agreement statistic, Kappa statistics, depletion curves, and

probability as a measure of uncertainty in cloud-obscured — or otherwise unavailable areas of — measurement maps. This process shows the value of Kappa as a summary statistic of the agreement between map two series. These procedures are now available to be updated for the analysis of other watersheds with other categories.

5.2 FINDINGS AND IMPLICATIONS

5.2.1 Usefulness of MODIS for Modeling The UKRW

Results confirm Déry et al. (2004) concerns that clouds hinder MODIS from making complete measurements in the UKRW. MODIS snow cover maps (Figure 4-4) and supporting quality assurance information show that clouds, during the winter-spring snowmelt of the year 2000 in particular, obscure the MODIS view of the ground during three and a half days between noon (UTC) at day 151 and the end of day 154 accounting for half the seven day melt period. The results also show that, in conjunction with cloud coverage, other factors help determine the usability of MODIS measurements. These factors include MODIS supporting quality assurance information described by NSIDC (2006) to create the Snow Cover PixelQA eight-bit layer — invalid data, broken detector bands, obtuse sensor angles, "highly uncertain" band 6 radiance, unusable sub-calculations — and also include time-of-day information. A combination of filters, described in Chapter Four, sift out the most usable MODIS measurements.

This research also agrees with Déry et al. (2004) in that both Level Two and Level Three MODIS results do not directly confirm SWE maps. For Level Two

measurements, MODIS does not measure SWE nor does MODIS report results in a grid format. For Level Three MODIS measurements, while they are more readily projected into grids because they are delivered in the GCS, the temporal composite inherent in them is longer than the melt-period in the UKRW. Level Three measurements, therefore, are better suited to confirm snow predictions of longer melt periods occurring across larger, global regions like the entire Kuparuk River watershed. For Level Two MODIS measurements, however, the methods in this study in-part overcomes these problems through the S2K procedure and a modal decision to generalize multi-category swaths into grids containing three category groups of cells: snow, snow-free, and unavailable. (For these groups, the snow group includes all "frozen" locations including ice, and the snow-free group includes both snow-free land and water.) Plots of MODIS and TOPLATS maps side-by-side (e.g. Figure 4-27) show that, despite factors that limit the spatiotemporal measurement information in MODIS measurements, MODIS data can reveal sub-watershed problems with a model during relatively cloud-free years. In the case of TOPLATS predictions for the year 2002, Figure 4-27 suggests TOPLATS relies on DEM information at, perhaps, the expense of other physical factors and other processes that need to be determined. This study's confidence in this conclusion is limited largely by the measurement quality assurance proportions in these cloud-free scenes, which range from 0.57 to 0.94, with an average proportion of 0.73 good quality cells.

This study can make the conclusion that image spectrometers on sun synchronous satellites like Aqua and Terra have the spatiotemporal resolution to monitor and confirm SCA predictions for short snow melt periods in watersheds that

are a similar size as the UKRW. Improvements in the quality and quantity of MODIS measurements during melt periods over areas like the UKRW, however, are limited by both natural (cloud coverage) and technological (small number of satellites and broken sensor) factors.

5.2.2 Quantifying Uncertainty In Scenes Containing Unavailable Measurements

Addressing the attempt to use probability to express measurement uncertainty (Section 2.4.3), this study defines unavailable locations in scenes as those that are cloud obscured or otherwise deemed poor quality by MODIS (Chapters Three and Four). Determining the probability distribution of the proportion of SCA for scenes containing unavailable measurements, based only on known information, only slightly increases this study's confidence in confirmation results because most scenes with *any* unknown coverage are generally filtered out based on time of day and quality assurance information before they can be considered. The final year 2002 series analyzed in Chapter Four, for example, contains zero cloud-obscured areas.

In summary, after filtering out MODIS data based on a combination of quality assurance layers inherent to the HDF-EOS granules, observed cloud coverage, and time of day, for each of three years, this study found only a small number of — and sometimes no — remaining usable scenes during the melt period to confirm TOPLATS results. In the usable scenes, only a marginal amount of unavailable pixels were left which could bear any impact on this study's conclusions for the UKRW.

5.2.3 Applicability of Kappa Statistics

With a limited sample size, the Kappa statistic and Kappa statistic variants plotted over the melt period do not indicate much more than the proportion of agreement between measured MODIS SCA measurements and inferred TOPLATS SCA model results over the same time period, but they do show some useful information. Three figures — (1) plots of Kappa comparison statistics in Figure 4-22b for the 0.80 albedo, 0.75 SWE threshold series, (2) plots of Kappa comparison statistics in Figure 4-23d for the 0.85 albedo, 2.50 cm SWE threshold series, and (3) the side-by-side measured and modeled results in Figure 4-27 — show the usefulness of Kappa statistics in comparison to the proportion of agreement. The remainder of this section reviews these plots from the beginning of the melt period to the end of the melt period. The beginning of the melt period for the 0.85 series shows the most useful information.

During the beginning of the melt period, from day 138 through day 140, shown in the first three rows of images in Figure 4-27, the 0.80 simulated series remains blanketed with snow while MODIS and the 0.85 simulated series both report snow depletion. In this beginning-of-melt period, therefore, the Kappa statistic cannot be calculated for the 0.80 series because there are uneven number of categories between the measured and modeled maps. There are always two categories in the measured data and only one category — snow — in the modeled data. In this case, the proportion of agreement can be considered the "alternative" Kappa. In the 0.85 series alternatively, two categories exist in both maps in each of the three early scenes. Kappa reveals, in this case, more than the proportion agreement does. While

the proportion of agreement shows relatively high values, and the proportion SCA points are close together in the SCA versus time plot, the low Kappa values reflect problems in the model maps. The side-by-side plots in Figure 4-27 of measured and modeled data for the 0.85 albedo series confirm the problems detected by the Kappa summary statistic. On the first scene shown in this plot (Day 138 at 00:05), for example, while the bulk of the maps look the same where snow covers the ground, the snow-free areas are in almost completely different locations. The two scenes from day 140 shows similar problems not revealed by the proportion of agreement. On all three scenes, Klocation is always lower than Khisto indicating that the spatial problems in the model are due to location problems more than quantity problems. In other words, the *quantity* of pixels in each of the two categories predicted by the model contributed less to the poor Kappa statistic than the *location* of the those pixels. The high maximum success rate of agreement P_{max} and the relatively low proportion of agreement (Equation 2-8) are the contributing factors to the lower Klocation.

During the middle of the melt period from day 141 through day 143, low and negative Kappa values confirm what the proportion of agreement already shows and do not reveal much more. When Kappa falls to values between 0.50 and -0.50 in the 0.80 albedo series for example, the proportion of agreement fall to values between 0.80 to 0.30. The 0.85 Kappa values show similar information. In both cases, however, the proportion of agreement and the Kappa values show more than the side-by-side proportion SCA plot where the proportion SCA values between the model and the measurements are relatively close. The Klocation and Khisto values in both

the 0.80 albedo series and the 0.85 albedo series show that, like at the beginning of the melt, spatial location errors influence the poor proportion of agreement and poor Kappa values in comparison to the influence of the quantity of cells in each category. This explains the close proportion of SCA results.

At the end of the melt period, from day 144 through day 145, the Kappa statistics are the least relevant and provide little information compared to the proportion of agreement. During these times, like in the beginning of the melt period, there are an uneven number of categories between the model maps (all snow-free in this case) and the MODIS maps. Klocation demonstrates, like it did in the beginning of the melt, the difficulty the model has in predicting patchy snow cover during the melt period (Figure 5-1).

Figure 5-1 Patchy Snow in the Kuparuk River
TOPLATS poorly predicts the patchy location of where snow melts, as shown in this south-facing photo, picture toward the end of the melt period. This photo was taken by G. W. Kling from the University of Michigan on May 28, 1996 (Déry et al. 2004).

5.3 CRITIQUE AND FUTURE WORK

In this research, model output is compared to measurements in the model coordinate system, Clark 1866 UTM Zone 6. The sensitivity of the error of measurement, however, has not been propagated through the intermediate Albers Equal Area projection. For interest areas that are smaller than, or on the order of magnitude in size of the resolution of the MODIS sensor (in this case 500 meters), the swath to grid operations could be subject to reduced comparison accuracy. A sensitivity analysis should be conducted in the future. One way to overcome the intermediate projection is to test other GIS products in performing directional transformations from GCS to UTM Zone 6 for the UKRW data.

Another piece of information that could be used is the MODIS Collection 5 fractional snow cover information. Besides reporting quality assurance information and Boolean snow information compared to unavailable information, fractional snow information could show how close a model might be in predicting snow cover over a watershed.

5.3.1 Other Statistics

This study's observations call for a similar analysis in a larger area with a longer melt period to determine the applicability of Kappa statistics over in these kinds of areas and timeframes. The entire Kuparuk River could be a candidate for such a study. These two factors — space and time, however, are not dependent on each other and an analysis of Kappa on the comparison between MODIS measurements and spatially simulated results over either a larger area or a longer time frame would increase the

sample of cells and make the Kappa statistics more relevant to review than they are in this research. Alternatively, several watersheds the size of the UKRW with a similar snow melt time frames as the UKRW could be reviewed in tandem to further determine the applicability of the Kappa statistics.

Other statistics could be used in a future analysis including a ratio of Kappa to the proportion of agreement. Simplifying this ratio where Kappa is defined by Equation 2-8

$$\frac{K}{PA} = \frac{1 - PE/PA}{1 - PE} \quad \textbf{5-1}$$

This ratio could show analysts if category location problems or category quantity problems in the model results could be present where the proportion of agreement between the two maps in the comparison fails to show any, or few, problems. This ratio is driven by the proportion of expected agreement due to a random relocation of cells (*PE*) over the proportion of agreement (*PA*). As *PE* gets higher in comparison to *PA*, analysts can expect the *K/PA* ratio to get lower indicating Kappa is a stronger test then the Proportion of Agreement. In future work, calculating this ratio for several watersheds like the UKRW during like snow-melt periods could reveal the potential of the Kappa statistic as an objective function for model evaluation.

Another statistic that could be evaluated is a fuzzy Kappa statistic (Dou et al. 2007; Hagen 2002). Fuzzy statistics summarize individual statistics taken at various resolutions. For example, a sixty-four-pixel square map could be composited into a forty-nine pixel square map, and these two maps could be compared in a fuzzy analysis. Most of the time, composites are conducted irrespective of physically-distributed features. If physical features are believed to influence criteria, however, perhaps the compositing process inherent in reducing the resolution of an image could be taken over physical features instead of in a grid. In this case, a triangular irregular network (TIN) could be used in place of a grid (Vivoni et al. 2005). The following

question could be addressed for a simple physical feature like DEM in determining if this feature influences snowmelt: Given two fuzzy Kappa series (a) Kappa statistics for maps with increasingly coarse pixel resolution and (b) Kappa statistics for maps with increasingly coarsely-defined elevation zones, can comparison of these two series quantify the dependence of a distributed snow-cover model on elevation at a particular interest area?

5.3.2 Variable Time-Rate Composite MODIS Data

This research, by employing Level Two MODIS data, highlights the fundamental problem with Level Three MODIS data described by Hall (2001, pers. com. 2006) in discussed in Chapter Two: The information in Level Three MODIS data is composited over an arbitrary fixed eight-day time interval. While this temporal composite potentially "eliminates unknown" measurement information at locations from cloud obscured and other unavailable regions in individual scenes, it (a) could hide sub-scene changes and physical process and (b) could composite information where no compositing is needed — between scenes with 100% measurement coverage. These problems from eight-day temporal compositing could greatly hinder the ability of Level Three MODIS data to evaluate the capabilities of a model during a relatively short time period. In the example of the UKRW where snow melts in less than eight days, the Level Three MODIS data is useless. Level Two data, in comparison however, is hindered by clouded and poor quality measurements. In conclusion, a variable time-rate composite could be created out of Level Two MODIS data that composites sequential scenes over variable time lengths. The criteria for

determining the time length could be spatial measurement availability and quality assurance information from the MODIS product. In an extreme example, if a ten-scene series contains all unavailable data during scenes one, two, four, five, seven, eight, and ten and all cloud-free, high quality scenes on days three, six, and nine, a variable time-rate composite could consist of three composites for (1) days one through four, (2) days five through seven, and (3) days eight through ten. In this example the composites last for four, three, and three days each with periods of no-data divided as evenly as possible between them. Similar to a variable bit-rate (VBR) music file on a computer (like modern mp3 file formats) where file size is optimized by varying the bit-rate dependent on the waveforms in a song, variable time-rate composites would optimize the useful information in a series of MODIS measurements for a given interest area. The composite scenes in such a series could depend on user-specified thresholds such as maximum number of scenes in a composite, minimum number of scenes in a composite, maximum time period of a composite, minimum time period of a composite, minimum proportion of available information in an interest area, and the product of the minimum probability of certainty – measured across time – with the number of cells in a scenes. Note that "cells" could be determined on a pixel-basis, or on a vector basis, grouped by physical areas like DEM as described in suggestions for Kfuzzy statistic analysis.

5.3.3 Comparing Data in Swath Format

In the case of UKRW, the model is based on DEM data in UTM Zone 6. Comparing measurements in the raster coordinate system of the model is the most common

method of using MODIS data to confirm model results. This way is usually used because common MODIS products, such as Level Three products, are already provided in grid formats that may easily be projected using GIS packages like those reviewed in Chapter Two. These packages, which did not work well to batch-convert Level Two MODIS data, are made specifically to convert Level Three data into UTM zone data. In future work, a different method could be used to confirm model results. Point data could be extrapolated from the raster model data and compared more directly with the measurements. In this analysis, the model would be used to produce results in the measurement format rather than transforming the measurements to the model format. It would reduce the propagation of measurement uncertainty and error through multiple projections. It would, however, also create the need to spatially weight Kappa statistic values according to point density. The weighting algorithm would need to be developed in future work.

Another way to compare the model and measurement maps, both given SCA categories (opposed to SCA and SWE categories) could be to compare raster model results with swath points projected, without bitmap interpolation, in the model projection system. Maps of these comparisons, visually, would contain measurement swath points overlaid on simulated model cells with color-coded categories. A raster-point comparison, like this, would enable use of hdf-eos information without geographic transformations that reduce measurement certainty. The analysis would require maximum distances to determine the influence of a measurement point on the simulated model cell. For example, the prediction of a model cell could be compared

to the data points within it, or with data points in a region nearby. This region could be defined by a distance or, perhaps, a physical feature.

5.3.4 Revaluate HEG-TOOL

Raytheon Company updated HEG-TOOL during the 2007-2008 International Polar Year since it was first evaluated for converting MOD10_L2 and MYD10_L2 swath graduals into projected grids. One notable update, the ability of HEG-TOOL to project data in the Albers Equal Area, could possible solve the batch-conversion problems described in Chapter Three. HEG-TOOL, thus, should be revaluated. If HEG-TOOL no longer halts during conversion of some HDF-EOS products, it could be used in place of a subset of the methods for converting swaths to grids created in this thesis.

5.3.5 Select Only High Quality Scenes Within Sub Time Intervals

Section 4.1 narrowed the selection of scenes down to morning scenes with a 0.50 or greater proportion of good quality swath points. In Section 4.2.1, the morning scenes alone showed that the 0.80 albedo simulation and the 0.85 albedo simulation performed better than the 0.75 series in terms of matching normalized SWE values to SCA values. Quality information can further narrow the selection of scenes to evaluate the model. For example, at the end of day 136, Figure 4-21 shows the point with 0.87 QA is more trustworthy than the point with 0.79 QA; and at the end of day 137, this study can have the most confidence in the scene with 0.84 QA. The candidate model that best matches the highest quality measurements within a given time interval could be identified.

5.4 RESEARCH SUMMARY

In summary, MODIS Level Two data and the Kappa statistic could be used in evaluating spatiotemporally distributed models. For model calibration, it would be necessary to calculate an objective function from the time series of different Kappa statistics. The methods in this study, however, would give more robust results in a larger watershed with a longer melt period: The duration and characteristics of the snow melt period in the UKRW proved to be problematic in terms of comparison with MODIS. The snow disappears in about a week, and in two of the three years the weather was cloudy during the entire period. So there were virtually no usable MODIS scenes available in those years. Even in the year 2002, which had a comparatively cloud-free melt period, other factors rendered a fraction of the MODIS scenes unusable. At the outset of this study, the selection of the UKRW with an area of 148 km^2 compared to a nominal swath resolution of 500 m seemed like it would provide enough data for a good comparison of maps and answer the conclusion that MODIS measurements "do not provide the location covered by snow within a single grid cell" (Déry et al. 2004) with the development of a a swath to grid conversion methodology. The time short melt period, "the persistence of low-level clouds in the Arctic during spring," and other problems with the data, however, proved to be greater limiting factors than problems with spatial resolution and comparing swaths to grids.

Level Two MODIS data best describe snow-melt situations with slightly longer melt periods and larger areas than the UKRW. Level Two data still, however, show more than the eight-day composite Level Three data. Funding for more

satellites and funding to repair existing satellite sensors would increase the chance of collecting good quality coverage data. A report generated by an online web-service found toward the end of this research called "Product Quality Documentation for MOD10_L2, C4," located at the "MODIS Land Quality Assessment web site" (NASA 2009), confirms this study's findings on the usability of data collected between the end of April in the year 2002 (day 120) and the end of the year 2002 (day 365). For these times, "Snow cover is mapped with reasonable accuracy. However, snow/cloud confusion and false snow detection do occur in some situations. Analysis of inaccuracies in snow mapping continues. Discretion should be exercised in use of this product." The report warns further that, "Snow mapping errors may occur on the perimeters of snow fields, cloud edges, and water boundaries," and the data is "being investigated" for further errors. For Collection Five data, not reviewed in this report, the web service reports similar problems. Additionally, while the Collection Five report confirms the data collected by MODIS during the 2002 UKRW melt has been "inferred" to pass a science quality test, the report marks the times right before (April 14 at day 104 through April 15 at day 105) and right after (three hours on June 19 at day 170) the winter-spring melt-window as "suspect" for quality errors.

The tools and methods in this study are now available for other researchers wishing to create maps from Level Two MODIS swath granules, select the MODIS scenes most useful for model evaluation, compare MODIS maps with model maps using Kappa statistics, and compare MODIS maps with model maps using the proportions of available (visible) snow coverage in each MODIS scenes as a measure of uncertainty for the snow coverage in cloud obscured, or otherwise unavailable,

areas of measurement maps. The Kappa statistic in this study shows small amount of information beyond the proportion of agreement statistic in the map comparison of the year 2002 data. Evaluation of a model that directly outputs SCA instead of SWE, could further reveal the usefulness of the Kappa statistic in map comparison for evaluation of a spatially distributed snow-melt models. Exploration of the Kappa family of statistics, overall, indicate that they are potentially useful in creating objective performance measures of spatially distributed models, and might eventually be useful for model calibration.

APPENDIX A. UNITED STATES GLOBAL CHANGE RESEARCH PROGRAM ORGANIZATIONS

Agency for International Development

Dept. of Agriculture

Dept. of Commerce, Natl. Oceanic & Atmospheric Admin.

Dept. of Defense

Dept. of Energy

Dept. of Health and Human Services, National Institutes of Health

Dept. of State

Dept. of Transportation

Dept. of the Interior, US Geological Survey

Environmental Protection Agency

National Aeronautics & Space Administration

National Science Foundation

Smithsonian Institution

APPENDIX B. PROJECTED MODIS MEASUREMENTS

See online images at http://choy.me/david/research.

APPENDIX C. SOFTWARE REQUIREMENTS

The following software is required to repeat or modify the methods described in Chapter Three and present the results in Chapter Four.

1. Microsoft Windows XP
2. Mathworks MATLAB® 7 with HDF-EOS support
3. Python 4 for Windows and Pythonwin
4. ESRI ArcGIS 9.1 or 9.2 with the Spatial Analyst extension

APPENDIX D. COMPARISON OVERVIEW DATAFLOW

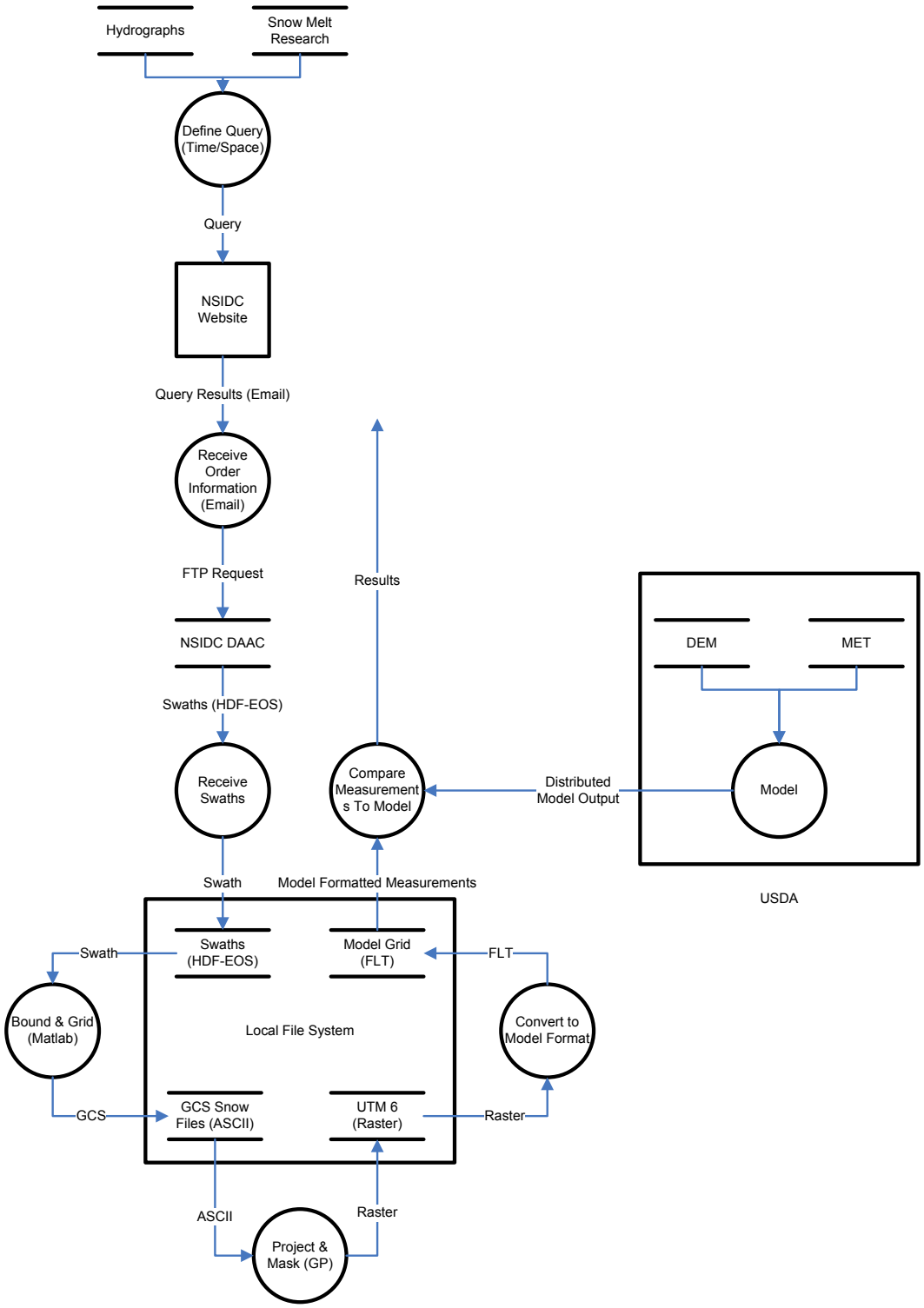

APPENDIX E. MODIS SWATH SCENE OBJECTS

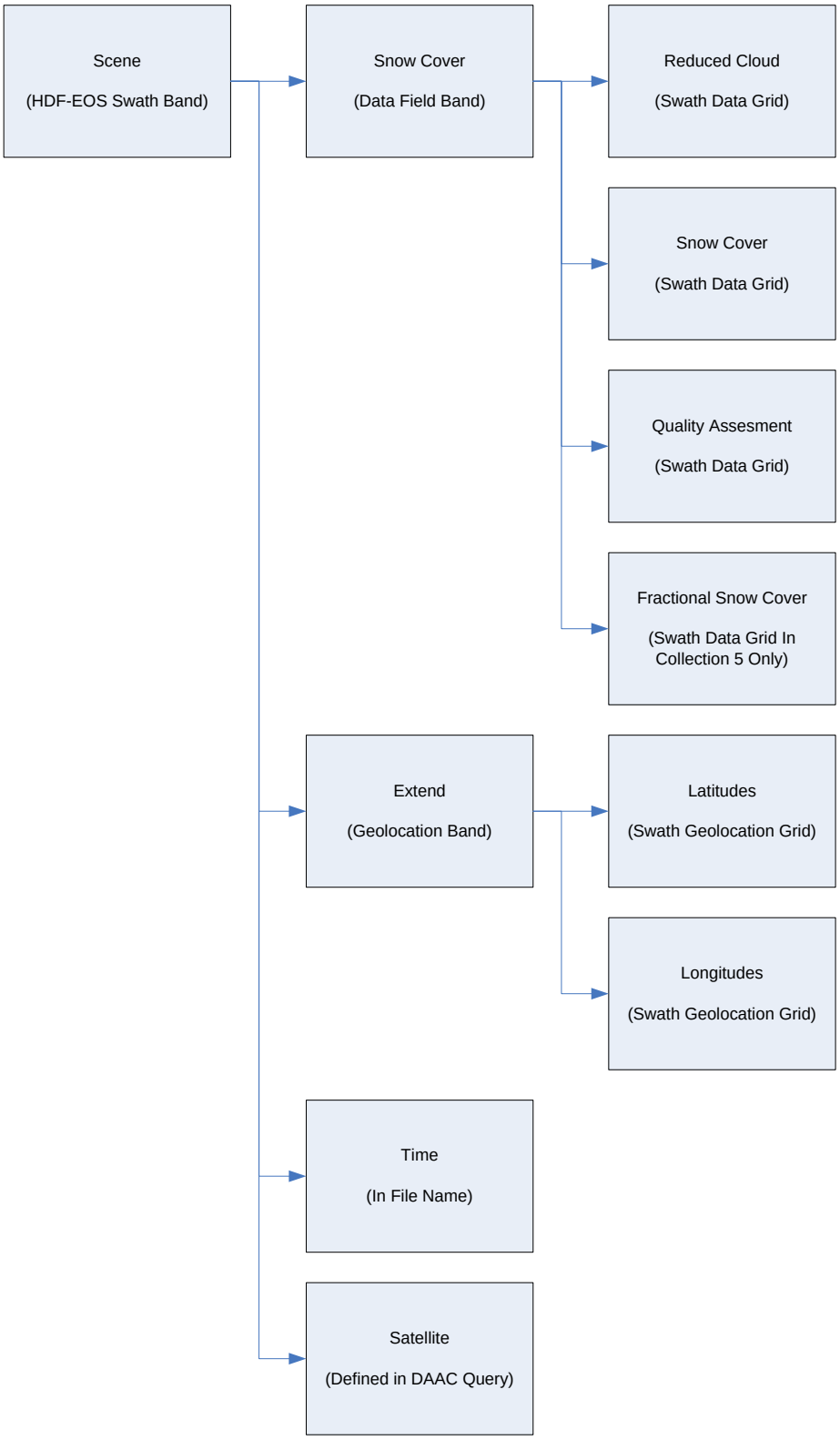

APPENDIX F. GLOBAL CHANGE ONLINE RESOURCES

Agency	Global Change Website Information
Agency for International Development	http://www.usaid.gov/our_work/environment/climate
Dept. of Agriculture	http://www.ars.usda.gov/main/main.htm
Dept. of Commerce, National Oceanic & Atmospheric Admin. (also, National Institute of Standards and Technology)	http://www.climate.noaa.gov/
Dept. of Defense	http://www.crrel.usace.army.mil/
Dept. of Energy	http://www.science.doe.gov/ober/CCRD_top.html
Dept. of Health and Human Services, National Institutes of Health	http://www.cancer.gov
Dept. of State	http://www.state.gov/g/oes/climate/ http://usinfo.state.gov/gi/global_issues/climate_change.html
Dept. of Transportation	http://climate.volpe.dot.gov/
Dept. of the Interior, US Geological Survey	http://geochange.er.usgs.gov/
Environmental Protection Agency	http://cfpub.epa.gov/gcrp/
National Aeronautics & Space Administration	http://science.hq.nasa.gov/earth-sun/science/water.html
National Science Foundation	http://www.nsf.gov/dir/index.jsp?org=GEO
Smithsonian Institution	http://www.serc.si.edu/research/searchresults.jsp?themeId=21

APPENDIX G. SWATH TO KUPARUK (S2K) CODE

Please contact the author for (a) python code for projecting, masking, and converting maps to little-endian floating point format and (b) MATLAB® code for converting HDF-EOS files to ASCII files.

APPENDIX H. COMPARING MODEL AND MEASUREMENTS

Please contact the author for MATLAB® code for creating the figures in this thesis and comparing model and measurements.

GLOSSARY

Aqua EOS satellite launched in. Collects MODIS data. To compliment Terra, Aqua crosses the equator in the afternoon. (http://aqua.nasa.gov/)

Advanced Very High Resolution Radiometer (AVHRR) Instrument aboard POES.

Catchment-Based Land Surface Model (CLSM) A catchment-based model used by Koster et al. (2000) and Ducharne et al. (2000) in a general circulation model.

Collection, MODIS A MODIS collection of data sets. Collection 5 includes fractional snow coverage.

Confusion Matrix (or Contingency Table) Shows agreement and disagreement between categorical results. The transformed confusion matrix with only two categories shows type 1 errors (producer risk) and type 2 errors (consumer risk). Confusion matrix has been used in computer science for testing data mining algorithms.

Distributed Active Archive Center (DAAC) Center for storing and distributing HDF-EOS data. The NSIDC DAAC stores relevant snow and ice MODIS measurements.

Enhanced Thematic Mapper Plus (ETM+) LANDSAT Sensor

Earth Observing System (EOS) NASA satellite program for measuring long-term, global changes (http://eospso.gsfc.nasa.gov/)

Geoproccessor The fundamental ArcGIS programming object (http://webhelp.esri.com/arcgisdesktop/9.2/pdf/Geoprocessor.pdf)

Geostationary Operational Environmental Satellite Program (GOES) Satalite program currently operated by NOAA, GOES refers to the satellite program and the satellites themselves. GOES satellites orbit the earth at the speed of the earth's rotation, enabling them to constantly hover above a single point on the earth.

Granule A single HDF-EOS dataset taken at a set time. Represents a single MODIS "scene" or "snapshot."

Granularity Increasing spatial resolution, in context with spatiotemporal data.

Grid The division of a quantity (in this study, usually space measured in meters), or multiple quantities (like quantities on the axis of a plot), into similar, smaller quantities. (A grid can also refer to different types of charts, like a comparison chart.)

griddata.m MATLAB® script used to fit swath surfaces to evenly spaced grids.

Earth Observing System (EOS) Project developed by NASA to study the earth. Includes the launch of Aqua and Terra. (http://eospso.gsfc.nasa.gov/)

Feature (called Feature Class by ESRI) Either a point, line, polygon, or pixel where the term line is generalized to include Bezier curves. ESRI excludes pixels from their definition of a feature and groups features into classes that can be assigned to layers of a map. ArcMap users cannot mix features within a layer, but can overlay layers in a single map. Three dimensional and four dimensional measurements can theoretically be called features. In practice

however, such measurements are usually described by composite layers across time series of maps.

HDF (Hierarchal Data Format) A data storage file format developed by NCSA. (http://www.hdfgroup.com/)

HDF-EOS Extension of the HDF file format used to store EOS data. Geographic data is stored in Swath, Grid, or Point formats in HDF-EOS files. (http://hdf.ncsa.uiuc.edu/hdfeos.html)

Interactive Multisensor Snow and Ice Mapping System (IMS) Software written by NOAA to create 25km, daily snow and ice data products. http://www.ssd.noaa.gov/PS/SNOW/ims.html

MS2GT The MODIS Swath-to-Grid Toolbox (http://nsidc.org/data/modis/ms2gt/)

Land Surface Model (LSM) A model that yields results that are distributed in a projected, Cartesian grid.

Moderate Resolution Imaging Spectroradiometer (MODIS) The tool that measures snow albedo, among other qualities, aboard AQUA and TERRA.

Nadir The direction directly below an observer, opposite from the zenith. In the case of a satellite, the direction towards the earth.

National Aeronautics and Space Administration (NASA) U.S. government agency that both observers the earth and explores space. Developed the HDF-EOS format based on the NCSA HDF format.

National Center for Supercomputing Applications (NCSA) Developed the HDF format.

(http://www.ncsa.uiuc.edu/)

National Snow and Ice Data Center (NSIDC) Maintains a DAAC of MODIS snow and ice data in HDF-EOS format.

(http://nsidc.org/)

National Oceanographic Are Agency

Polar Operational Environmental Satellite (POES) Satellite program launched by NASA and operated by NOAA. Used primarily for meteorological forecasting.

Permafrost Rock or soil that has been frozen for two or more years.

Projection

Albers Equal Area An equal area projection from the view of a pole

Cylindrical Equidistant A global project with latitude an longitude units

Robinson A common Pseudo-Cylindrical global projection.

qHull or QuickHull. Algorithm used by MATLAB® script "griddata.m" to perform nearest-neighbor Delaunay triangulation. See http://qhull.com.

Scene A segment of a swath.

Swath One of three ways HDF-EOS data is stored (Swath, Grid, Point)

Snow Covered Area (SCA) sdf

Solar Noon The time midway between sunrise and sunset. At Solar Noon, MODIS sensors view the earth near nadir, the best possible angle.

Level 2 Swath to TOPLATS Grid Tool for the Upper Kuparuk River Watershed (S2K) Procedure to convert MODIS swaths to grids comparable to TOPLATS output in the Upper Kuparuk River Watershed.

Terra EOS satellite launched in . Collects MODIS data. To compliment Aqua, Terra crosses the equator in the morning. (http://terra.nasa.gov/)

TOPMODEL-based Land-Atmosphere Transfer Scheme (TOPLATS) A distributed snowmelt model created by Pauwels and Wood 1999.

Triangular Irregular Network (TIN) A delineation of space into irregular triangle shapes, suggested in this study for evaluating maps with consideration to physical map features like land use or elevation.

United States Global Change Research Program (USGCRP) U.S government program that appropriates funds to 13 federal agencies to study global change, with a focus on climate change.

Universal Transverse Mercator (UTM) Alaska lies in UTM zones 1 through 10. The Upper Kuparuk is in UTM Zone 6. (http://erg.usgs.gov/isb/pubs/factsheets/fs07701.html) (http://rockyweb.cr.usgs.gov/outreach/gps/UTM_Zones_AK.pdf#search=%22alaska%20utm%22)

REFERENCES

Abbott, M.B. and Refsgaard, J.C. (1996). *Distributed Hydrological Modeling*, Kluwer Academic Publishers, Maine.

Advanced Very High Resolution Radiometer (AVHRR). http://noaasis.noaa.gov/NOAASIS/ml/avhrr.html, accessed 2008.

Alaska Bureau of Land Management (2006). "The Dalton Highway." Anchorage, AK: Alaska Natural History Association. Online: http://www.blm.gov/ak/dalton/assets/documents/DaltonGuide06.pdf.

Ayyub, B.M. and McCuen, R.F. (2003). *Probability, Statistics and Reliability for Engineers and Scientists 2nd Ed*, Chapman & Hall/CRC Press LCC, Boca Raton, FL.

Bergers (2006). "U.S. Readies 'LANDSAT 8' Acquisition." *Space.com*. http://www.space.com/spacenews/archive06/LANDSAT_022706.html, accessed May 2007.

Beven, K.J. (1998a). *Distributed Hydrological: Applications of the TOPMODEL Concept*, Wiley, England.

——, —— (1998b). "TOPMODEL User Notes Windows Version 97.01." Centre for Research on Environmental Systems and Statistics, Institute of Environmental and Biological Sciences, Lancaster University, Lancaster LA1 4YQ, UK.

Cohen, J. (1960). "A Coefficient of Agreement for Nominal Scales" *Educational and Psychological Measurement*, 20, 37-46.

Colee, M.T. (2000) "A High-Resoultion Distributed Snowmelt Model in an Alpine Catchment." MA thesis, University of California Santa Barbara.

CUAHSI (2009). "CUAHSI Hydrologic Information System." http://his.cuahsi.org/, accessed 2009.

Delaunay, B. (1934). "Sur la sphère vide." *Izvestia Akademii Nauk SSSR*, Otdelenie Matematicheskikh i Estestvennykh Nauk, 7, 793–800

Déry, S.J., Crow, W.T., Stieglitz, M., and Wood, E.F. (2004). "Modeling Snow-Cover Heterogeneity over Complex Arctic Terrain for Regional and Global Climate Models." *J. Hydrometeorology*, Feb 2004, 33-48.

Déry, S.J., Stieglitz, M., Rennermalm, A.K., and Wood, E.F. (2005). "The water budget of the Kuparuk River Basin, Alaska." *J. Hydrometeorology*, Oct 2005, 633–655.

Déry, S.J., Salomonson, V.V., Stieglitz, M., Hall, D.K., and Appel, I. (2005). "An approach to using snow aerial depletion curves inferred from MODIS and its applications to land surface modeling in Alaska." *Hydrological Processes*, 19, 2755–2774.

Dou, W., Ren, Y., Wu, Q., Ruan, S., Chen, Y., Bloyet, and D. Constans, J. (2007). "Fuzzy Kappa for the agreement measure of fuzzy classifications." *Neurocomputing*, 70(4-6), 726–734.

Ducharne, A., Koster, R.D., Suarez, M. J., Stieglitz, M., and Kumar, P. (2000). "A catchment-based approach to modeling land surface processes in a general circulation model. 2. Parameter estimation and model demonstration." *J. Geophys. Res.*, 105(24) 823–838.

Famiglietti, J. S. and Wood, E. F. (1994a). "Multiscale modeling of spatially variable water and energy balance processes." *Water Resour. Res.*, 30, 3061–3078.

—— and —— (1994b) "Application of multiscale water and energy balance models on a tallgrass prairie." *Water Resour. Res.*, 30, 3079–3093.

French, H.M. (2007). "Quaternary Periglacial Conditions" Chapter 11 of *The Periglacial Environment, Third Edition*, John Wiley & Sons, England.

Garret, J.J. (2005). "Ajax: A New Approach to Web Applications." http://www.adaptivepath.com/publications/essays/archives/000385.php, accessed 2005.

Geostationary Operational Environmental Satellite Program (GOES). http://goespoes.gsfc.nasa.gov/goes/project/index.html, accessed 2008.

Hagen, A. (2002). "Comparison of Maps Containing Nominal Data." Research Institute for Knowledge Systems, Maastricht. The Netherlands.

Hall, D.K., Riggs, G.A., Salomonson, V.V. (2001). "Algorithm Theoretical Basis Document (ATBD) for the MODIS Snow and Sea Ice-Mapping Algorithms." http://modis-snow-ice.gsfc.nasa.gov/atbd.html, accessed November 2006.

Hamilton, T.D. (1986). "Late Cenezoic glaciation of the Central Brooks Range." Vol. 99 of: *Glaciation in Alaska: The geologic record*, T. D. Hamilton, K. M. Reed, and R. M. Thorson, ed. Alaska Geol. Soc., Anchorage, 9–49.

Johnson, D.B. (1996). "Satellite Coverages and Orbits" http://www.rap.ucar.edu/~djohnson/satellite/coverage.html, accessed 2007.

Kane, D.L. and Hinzman, L.D., (2009). "Climate data from the North Slope Hydrology Research project." University of Alaska Fairbanks, Water and Environmental Research Center, Fairbanks, Alaska. http://www.uaf.edu/water/projects/NorthSlope/, accessed May 2009.

——, ——, McNamara, J.P., Yang, D., Olsson, P., Gieck, R. E. (2003). "An Extreme Rainfall/Runoff Event in Arctic Alaska." *J. Hydrometeorology*, 4, 1220–1228.

——, ——, McNamara, J.P., Zhang, Z., and Benson, C.S. (2000). "An overview of a nested watershed study in Arctic Alaska." *Nord. Hydrol.*, 31, 245–266.

Kaufman, D.S. and Manley, W.F. (2004). "Pleistocene Maximum and Late Wisconsinan glacier extents across Alaska, U.S.A." *Quaternary Glaciations—Extent and Chronology, Part II: North America. Developments in Quaternary Science Volume 2*. Ehlers, J. and Gibbard, P.L., eds., Elsevier, Amsterdam.

Koster, R. D., A. Ducharne, M. Stieglitz, and P. Kumar (2000). "A catchment-based approach to modeling land surface processes in a general circulation model." *J. Geophy. Res.*, 105, 24 809-24 822.

Landis, J.R and G.G. Koch (1977). "The Measurement of Observer Agreement for Categorical Data" *Biometrics*, 33(1), 159–174.

Liston, G.E. (1998). "Interrelationships among Snow distribution, Snowmelt, and Snow Cover Depletion: Implications for Atmospheric, Hyrologic, and Ecologic Modeling." *J Hydrometeorology*, 38, 1474–1487.

Matson, M., Ropelewski, C.F., and Varnadore, M.S. (1986). "An atlas of satellite-derived northern hemisphere snow cover frequency" National Weather Service, Washington, D.C.

McCuen (2003). "Introduction to Time Series Modeling." Chap. 2 of: *Modeling Hydrologic Change*, CRC Press LLC, Boca Raton, FL, 9–36.

Mokus, V. (1972). "Estimation of Direct Runoff from Storm Rainfall." Chapter 10 of: *National Engineering Handbook*, 10.1–10.24.

National Aeronautics and Space Administration (NASA) (2009). "MODIS Land Quality Assessment web site." http://landdb1.nascom.nasa.gov/cgi-bin/QA_WWW/newPage.cgi, accessed 2009.

National Oceanic and Atmospheric Administration (2006). “Ocean Explorer.” http://www.oceanexplorer.noaa.gov/technology/tools/satellites/satellites.html, accessed 2007.

——, —— (2009). “Earth System Research Laboratory Sunrise/Sunset Calculator.” http://www.srrb.noaa.gov/highlights/sunrise/sunrise.html, accessed 2009.

National Operational Hydrologic Sensing Center (NOHRSC) (2009). http://www.nohrsc.noaa.gov/, accessed 2009.

National Snow and Ice Data Center (NSIDC) (2003) “MS2GT: The MODIS Swath-to-Grid Toolbox” http://nsidc.org/data/modis/ms2gt, accessed 2008.

—— (2006a) “MODIS Snow Cover Quality Assurance Fields” http://nsidc.org/data/docs/daac/mod10_modis_snow/snowcover_qa.html, accessed 2009.

—— (2006b). “Comparison of Distributed vs. Archived Volume for MODIS Cryosphere L2, L2 Products.” *Proceedings of DAAC Data Priority Workshop January 11-12, 2006*, NSIDC, Goddard Spaceflight Center, Greenbelt, MD. http://nsidc.org/daac/users/data_workshop_report_2006.pdf, accessed 2008

—— (2007). “Data” http://nsidc.org/data/arcss017.html, accessed 2007.

—— (2008a) “Distributed Active Archive Center Overview” http://nsidc.org/daac, accessed 2008.

—— (2008b) “MODIS Data at NSIDC” http://nsidc.org/data/modis, accessed 2008.

—— (2008c) “EOS Data Gateway at NSIDC” http://nsidc.org/~imswww/pub/imswelcome/index.html, accessed 2008.

Nolan, M (2003). “Research at the Kuparuk Watershed.” http://www.uaf.edu/water/faculty/nolan/kuparuk/index.htm, accessed 2007.

Nolin, A., and Liang, S. (2000). “Progress in bidirectional reflectance modeling and applications for surface particulate media: Snow and soils.” *Remote Sensing Reviews*, 14, 307–342.

Oatley, J.A. (2002). “Ice, bedload transport, and channel morphology on the Upper Kuparuk River; a thesis.” *University of Alaska Fairbanks*.

Office of Management and Budget (2007). “Federal Climate Change Expenditures Report to Congress.” http://www.whitehouse.gov/omb/legislative/fy08_climate_change.pdf, accessed 2007.

Osterkamp, T.E., and Payne, M.W. (1981). “Estimates of permafrost thickness from well logs in northern Alaska.” *Cold Reg. Sci. Technol.*, 5, 13–27.

Polar Operational Environmental Satellite Program (POES). http://goespoes.gsfc.nasa.gov/poes/project/index.html, accessed 2008.

Pontius Jr., R.G. (2000). “Quantification error versus location error in comparison of categorical maps.” *Photogrammetric Engineering & Remote Sensing*, 66(8), 1011–1016.

——, —— and Schneider, L.C. (2001). "Land-cover change model validation by an ROC method for the Ipswitch watershed" *Agriculture, Ecosystems and Environment*, 85(1-3), 239–248.

——, —— (2002). "Statistical Methods to Partition Effects of Quantity and Location During Comparison of Categorical Maps at Multiple Resolutions." *Photogrammetric Engineering & Remote Sensing*, 68(10), 1041–1049.

——, ——, Shusas, E., and McEachern, M. (2004). "Detecting important categorical land changes while accounting for persistence." *Agriculture, Ecosystems and Environment*, 101, 251–268.

——, —— and Lippitt, C.D. (2006). "Can Error Explain Map Differences Over Time?" *Cartography and Geographic Information Science*, 33(2), 159–171

Porter, S.C (1964). "Late Pleistocene Glacial Chronology of North-Central Brooks Range, Alaska." *American Journal Of Science*, 262, 446–460.

Riggs, G.A., D.K. Hall, V.V. Salomonson. (Nov 2006). *MODIS Snow Products User Guide to Collection 5*.

Robinson, D.A. (2003). "An Informed Guide to Climate Data Sets." www.cgd.ucar.edu/cas/guide/Data/robinson.html, accessed 2008.

——, ——, Dewey, K.F., and Heirm, Jr. R.R. (1993). "Global Snow Cover Monitoring: An Update." *Bulletin of the American Meteorological Society*, 74(9), 1689–1696.

Salomonsona, V.V., and Appelb, I. (2004). “Estimating fractional snow cover from MODIS using the normalized difference snow index.” *Remote Sensing of Environment*, 89, 351–360.

Sim, J. and Write, C.C. (2005). “The Kappa Statistic in Reliability Studies: Use, Interpretation, and Sample Size Requirements.” *Physical Therapy*, 85, 235–268.

Turpin, O., Ferguson, R., and Johansson, B. (1999). “Use of remote sensing to test and update simulated snow cover in hydrological models.” *Hydrological Processes*, 13, 2067–2077.

United States Geological Survey (2008). “Water Resources Applications Software Summary of HSPF.” http://water.usgs.gov/cgi-bin/man_wrdapp?hspf, accessed 2008.

United States Global Change Research Program (USGCRP) (2003). “Strategic Plan for the U.S. Climate Change Science Program.” http://www.climatescience.gov/Library/stratplan2003/final/ccspstratplan2003-all.pdf, accessed 2007.

—— (2008). “Revised Research Plan for the U.S. Climate Change Science Program.” http://www.climatescience.gov/Library/stratplan2008/CCSP-RRP-FINAL.pdf, accessed 2008.

—— (2007). "Preview of Our Changing Planet: The U.S. Climate Change Science Program for Fiscal Year 2008." http://www.usgcrp.gov/usgcrp/Library/ocp2008preview/OCP08-preview.pdf, accessed 2007.

United States Naval Observatory Astronomical Applications Department (2009). "Sun or Moon Rise/Set Table for One Year." http://aa.usno.navy.mil/data/docs/RS_OneYear.php, accessed 2009.

United States Senate and House of Representatives (1990). "U.S. Global Change Research Act of 1990; Public Law 101-606(11/16/90) 104 Stat. 3096-3104." http://www.gcrio.org/gcact1990.html, accessed 2007.

Vieux, B.E. (2004). *Distributed Hydrologic Modeling Using GIS 2nd ed*, Kluwer Academic Publishers, Maine.

Vivoni, E. R., V.Y. Ivanov, R.L. Bras, and D. Entekhabi (2005). "On the effects of triangulated terrain resolution on distributed hydrologic model response." *Hydrological Processes*, 19(11), 2101–2122.

Voss, O. (2006). Dalton Highway (Alaska 11) Photo Journey. http://www.alaskaroads.com/photos-Dalton-Hwy.htm, accessed December 2006.

Walker, D.A., Hamilton, T.D., Balser, A.W., and Anderson, J.A. (2003). "Glacial Geology Map of the Toolik Lake and Upper Kuparuk River Region, Alaska

Digital media." National Snow and Ice Data Center, Boulder, CO. http://nsidc.org/data/docs/arcss/arcss117/index.html, accessed 2006.

Williams, D. (2007). "Orbit & Coverage." Chapter 5 of: *LANDSAT 7 Science Data Users Handbook*, Goddard Spaceflight Center, MD. http://landsathandbook.gsfc.nasa.gov/handbook/handbook_toc.html, accessed September 2007.

Wolfe, R.E. (2002, February 3) *Modis Summary* Presented at EDC LP DAAC Science Advisory Panel Meeting. http://edcdaac.usgs.gov/landdaac/presentations/MODIS_Status-Wolfe.pdf, accessed February 2007.

Zhang, Z., Kane, D.L., and Hinzman, L.D. (2000). "Development and application of a spatially-distributed Arctic hydrological and thermal process model (ARHYTHM)" *Hydrological Processes*, 14, 1017–1044.